EYE-CLIMA
Verifying emissions of climate forcers

Final fluxes of CO_2, CH_4 and N_2O at 0.5° from 2005

DELIVERABLE D3.2

Author(s):	LSCE: Grégoire Broquet, Antoine Berchet Science Partners: Audrey Fortems-Cheiney FMI: Anteneh Getachew Mengistu, Maria Tenkanen, Tuula Aalto NILU: Nalini Krishnankutty
Date of submission:	26-01-2026
Version:	1.0
Responsible partner:	NILU
Deliverable due date:	30-04-2025
Dissemination level:	Public

Call:	HORIZON-CL5-2022-D1-02
Topic:	Climate Sciences and Responses
Project Type:	Research and Innovation Action
Lead Beneficiary:	NILU - Norsk Institutt for Luftforskning

This project has received funding from the European Union's Horizon Europe research and innovation programme under grant agreement No 101081395

Document History

Version	Date	Comment	Modifications made by
0.1	08.09.2025	First complete draft	A. Fortems-Cheiney, N. Krishnankutty, G. Broquet, A. Berchet, Anteneh Getachew Mengistu, M. Tenkanen, and T. Aalto
0.2	11.09.2025	Internal review	R. Thompson
0.3	26.09.2025	Second version	A. Fortems-Cheiney, N. Krishnankutty, G. Broquet, A. Berchet, Anteneh Getachew Mengistu, M. Tenkanen, and T. Aalto
1.0	23.01.2026	Revision to CO_2 and N_2O	A. Fortems-Cheiney, N. Krishnankutty
1.1	24.01.2026	Final version	N. Krishnankutty
1.1	26.01.2026	Submitted to commission	R. Thompson

This project has received funding from the European Union's Horizon Europe research and innovation programme under grant agreement No 101081395

Summary

One of the main objectives of EYE-CLIMA is to use the atmospheric inversion methodology, which can be used to estimate the surface-atmosphere fluxes of various greenhouse gases, to verify and support National Greenhouse Gas Inventories (NGHGIs). By carrying-out long-term atmospheric inversions of the three most important GHGs, carbon dioxide (CO_2), methane (CH_4) and nitrous oxide (N_2O) for Europe, EYE-CLIMA aims to support the monitoring of emissions for European Union countries (EU27) plus the United Kingdom, Switzerland, and Norway (EU27+3) and provide valuable information for the assessment of emission mitigation policy.

The inversions of CH_4 and N_2O are at monthly temporal resolution, while for CO_2, the inversions have a temporal resolution of monthly with a sub-daily time step of 6 hours to allow the diurnal cycle in CO_2 fluxes to also be optimized. These inversions are based on observations from ground-based sites (e.g., from ICOS, INGOS, GAW, and NOAA networks) with long-term records for consistency over all years. For CO_2, additional inversions using satellite observations from OCO-2 have been performed. For the inversions, prior flux information is obtained from Work Package 2, along with global emission estimates. Inversions are computed with the inversion framework, the Community Inversion Framework (CIF), combined with CHIMERE for CO_2 and FLEXPART for CH_4 and N_2O. The boundary conditions for the regional simulations are global optimized fields of mixing ratios, choosing the product for each species that contributes the least error.

The spatial resolution of the fluxes is 0.5°×0.5°. Presently, CO_2 inversions using surface measurements have been performed for the period 2005-2023 while the inversions using satellite observations have been conducted for the period 2015-2021. For N_2O and CH_4, the inversions are performed for the periods 2005-2023.

For CO_2, the inversions using surface measurements and OCO-2 satellite observations both significantly improved the fit between the simulated and observed CO_2 mole fractions. European ecosystems act as CO_2 sinks, but surface-based inversions generally result in positive corrections (decreasing the CO2 sink), while the satellite-based inversions result in negative corrections. The posterior estimates of the NEE+F_{LUC} average annual budget for EU27+3 over 2015-2021 is of about -0.34 PgC.yr^{-1} from the surface-based inversions and of about –0.84 PgC.yr^{-1} from the satellite- based inversions compared to the prior estimates of about -0.55 PgC.yr^{-1}, with the weakest sinks seen in 2018, when Europe experienced an extensive heatwave and drought.

For CH_4, the optimized fluxes resulted in a notable improvement in agreement of modelled and observed CH_4 mole fractions. For the EU27+3 region, averaged over 2005–2023, total emissions shift from a prior estimate of 23.11 ± 1.79 Tg yr^{-1} to a posterior estimate of 23.47 ± 1.52 Tg yr^{-1}, representing a modest ~2% increase (± values indicate the standard deviation of the mean). This modest change masks substantial regional and sectoral changes: agricultural emissions increased by around 10% across the EU27+3, with particularly large increases in Germany, France, and the Benelux, while decreases occurred in the UK, Poland, Switzerland, and Italy. Wetland emissions declined across northern Europe, and fossil and geological fluxes underwent localized adjustments.

For N_2O, the forward transport model run with the optimized fluxes showed an improved agreement with the observations compared to using the prior fluxes. The inversion resulted in increased emissions in the Netherlands, western Germany, northwest France, and the UK, while decreases were observed over Northern Italy. Total mean prior emissions over the whole inversion period from 2005-2023 is 1.038 Tg(N_2O) yr^{-1} and increased to 1.519 Tg yr^{-1} after inversion. The emissions show a seasonal cycle with a maximum in early summer.

This project has received funding from the European Union's Horizon Europe research and innovation programme under grant agreement No 101081395

TABLE OF CONTENTS

Document History 2
Summary 3
1. Introduction 6
2. Methodology 6
2.1 Inversion framework 6
2.2. Model descriptions 7
2.2.1. The Community Inversion Framework (CIF) 7
2.2.2. CHIMERE 7
2.2.3. FLEXPART 7
3. CO_2 inversions 7
3.1 Inverse modelling system and experimental framework 8
3.1.1 Configuration of the regional CHIMERE chemistry-transport model 8
3.1.2 Land biosphere fluxes 8
3.1.3 Land fluxes from the “lateral” export of carbon from the ecosystems (including biofuel emissions) 9
3.1.4 Prior and fixed estimates of the land fluxes 9
3.1.5 Fossil emissions 9
3.1.6 Open and coastal ocean fluxes 10
3.1.7 Prior / Fixed estimate of the boundary conditions and completion of the stratosphere 10
3.1.8 Meteorological forcing 10
3.2. Observations 10
3.2.1. Near-surface in-situ measurements 10
3.2.2. OCO-2 satellite observations 11
3.4. The inversion framework 12
3.4.1. Experiments 13
3.5. Results 14
3.5.1. Fit to the assimilated observations 14
3.5.2. Spatial variability of the annual corrections applied to the prior terrestrial ecosystem fluxes from surface and OCO-2 observations 15
3.5.4. Long-term mean and inter-annual variability of the EU27+3 NEE+F_{LUC} budget 18

This project has received funding from the European Union's Horizon Europe research and innovation programme under grant agreement No 101081395

4. CH_4 inversions 20
4.1 Inversion framework and transport model 20
4.2. Prior fluxes 20
4.3. Observations 23
4.4 Results 24
4.4.1 Comparison of Modelled and observed CH_4 mixing ratio 24
4.4.2 Spatial distribution of prior and posterior fluxes 26
4.4.3 Annual and monthly emission estimates 29
5. N_2O inversions 30
5.1 Inversion framework and transport model 30
5.1 Prior Fluxes 31
5.3 Observations 32
5.4 Results 34
5.4.1 Modelled and observed atmospheric N_2O mole fractions 34
5.4.2 Spatial and temporal distribution of prior and posterior emissions 37
6. Conclusions 40
7. References 41
Appendix A: Inversion Protocol for CO_2 47
Appendix B: Inversion Protocol for CH_4 56
Appendix C: Inversion Protocol for N_2O 62

This project has received funding from the European Union's Horizon Europe research and innovation programme under grant agreement No 101081395

1. Introduction

To mitigate global warming, the emissions of greenhouse gases (GHGs) need to be reduced. Up to present, the standard method to monitor GHG emissions has been the use of national greenhouse gas inventories (NGHGIs), which are typically compiled using activity data and emission factors. However, NGHGIs contain uncertainties due to uncertainty in the emission factors as well as in the activity data.

One of the main objectives of EYE-CLIMA is to provide independent verification of NGHGIs by developing top-down methods based on atmospheric inversion to a level of readiness where they can be used to determine emissions at national and sub-national scales.

This deliverable presents the final atmospheric inversion results for the three main GHGs, carbon dioxide (CO_2), methane (CH_4) and nitrous oxide (N_2O) for Europe for the target period 2005-2023. This long timeseries of observation-based emissions estimates provides valuable information on the trends in the emissions and help support policy decisions regarding emission mitigation.

Atmospheric inversion is a way to use atmospheric observations, e.g., mixing ratios of GHGs, to estimate surface-atmosphere fluxes and their uncertainties. The method involves using an atmospheric chemistry transport model (ACTM) to relate an existing independent estimate of the fluxes (the prior estimate) to atmospheric mixing ratios and to determine the model-observation error. This error is then used to update the prior estimate by effectively inverting the transport to relate the difference in mixing ratio to a difference in flux.

The 0.5°×0.5° resolution inversion used in this deliverable is assumed to be sufficient to reliably estimate the annual country totals for mid to large European countries and is the typical resolution of inversion systems for estimating GHG budgets at the European scale. Moreover, due to the sparsity of observations in the 2000s and up to the start of the ICOS network, it is not possible to reliably constrain the emissions at higher resolution over the entire target time period.

2. Methodology

2.1 Inversion framework

Atmospheric inversions work by relating the difference between prior modelled and observed mixing ratios to a correction to the prior flux estimate. In other words, the method minimizes the following cost function $J(\mathbf{x})$ with respect to the state vector $\mathbf{x}$:

$$J(\mathbf{x}) = \frac{1}{2}(\mathbf{x}-\mathbf{x_b})^{\mathrm{T}}\mathbf{B}^{-1}(\mathbf{x}-\mathbf{x_b}) + \frac{1}{2}(H(\mathbf{x})-\mathbf{y})^{\mathrm{T}}\mathbf{R}^{-1}(H(\mathbf{x})-\mathbf{y}) \quad (1)$$

Here, $\mathbf{x}$ represents the state vector of model variables, $\mathbf{x_b}$ is the initial guess or prior state vector, $\mathbf{B}$ denotes the prior error covariance matrix reflecting uncertainties in $\mathbf{x_b}$, $\mathbf{y}$ is the vector of observed data, $H(\mathbf{x})$ is the observation operator mapping $\mathbf{x}$ to the observation space, and $\mathbf{R}$ is the observation error covariance matrix accounting for uncertainties in $\mathbf{y}$. The first term on the right-hand side of Eq. 1 accounts for deviation from the prior state $\mathbf{x_b}$ and second term represents the observational constraints on the prior fluxes.

To minimize $J(\mathbf{x})$ in CIF-CHIMERE and CIF-FLEXPART, the gradient $\nabla J(\mathbf{x})$ is computed as:

$$\nabla J(\mathbf{x}) = \mathbf{B}^{-1}(\mathbf{x}-\mathbf{x_b}) + H^{*}\mathbf{R}^{-1}(H(\mathbf{x})-\mathbf{y}) \quad (2)$$

This project has received funding from the European Union's Horizon Europe research and innovation programme under grant agreement No 101081395

The conjugate gradient algorithm (Lanczos, 1950) utilizes $\nabla J(\mathbf{x})$ to iteratively update $\mathbf{x}$, continuing until the gradient norm falls below a predefined threshold or a maximum number of iterations is reached. In Eq. 2, H^* denotes the adjoint of the operator H and for FLEXPART this is equivalent to the matrix transpose, $\mathbf{H}^T$.

2.2. Model descriptions

The Community Inversion Framework (CIF) (Berchet et al. 2021) has been used with the atmospheric transport models, CHIMERE and FLEXPART, for inversions of CO_2, CH_4, and N_2O, respectively.

2.2.1. The Community Inversion Framework (CIF)

The CIF is an open-source Bayesian inversion framework, which was developed under the previous Horizon Europe project, VERIFY. The concept of the CIF is to have a community inversion framework that can be interfaced with multiple atmospheric transport models to enable a consistent inter-comparison of inversions run with different transport operators (Berchet et al. 2021). The CIF has been interfaced with the Lagrangian particle dispersion model, FLEXPART, as well as the regional Eulerian model, CHIMERE, which are used in EYE-CLIMA. CIF has also been interfaced with the TM5-MP model, which is also used in EYE-CLIMA.

2.2.2. CHIMERE

CHIMERE is a Eulerian chemistry transport-model. CHIMERE and its adjoint code are coupled to the CIF to simulate CO_2 atmospheric mole fractions and CO_2 vertical columns over Europe. The CHIMERE domain for Europe covers latitudes 31.75 - 73.75°N and longitudes 15.25°W - 34.75°E with a 0.5°×0.5° horizontal resolution and 17 vertical layers up to 200 hPa. Meteorological forcing for CHIMERE is generated using operational forecasts from the Integrated Forecasting System (IFS) of the European Centre for Medium Range Weather Forecasting (ECMWF).

2.2.3. FLEXPART

FLEXPART is a Lagrangian Particle Dispersion Model and is described in Pisso et al. (2019) (and the most recent version 11 in Bakels et al. 2024). FLEXPART simulates atmospheric transport both forward in time and backwards in time, a key capability for inverse modeling. Backwards in time simulations are used to generate source-receptor relationships (SRRs), which form Jacobian matrices linking changes in surface fluxes to observed mole fractions. These SRRs describe the sensitivity of each observation to emissions across the domain and are used within CIF to model atmospheric CH_4 and N_2O mole fractions and to relate observation–model differences to corrections to the prior fluxes.

3. CO_2 inversions

This section describes the final inversions of the CO_2 land ecosystem fluxes.

These final inversions cover the period 2005 to 2023 and have a 0.5°×0.5° resolution. They rely on a configuration of the CIF-CHIMERE inversion system, following the new protocol for CO_2 regional inversions established in the frame of EYE-CLIMA (see Appendix A). The datasets used for these final inversion experiments at the 0.5°×0.5° resolution, described in the protocol, better account for various fluxes, including fluxes to the atmosphere from fires, from inland waters and from harvested wood and crops. In particular, harvest fluxes provided by ORCHIDEE now have a more realistic spatial distribution

This project has received funding from the European Union's Horizon Europe research and innovation programme under grant agreement No 101081395

(see Section 3.1.3). As boundary conditions have a strong impact on the annual NEE budgets (see D3.1), our inversions also now better consider boundary conditions.

Different CO_2 inversion results have been derived with this new inversion configuration by assimilating surface (mainly from ICOS sites) or satellite (NASA/JPL OCO-2) observations.

This section details the CIF-CHIMERE inversion configuration and the analysis of the system behaviour and of the resulting land ecosystem flux estimates. In line with the objective of these inversions, which should provide a benchmark for further developments and analysis in EYE-CLIMA, the presentation focuses on general patterns of the spatial variability of the corrections applied to the prior terrestrial ecosystem fluxes from surface and OCO-2 observations, on the seasonal cycle and on the long-term mean, trends and inter-annual variability of annual NEE budget for the European Union + UK + Switzerland + Norway (EU27+3), i.e., on the type of general diagnostics analysed in recent inter-comparisons of European scale inversions (Monteil et al., 2020, Thompson et al., 2020, McGrath et al., 2023) and in D3.1.

3.1 Inverse modelling system and experimental framework

The inversion system relies on the coupling between the variational mode of the Community Inversion Framework (CIF, Berchet et al., 2021), the regional chemistry transport model CHIMERE (Menut et al., 2013; Mailler et al., 2017) and the adjoint of this model (Fortems-Cheiney et al., 2021b).

3.1.1 Configuration of the regional CHIMERE chemistry-transport model

The inversions generally do not take the atmospheric source of CO_2 from the oxidation of CO into account, assuming this source is negligible. As the impact of this atmospheric CO source of CO_2 on the CO_2 concentrations and on the CO_2 land ecosystem fluxes estimated from the inversions is negligible (MS3), CO_2 is still considered as a passive tracer at the time scales considered in this study.

Consequently, when using the CHIMERE CTM and its adjoint code, here, only the atmospheric transport modelling components are used, and the chemistry modelling components are deactivated.

3.1.2 Land biosphere fluxes

Two products are used to derive prior or fixed estimates of the land-biosphere fluxes of CO_2:

ORCHIDEE simulation using CRUERA-v5 meteorological forcing at 0.125° resolution over Europe (35°-73°N and 25°W-45°E) and at hourly temporal resolution, providing:

- NPP and Rh at 3-hour resolution
- F_{LUC} (land use change fluxes restricted, here in practice, to emissions of carbon due to deforestation)
- Local emissions of the total amount of carbon removed (without spatial displacement in ORCHIDEE) from the local carbon stocks by wood and crop harvest: $F_{WOODHARVEST}$ and $F_{CROPHARVEST}$ at annual resolution but spread at 1-hour resolution as a constant flux over the year

GFASv1.2 estimate of net biomass burning emissions at 0.1° resolution, until year 2025:

- F_{BB} at 1-day resolution

The F_{BB} fluxes from GFAS are used as a fixed flux component in the inversions.

This project has received funding from the European Union's Horizon Europe research and innovation programme under grant agreement No 101081395

3.1.3 Land fluxes from the "lateral" export of carbon from the ecosystems (including biofuel emissions)

The estimate of land fluxes due to "lateral" export of carbon from the ecosystems are derived using the last version of the database of Ciais et al. (2021). These estimates are provided globally at 0.083°×0.083° and 1-year resolution over 1961 - 2022. The estimates for 2022 have been used to impose the values for 2023. The following selection of fluxes from this database have been used:

- ALLWOODSOURCE (emissions from wood biofuel combustion and other wood products)
- ALLCROPSOURCE (emissions from crop biofuel combustion and other crop products such as human/animal respiration)
- ALLCROPSINK (estimate of the carbon sink corresponding to the crop harvest)
- ALLWOODSINK (estimate of the carbon sink corresponding to the wood harvest)
- RIVERSINK (transfer from soils to rivers)
- LAKERIVEREMIS (inland water outgassing)

3.1.4 Prior and fixed estimates of the land fluxes

For consistency between the sinks and sources associated with these lateral transfers in the prior estimate of the fluxes, the prior estimate of the NEE from ORCHIDEE is adjusted by adding a linear scaling of the ORCHIDEE $F_{CROPHARVEST}$ and $F_{WOODHARVEST}$ fields α x ($F_{CROPHARVEST}$ or $F_{WOODHARVEST}$) with α_{crop} and α_{wood} respectively defined so that the integral of this correction over Europe and the year equals the differences between the EU27+3 and 1-year scale budget of $F_{CROPHARVEST}$ and $F_{WOODHARVEST}$ versus the ALLCROPSINK and ALLWOODSINK estimates from Ciais et al. (2021), implicitly assuming that the budget from the latter is more accurate. Of note, is that there is no sub-annual temporal resolution for the $F_{CROPHARVEST}$ and $F_{WOODHARVEST}$ fields from the ORCHIDEE simulations. Therefore, these fluxes are prescribed as constant fluxes within a year, which thus applies to the adjustment of ORCHIDEE.

The estimates of $F_{WOODSOURCE}$ (=ALLWOODSOURCE), $F_{CROPSOURCE}$ (=ALLCROPSOURCE), and $F_{LAKERIVER}$ (=LAKERIVEREMIS+RIVERSINK) are used as a fixed flux components in the inversions. The ORCHIDEE $F_{CROPHARVEST}$ and $F_{WOODHARVEST}$ from ORCHIDEE themselves, which are redundant with the ALLWOODSOURCE and ALLCROPSOURCE but which are assumed to rely on a less accurate estimate of the harvests, and which ignore the import/export of harvest across the boundaries of Europe, are discarded.

3.1.5 Fossil emissions

Anthropogenic emissions from EDGARv8 are used as recommended by WP2 (MS 2). These are provided at monthly resolution for the following sectors (the sector codes are given in parentheses): i) Energy for buildings (BUILDINGS), ii) Fuel exploitation (FUEL_EXPLOITATION), iii) Industrial combustion (IND_COMBUSTION), iv) Industrial processes (IND_PROCESSES), v) Power industry (POWER_INDUSTRY), vi) Transport (TRANSPORT) and vii) Waste (WASTE).

EDGARv8 provides separate estimates for CO_2 emissions from fossil sources (F_{CO2}) versus bio-fuel sources for the above sectors. The biofuel files include "CO2bio" in the file name and are excluded. EDGARv8 provides weekly and hourly profiles per country and source sector, which should be used to calculate hourly varying emissions.

The F_{CO2} flux from EDGARv8 are used as a fixed flux component in the inversions.

This project has received funding from the European Union's Horizon Europe research and innovation programme under grant agreement No 101081395

3.1.6 Open and coastal ocean fluxes

The estimate of sea/ocean fluxes within the inversion domain should be based on a hybrid product combining the coastal ocean flux estimates from the University of Bergen and a global ocean estimate from MPI-BGC-Jena (Rödenbeck et al., 2014; McGrath et al., 2023). The data is provided from 2005 to 2020 at a 0.125°×0.125° horizontal resolution and at daily temporal resolution. The estimates for 2020 are used to impose the values for more recent years.

This product is used as a prior estimate of the F_{OCEAN} fluxes in the inversions.

3.1.7 Prior / Fixed estimate of the boundary conditions and completion of the stratosphere

For the estimate of the prior initial, lateral and top boundary conditions, inversions use the CAMS global greenhouse gas inversion product, v22r1, available up to 2022-12.

This global inversion product is also used to complement the vertical columns of CO_2 above the top boundary of the CHIMERE CTM when comparing the model to XCO_2 satellite observations.

3.1.8 Meteorological forcing

The CHIMERE CTM is driven by European Centre for Medium-Range Weather Forecasts (ECMWF) meteorological forecasts.

3.2. Observations

3.2.1. Near-surface in-situ measurements

The inversion assimilates measurements of CO_2 mole fraction from the European Obspack compilation of atmospheric CO_2 data from ICOS and non-ICOS European ground based continuous measurement stations for the period 1972-2024 called “obspack_co2_466_GVeu_v10_20240729” (ICOS RI et al., 2024).

ICOS-labelled stations have provided CO_2 data since 2015. The database also includes measurements from non-labelled sites for the full period of inversion. However, before 2015, the data coverage is relatively sparse (Figure 3.1). Following the protocol and usual observation selection strategies (Broquet et al., 2013, Monteil et al., 2020), the inversion assimilates 1-hour averages of the measured CO_2 mole fractions during the time windows 12:00-17:00 UTC for low altitude stations (below 1000 masl) and 0:00-6:00 UTC for high altitude stations (above 1000 masl). When several levels of measurements are available at a given station, the inversions assimilate the data from the highest level only.

The stations selected for the period 2005-2023 are shown in Figure 3.1. We have excluded the urban stations HEI (Heidelberg in Germany) and GIF (Gif sur Yvette in France) and some stations which are challenging to represent with meso-scale atmospheric transport models and/or which provide data over a relatively short time over the entire period 2005-2023 (LMU, VAC, GIC, SGC and EEC in Spain) from the dataset.

This project has received funding from the European Union's Horizon Europe research and innovation programme under grant agreement No 101081395

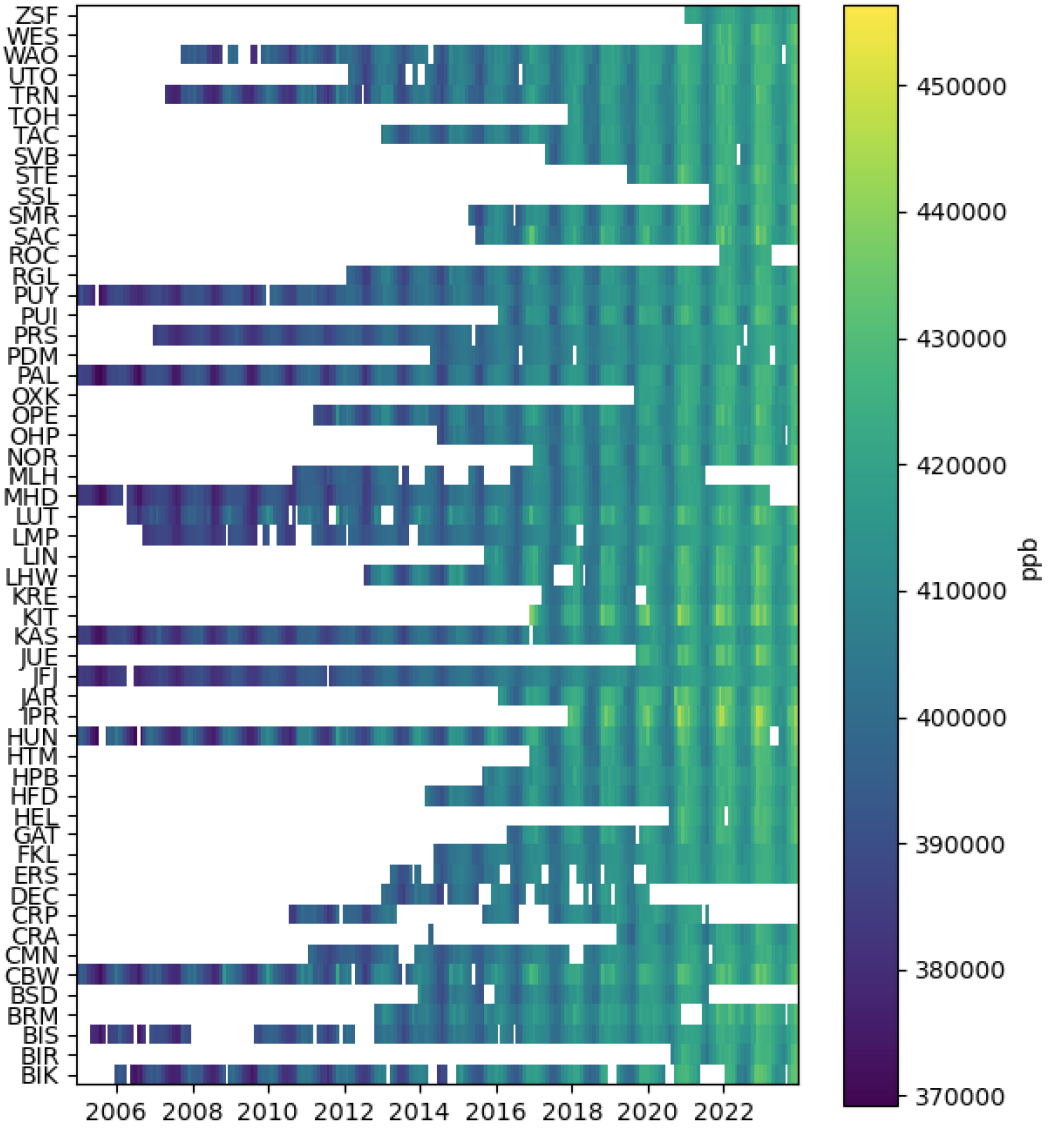

Figure 3.1: Observation temporal coverage at the different stations from 2005 to 2023: the months during which measurements are available at a given site are coloured. Blue to yellow colour scale denotes monthly averaged CO_2 mole fractions (ppb).

3.2.2. OCO-2 satellite observations

The inversion alternatively assimilates the relatively high-resolution satellite total column CO_2 mole fraction (XCO_2) observations from the OCO-2 NASA-JPL mission (the v11 dataset), launched in July 2014. The OCO-2 satellite carries high-resolution spectrometers that return high-precision measurements of reflected sunlight received within the CO_2 and O_2 bands in the short-wave infrared spectrum (Crisp et al., 2012) and flies on a 705 km sun-synchronous orbit with a 16-day (233 orbits) ground track repeat cycle. The nominal footprint of the OCO-2 ground pixels is 1.29 × 2.25 km^2 (across × along track) at nadir, with a cross-track swath width of about 10 km. We only consider "good" retrievals as identified by the XCO_2 quality flag of the product.

Although the biases in OCO-2 over the ocean acquired in glint mode have been substantially reduced since the initial version 7 (O'Dell et al., 2018), Chevallier et al. (2019) claimed that the assimilation of OCO-2 ocean observations still produced unrealistic results in their global atmospheric inversions. They

This project has received funding from the European Union's Horizon Europe research and innovation programme under grant agreement No 101081395

are, therefore, not considered in this study, as in D3.1. After this selection, all individual observations are assimilated and compared to their corresponding horizontal grid-cells in CHIMERE (i.e. to the CHIMERE CO_2 vertical column in this horizontal grid cell), defined for a given observation as that containing the centre of the ground projection of the OCO-2 pixel at the observation time: there is no aggregation of the observations at the model resolution. The average number of observations illustrates the higher coverage over Southern Europe than in Northern Europe during the whole period of observation (D3.1).

The CAMS global CO_2 inversions are used to complement the vertical columns of CO_2 above the top boundary of CHIMERE when comparing the model to XCO_2 observations. To make suitable comparisons between simulations and satellite observations, the vertical profiles of CO_2 mole fraction in the corresponding atmospheric columns of the model simulations are first interpolated on the satellite CO_2 retrieval levels (with a vertical mass-conserving interpolation on pressure levels). Then, the appropriate simulated XCO_2 values are computed using both the OCO-2 averaging kernels and prior estimates provided in the OCO-2 retrieval product. As an example, the average of the OCO-2 observations for the year 2015 is presented in Figure 3.2a while the average of the simulated XCO_2 values corresponding to these observations is presented in Figure 3.2b.

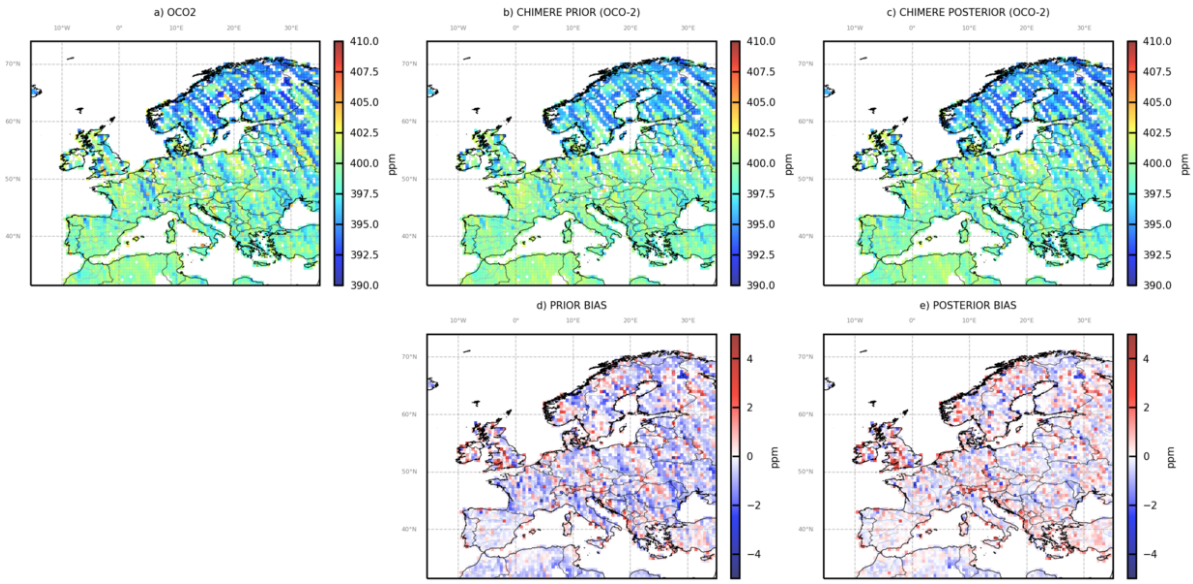

Figure 3.2: Comparison between the a) OCO-2 XCO_2 observations and b-c) the corresponding CHIMERE XCO_2 simulations in 2015; averages over the year of the XCO_2 values per grid cell of the model (observations, prior simulations, posterior simulations and bias), in ppm.

3.4. The inversion framework

The inversions of CO_2 land ecosystem fluxes consist here in correcting the "prior" estimate of the sum of the Net Ecosystem Exchange (NEE) and of the fluxes F_{LUC} of CO_2 due to the Land Use Change (LUC), being limited here to emissions from deforestation. This prior estimate is corrected to derive “posterior” estimates with an improved fit between CHIMERE and the surface measurements of CO_2 mole fractions or XCO_2 satellite observations.

Series of independent 13-month inversions have been performed to provide a posterior estimate of NEE+F_{LUC} from 2005 when using the surface measurements or from 2015 when using the satellite data. These 13-month inversions target individual years *y*, beginning on December 15th of the year *y-1* and

This project has received funding from the European Union's Horizon Europe research and innovation programme under grant agreement No 101081395

ending on January 15th of the year *y+1* (to account for the lag-time between observations and the fluxes which impacted them, and for the temporal correlations of the prior uncertainties (see below), which connects observations at a given time to fluxes few weeks before or after), and we retain their results over the period January 1st to December 31st only when combining all results into time series of flux maps.

The inversion optimizes 6-hourly mean NEE+F_{LUC} fluxes at the 0.5°×0.5° resolution of CHIMERE. The covariance matrix associated to the prior estimate of NEE+F_{LUC} (the prior uncertainty) is specified using the ORCHIDEE heterotrophic respiration for uncertainties at the control resolution, similarly to what is classically done in CO_2 inversions over Europe (Broquet et al., 2011; Monteil et al., 2020). Following the diagnostics of Kountouris et al. (2015), the temporal and spatial correlation scales for the prior uncertainty are set to ≈1 month and 200 km, with no correlation between the four 6-hour windows of the same day. The inversions also control the ocean fluxes and the initial and lateral CO_2 boundary conditions (see Table 4 of the protocol in Appendix A).

The observation error covariance matrix characterizing the transport model, CO_2 measurement and XCO_2 retrieval errors is set-up to be diagonal, ignoring the correlations between errors for different hourly averages of the CO_2 measurements (which has been justified by the analysis of Broquet et al., 2011), or between errors for different XCO_2 observations. The variance of the observation errors corresponding to individual observations correspond to the Root Sum Square of the observation error values provided in the observation products and of values assigned to characterize the transport model error (see Table 3 of the protocol in Appendix A).

About 6 iterations are needed to reduce the norm of the gradient of the cost function *J* by 85% with the M1QN3 limited-memory quasi-Newton minimisation algorithm that we use (Gilbert and Lemaréchal, 1989).

3.4.1. Experiments

The different inversions performed in this study are presented in Table 3.1. Inversions following the new protocol are labelled as “reference”. These reference inversions using surface measurements have been respectively performed for the period 2005-2023. The reference inversions using satellite observations have been conducted for the period 2015-2021. Sensitivity tests have been also performed by directly using both the NEE+FLUC and the FCROPHARVEST and FWOODHARVEST fluxes from ORCHIDEE, and ignoring the lateral flux products, as would have been done following a more traditional inversion configuration and as done in D3.1. These sensitivity tests are mainly exploited for the analysis of the NEE+FLUC annual budgets in Section 3.5.4.

Table 3.1: Description of the inversions performed in this study.

Name	**Observations**	**Period**	**NEE Prior estimate**	**Crop and wood harvest source** (fixed component)
Reference	surface	2005-2023	ORCHIDEE CRUERA-v5 adjusted by adding a linear scaling of the ORCHIDEE $F_{CROPHARVEST}$ and $F_{WOODHARVEST}$ fields to balance the difference between ORCHIDEE crop and wood harvest and the crop and wood sink from Ciais et al. (2021)	$F_{WOODSOURCE}$ and $F_{CROPSOURCE}$ from Ciais et al. (2021)

This project has received funding from the European Union's Horizon Europe research and innovation programme under grant agreement No 101081395

	OCO-2	2015-2021	ORCHIDEE CRUERA-v5 v5 adjusted by adding a linear scaling of the ORCHIDEE $F_{CROPHARVEST}$ and $F_{WOODHARVEST}$ fields to balance the difference between ORCHIDEE crop and wood harvest and the crop and wood sink from Ciais et al. (2021)	$F_{WOODSOURCE}$ and $F_{CROPSOURCE}$ from Ciais et al. (2021)
Traditional	surface	2015-2023	ORCHIDEE CRUERA-v5	$F_{WOODHARVEST}$ and $F_{CROPHARVEST}$ from ORCHIDEE CRUERA-v5
	OCO-2	2015-2021	ORCHIDEE CRUERA-v5	$F_{WOODHARVEST}$ and $F_{CROPHARVEST}$ from ORCHIDEE CRUERA-v5

3.5. Results

3.5.1. Fit to the assimilated observations

The reduction of the misfits between the simulation and the assimilated observations due to the corrections applied by the CIF-CHIMERE surface-based reference inversions to the prior estimates of the NEE+F_{LUC} and ocean fluxes and of the boundary conditions is illustrated in Table 3.2 from 2015 to 2023. When taking all the selected hourly observations of the stations into account in the year, the determinant coefficient R^2 is increased and the RMSE and the bias (from the prior to the posterior simulations) misfits between simulated versus measured CO_2 during the assimilation windows are often reduced (Table 3.2).

Table 3.2: Performance statistics of CHIMERE CTM compared to assimilated mole fraction measurements, before and after the inversions. Mean prior, posterior and relative difference (RDiff) of determinant coefficient (R^2), Root mean squared error (RMSE) and bias, considering all the selected hourly measurements, from 2015 to 2023.

Inversion	**R^2**			**RMSE (ppm)**			**Bias (ppm)**		
	prior	**post**	**rdiff**	**prior**	**post**	**rdiff**	**prior**	**post**	**rdiff**
2015	0.6	0.8	+32%	4.75	3.41	-28%	-0.49	0.13	-74%
2016	0.61	0.79	+30%	5.41	3.88	-28%	-1.08	0.22	-80%
2017	0.66	0.81	+24%	5.01	3.65	-27%	-0.79	-0.03	-96%
2018	0.63	0.8	+28%	5.46	4.02	-26%	-0.67	0.48	-29%
2019	0.62	0.79	+27%	5.21	3.80	-27%	-0.76	0.19	-75%
2020	0.62	0.79	+27%	5.32	3.94	-26%	-0.54	0.1	-99%
2021	0.62	0.79	+26%	5.53	3.99	-28%	-1.25	0.07	-94%
2022	0.46	0.69	+48%	6.68	4.95	-26%	0.27	0.09	-65%
2023	0.56	0.75	+35%	6.19	4.04	-35%	-2.9	0.1	-97%

This project has received funding from the European Union's Horizon Europe research and innovation programme under grant agreement No 101081395

In the reference inversions assimilating OCO-2 observations, the prior misfits between these observations and the prior simulation are also generally strongly decreased (Figure 3.2d). For example, the reduction of the bias between simulated versus observed CO_2 reaches about 57% in 2015 at the domain scale.

Corrections to the NEE+F_{LUC} fluxes seem to conduct to a clear improvement of the fit of simulated mole fractions to the observations. These results raise a good confidence in the posterior NEE+F_{LUC} estimates, whose main characteristics are presented in the following sections.

3.5.2. Spatial variability of the annual corrections applied to the prior terrestrial ecosystem fluxes from surface and OCO-2 observations

Figure 3.3 presents maps of the annual corrections provided by the reference inversions to the adjusted ORCHIDEE CRUERA prior estimates for NEE+F_{LUC} when assimilating surface and OCO-2 observations from 2015 to 2021. The inversions assimilating surface observations show more positive corrections over the domain than in D3.1. On the contrary, the inversions using OCO-2 satellite data as observations often present annual negative correction to the prior estimates, particularly over Eastern Europe where there are only few surface stations. There is therefore a distinct impact in certain regions of the surface or satellite observations, potentially explained by the difference of spatial and temporal coverage of the footprints on the fluxes from the two measurement datasets.

This project has received funding from the European Union's Horizon Europe research and innovation programme under grant agreement No 101081395

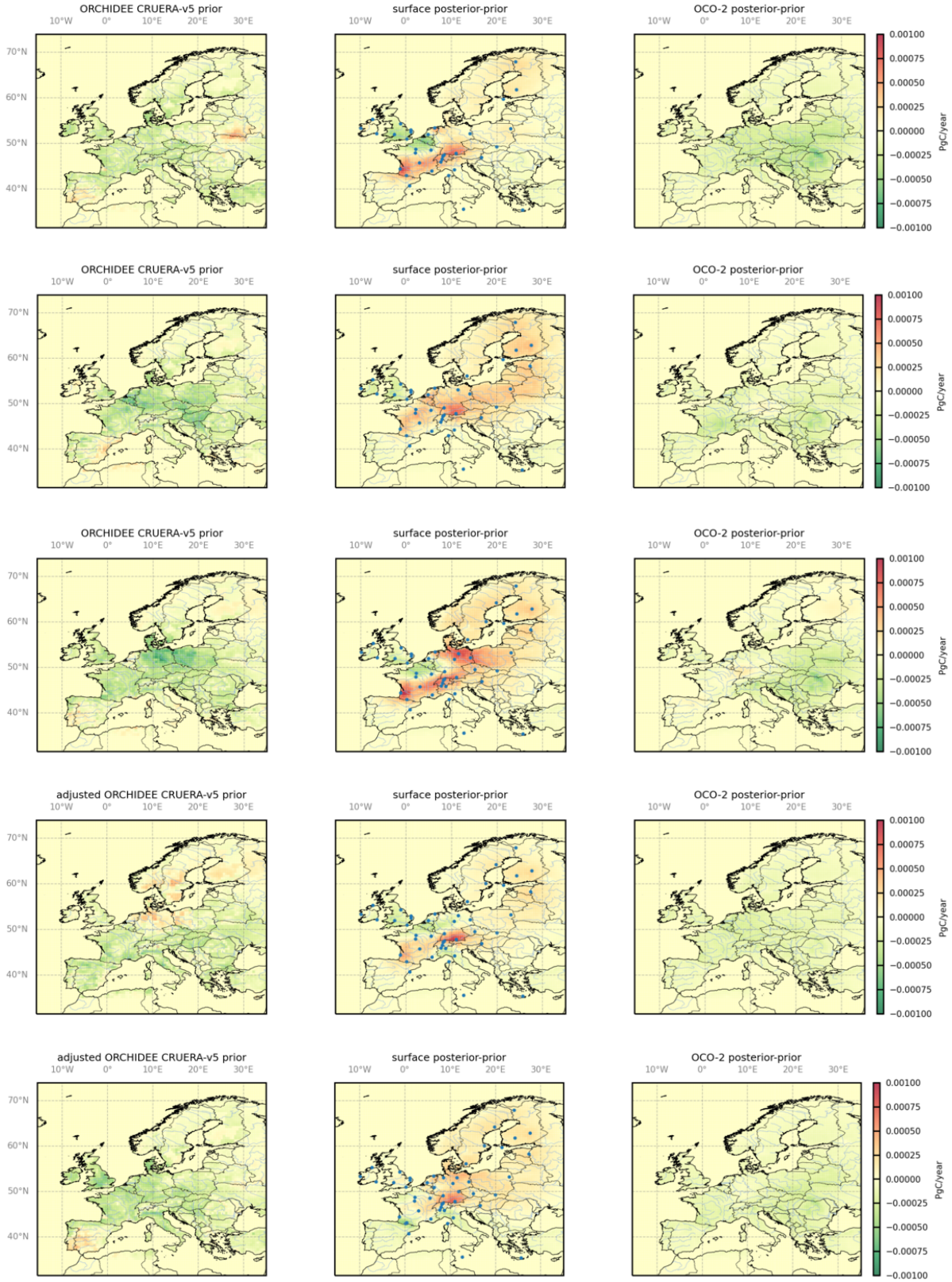

This project has received funding from the European Union's Horizon Europe research and innovation programme under grant agreement No 101081395

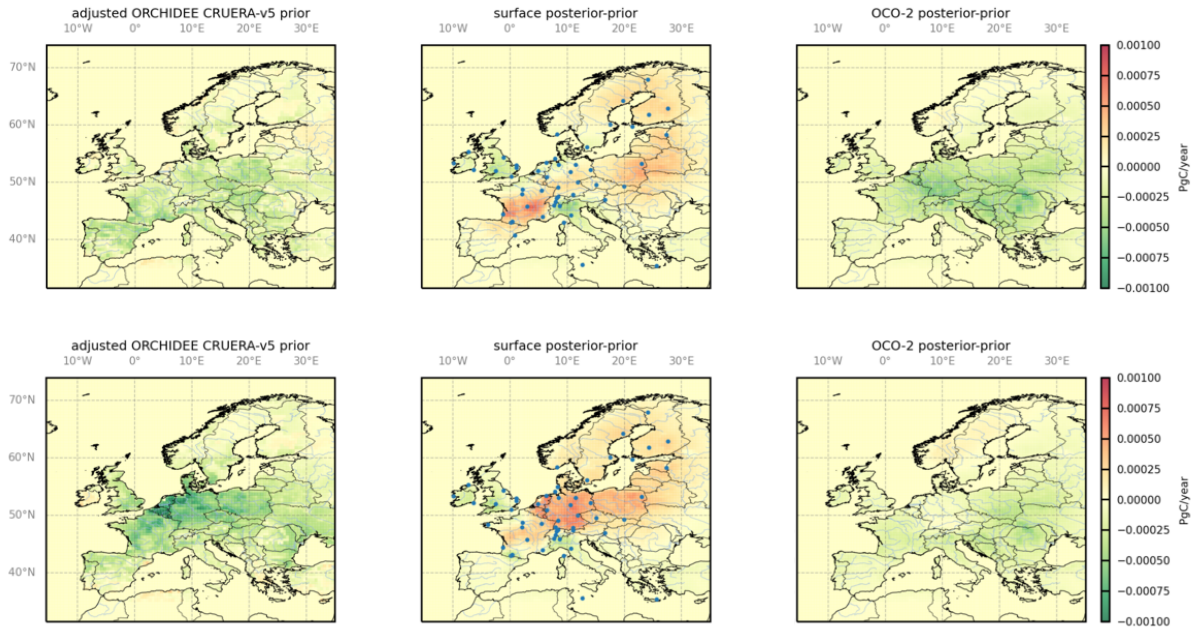

Figure 3.3: Maps of the adjusted ORCHIDEE CRUERA-v5 NEE+F_{LUC} prior estimates and of the annual corrections provided by the reference inversions to these priors when assimilating surface measurements and OCO-2 observations, in PgC/year, from 2015 to 2021.

3.5.3. Seasonal cycle of the EU27+3 NEE+F_{LUC} budget

Figure 3.4 presents a times series of monthly estimates of the CO_2 NEE+F_{LUC} from prior and posterior estimates from surface measurements and from satellite observations, from January 2015 to December 2021.

Except in 2016, the CO_2 positive maximum often occurs in October (in 2017, 2018, 2019, 2020, 2021) or in November (in 2015) in the prior estimates. It also occurs in October or in November in the posterior estimates from the surface and satellite based inversions and the inversions generally agree between them about the timing of this maximum (except in 2016). The maximum of the CO_2 peak uptake is often identified in May, both in the prior estimates and in the posterior estimates from the surface and satellite -based inversions (except in 2015 where the maximum of the CO2 peak uptake occurs in April).

The monthly NEE+F_{LUC} alternates between being a neutral flux and a positive net CO_2 source between July/August and February/March in the adjusted ORCHIDEE prior while in the posterior estimates the corresponding period can also occur between August/September and February/March from surface and OCO-2 inversions. The high positive NEE found by the adjusted ORCHIDEE at the end of the summer (~ 0.10 PgC per month in September) is at odds with the average seasonal cycles derived in Monteil et al. (2020). In our estimates from surface and OCO-2 inversions, the NEE is consistently lower than 0.10 PgC for this month.

This project has received funding from the European Union's Horizon Europe research and innovation programme under grant agreement No 101081395

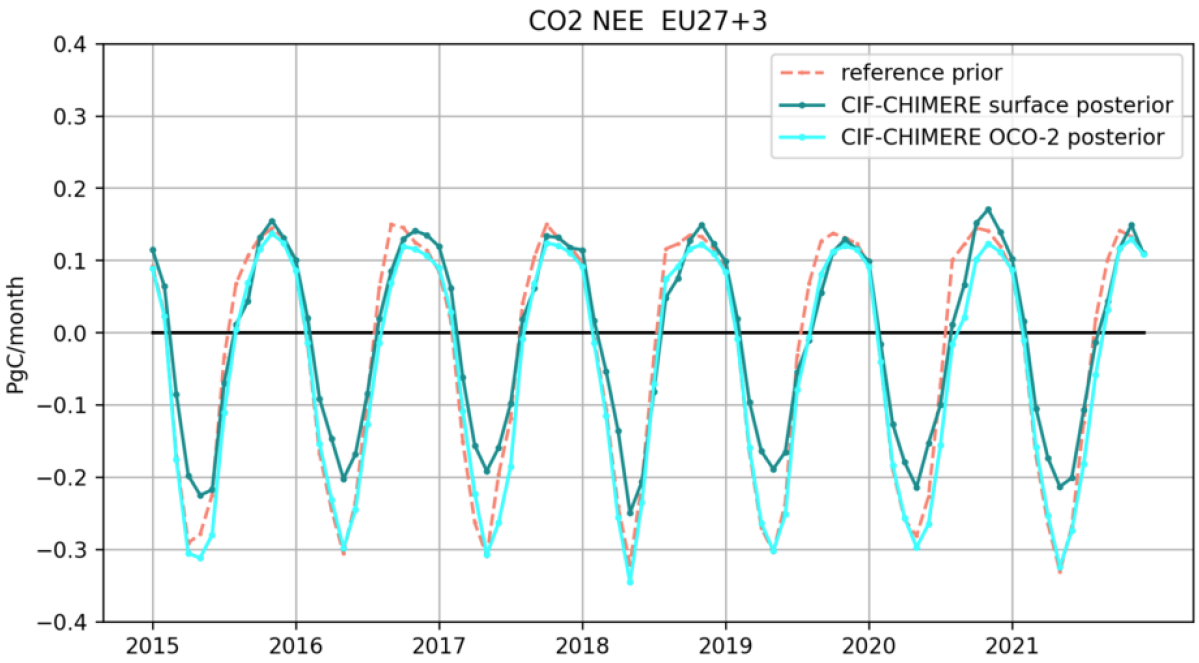

Figure 3.4: Times series of monthly estimates of the CO_2 NEE+FLUC, in PgC/month, from 2015 to 2021, for the EU-27+3 area. The dashed orange line is for the adjusted ORCHIDEE-CRUERA-v5 prior while the solid lines are for posterior estimates.

3.5.4. Long-term mean and inter-annual variability of the EU27+3 NEE+F_{LUC} budget

The reference and the traditional configuration of the inversions (see Table 3.1) show consistent inter-annual variability from 2005 to 2023 but different annual budgets. The traditional configuration indeed presents a larger CO_2 sink for the NEE estimates, both with the surface- and satellite-based inversions. Using the spatial distribution and different amplitude of the harvest source fluxes from Ciais et al. (2021) tends to lead to more positive corrections than when using the ones from ORCHIDEE. This be explained by the shift of this source further from the measurements to more localized areas when considering the actual location of the harvest consumption with the product by Ciais et al. (2021) than when emitting it where the harvest occurs as in ORCHIDEE. A consequence of such a fit is larger sinks of CO2 in the vicinity of the observations, which tends to drive the inversions towards more positive corrections.

The posterior estimates of the NEE+F_{LUC} average annual budget for EU27+3 over the period 2005-2023 from the surface-based reference inversions is of about -0.35 PgC.yr^{-1} compared to the prior estimates of about -0.52 PgC.yr^{-1}. As already seen in Figure 3.3, the satellite-based inversions produce higher sinks at the scale EU-27+3. The posterior estimates of the NEE+F_{LUC} average annual budget over the period 2015-2021 is about –0.34 PgC.yr^{-1} from the surface-based inversions and about –0.84 PgC.yr^{-1} from the satellite-based inversions (compared to the prior of about -0.55 PgC.yr^{-1}), which is 145% larger than the surface-based ones. The sinks are the weakest in 2022 with the reference surface-based inversions (Figure 3.5). With the satellite-based inversions, the sinks are the weakest in 2018. Europe experienced extensive heatwave and drought in 2018 (Thompson et al., 2020), and in 2022.

By construction, the raw inversion results from recent studies such as Monteil et al., 2020; Chevallier, 2021; Petrescu et al., 2021; Munassar et al., 2022; and McGrath et al., 2023 tend to correspond Net Biome Production fluxes, since the corresponding inverse modelling frameworks do not explicitly account for the sources from the crop and wood harvested products as a separate component of the land fluxes. A comparison between the inversions conducted here and such inversions, requires the derivation of total land fluxes, excluding the fossil fuel emissions, i.e. adding the balance between the sources and sinks associated to river lateral export of carbon and the harvest source terms.

This project has received funding from the European Union's Horizon Europe research and innovation programme under grant agreement No 101081395

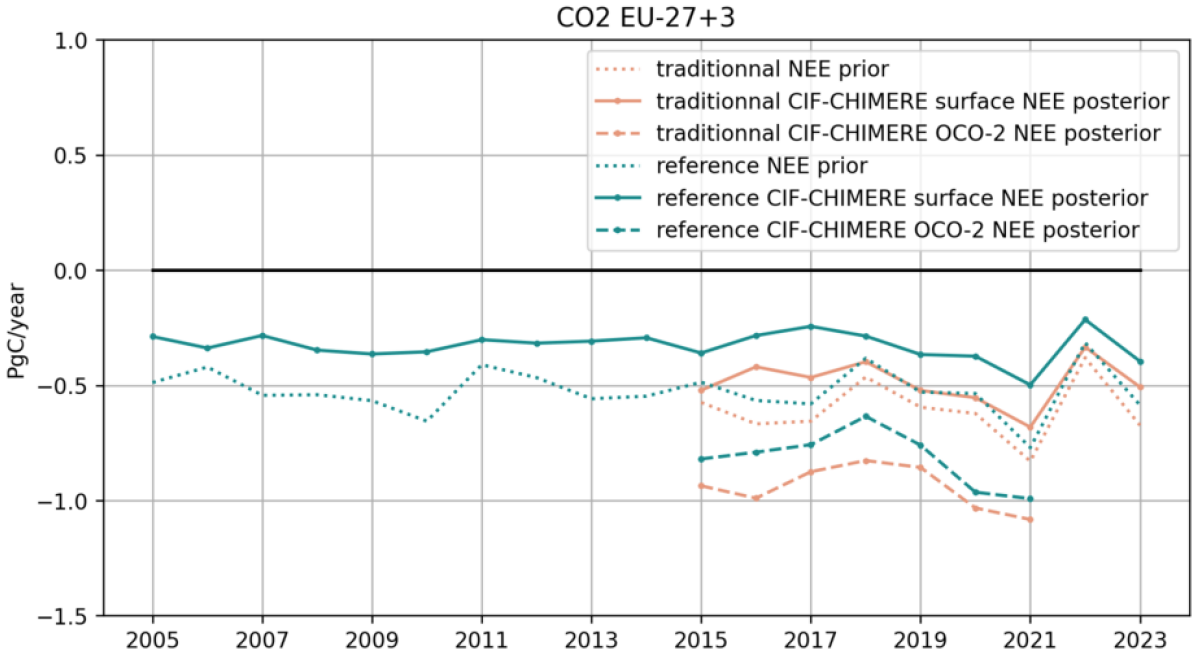

Figure 3.5: Figure 3.5: Times series of annual prior estimates of the CO_2 NEE+F_{LUC} and posterior estimates from the reference and traditional surface- and satellite-based inversions, in PgC/year, from January 2005 to December 2023 for the EU27+3 area.

This project has received funding from the European Union's Horizon Europe research and innovation programme under grant agreement No 101081395

4. CH_4 inversions

This section describes the CIF-FLEXPART CH_4 inversion configuration for Europe, spanning 11°W to 35°E and 34°N to 72°N, at a spatial resolution of 0.5°×0.5°, covering the period 2005 – 2023. The inversion employs a 4D-Var framework to optimize CH_4 flux estimates from different sectors at the grid cell level. Source–receptor relationships are quantified using the FLEXPART Lagrangian particle dispersion model, which provides the sensitivity matrix required for the inversion.

4.1 Inversion framework and transport model

To optimize CH_4 emissions over Europe, we employed the Community Inversion Framework (CIF) together with the Lagrangian particle dispersion model FLEXPART v10.4, hereafter referred to as CIF-FLEXPART. The inversion was performed at a base resolution of 0.5°×0.5° using atmospheric CH_4 mole fraction data from ground-based observation networks, covering the period 2005 – 2023.

All FLEXPART runs were driven by hourly ECMWF ERA5 meteorological data at 0.5°×0.5° resolution, including wind velocity, temperature, and boundary layer height, which are critical for accurate particle transport. For each observation, a 10-day backward simulation was performed to produce SRRs, which were stored at 0.5°×0.5° resolution over the European nested domain and 2°×2° resolution for the global domain, at hourly intervals. To account for the long atmospheric lifetime of CH_4, background mixing ratios were determined by coupling the endpoints of particle trajectories to 3D initial fields from a global model (Thompson and Stohl, 2014).

We applied grid-cell-wise optimization, maintaining the native 0.5°×0.5° resolution for all grid cells. This approach preserves the full spatial detail of emissions at 0.5°×0.5° and avoids potential aggregation-induced errors.

4.2. Prior fluxes

The prior CH_4 emission estimates were categorized into 8 sectors: i) Fugitives from fossil fuels (FFF), ii) Combustion (COM), iii) Agriculture and waste (AGW), iv) Wetlands, freshwater, and soil sinks (WET), v) Biomass burning (BBR), vi) Geological (GEO), vii) Termites (TER), and viii) Ocean (OCE). Figure 4.1 displays the spatial distribution of these fluxes over the inversion domain. All sectors were independently optimized using predefined prior uncertainties as summarized in Table 4.1, except for termite and ocean fluxes, which were kept fixed during the inversion.

For anthropogenic emissions, monthly prior fluxes were obtained from the GAINS v2 inventory for EU27+3 countries (Deliverable D2.8) and from EDGAR2024 for the rest of the world (hereafter GAINS–EDGAR). Both GAINS and EDGAR provide data at a spatial resolution of 0.1° × 0.1° and monthly temporal resolution. Within GAINS v2, the subcategories include:

- *Fugitives (FFF): fugitive emissions from fossil fuels (D_Fugitives),*
- *Combustion (COM): emissions from public power (A_PublicPower), industry (B_Industry), other stationary combustion (C_OtherStationaryComb), and road transport (F_RoadTransport),*
- *Agriculture and waste (AGW): emissions from waste (J_Waste), livestock (K_AgriLivestock), and other agricultural activities (L_AgriOther).*

Biomass burning (BBR) emissions were taken from GFAS, covering emissions from open biomass burning. For wetland and soil fluxes, prior estimates within the European domain were derived from the

This project has received funding from the European Union's Horizon Europe research and innovation programme under grant agreement No 101081395

JSBACH–HIMMELI ecosystem model (Deliverable D2.4). This model framework combines JSBACH land-ecosystem model with HIMMELI wetland model to simulate peatland, inundated soil, and mineral soil fluxes, and provides wetland and soil CH_4 fluxes at a spatial resolution of 0.125°×0.125° and daily temporal resolution. Additionally, freshwater fluxes were included following Johnson et al. (2022) for lakes and Rocher-Ros et al. (2023) for rivers, with global lake totals scaled to 13 Tg yr^{-1}, consistent with the lower-limit estimate of the Global Methane Budget (Saunois et al., 2024). The freshwater fluxes were originally at a spatial resolution of 0.25°×0.25° and temporal resolutions of daily (lakes) and monthly (rivers). Geological fluxes (GEO) were taken from Etiope et al. (2019), representing onshore geological sources, and scaled globally to 15 Tg yr^{-1} following Saunois et al. (2024). Ocean emissions (OCE) were based on the climatological dataset of Weber et al. (2019), which accounts for both diffusive and ebullitive fluxes. Finally, termite emissions (TER) were prescribed from Castaldi (2013) and Saunois et al. (2024). As with the ocean fluxes, termite emissions were not optimized in the inversion but retained as fixed prior contributions. Geological, ocean and termite emissions were originally at a spatial resolution of 1°×1° and monthly temporal resolution. All data are re-gridded to 0.5°×0.5° and monthly resolution for the inversions.

Table 4.1. Prior CH_4 flux categories, source sectors, and inversion settings (optimization resolution, uncertainties, and correlations). TER and OCE are prescribed but not optimized. CH_4 estimates represent mean values for the sample year 2021.

Category abbreviations	**Source Sectors**	**Optimization resolutions**		**Uncertainties**	**Correlations**	
		Spatial	Temporal		Spatial	Temporal
FFF	Fugitives from fossil fuels	0.5° × 0.5°	Monthly	15%	100 km	1M
COM	Combustion	0.5° × 0.5°	Monthly	51%	100 km	3M
AGW	Agriculture and waste	0.5° × 0.5°	Monthly	80%	100 km	3M
WET	Wetlands, soil sinks and freshwater	0.5° × 0.5°	Monthly	100%	100 km	1M
BBR	Biomass burning	0.5° × 0.5°	Monthly	50%	50 km	1M
GEO	Geological	0.5° × 0.5°	Monthly	100%	300 km	6M
TER	Termites	N/A	N/A	N/A	N/A	N/A
OCE	Ocean	N/A	N/A	N/A	N/A	N/A

This project has received funding from the European Union's Horizon Europe research and innovation programme under grant agreement No 101081395

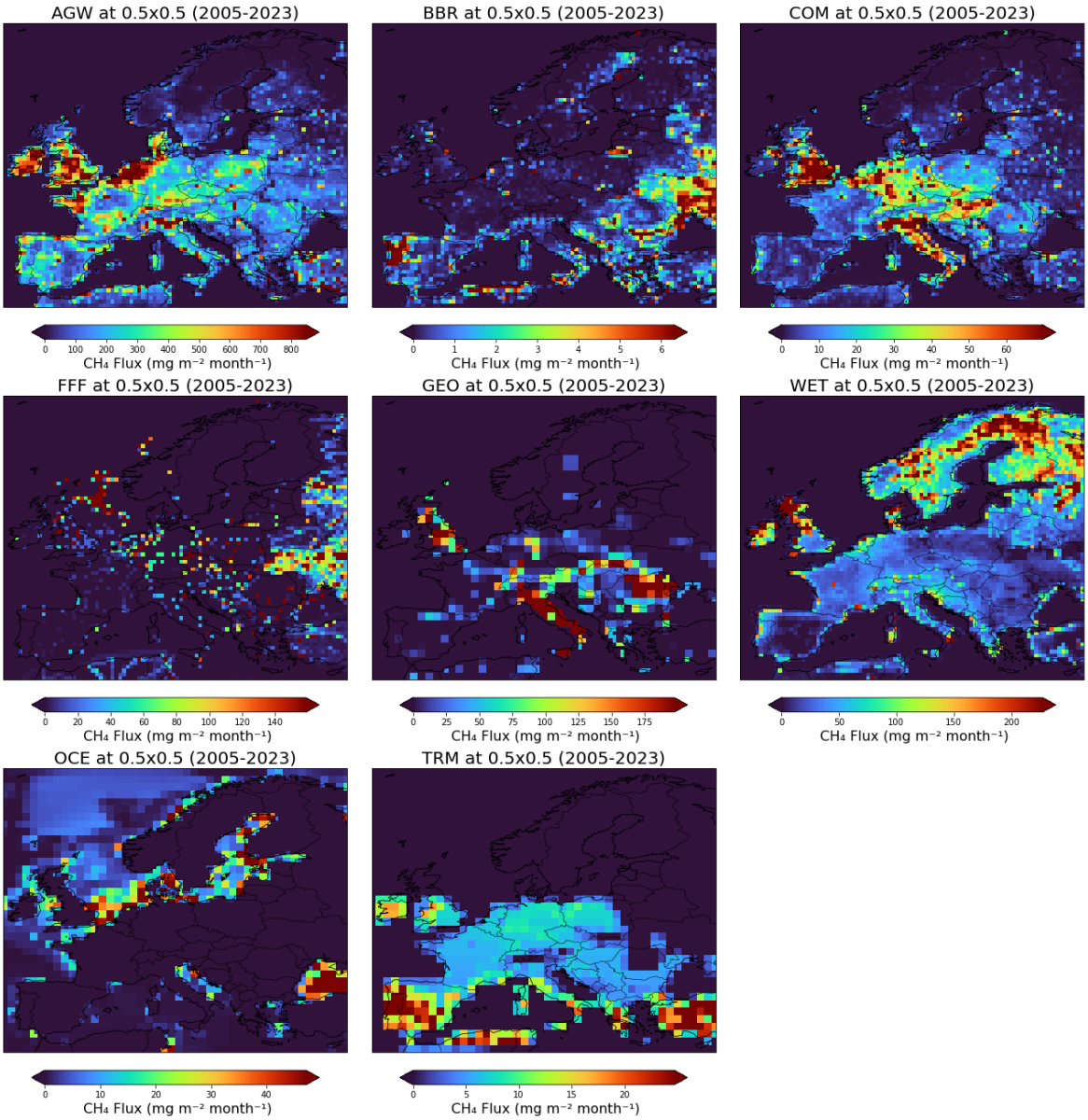

Figure 4.1: Prior methane emissions by source averaged in the years (2005-2023) at a spatial resolution of 0.5°×0.5°. Note that the colour scales of the maps vary.

This project has received funding from the European Union's Horizon Europe research and innovation programme under grant agreement No 101081395

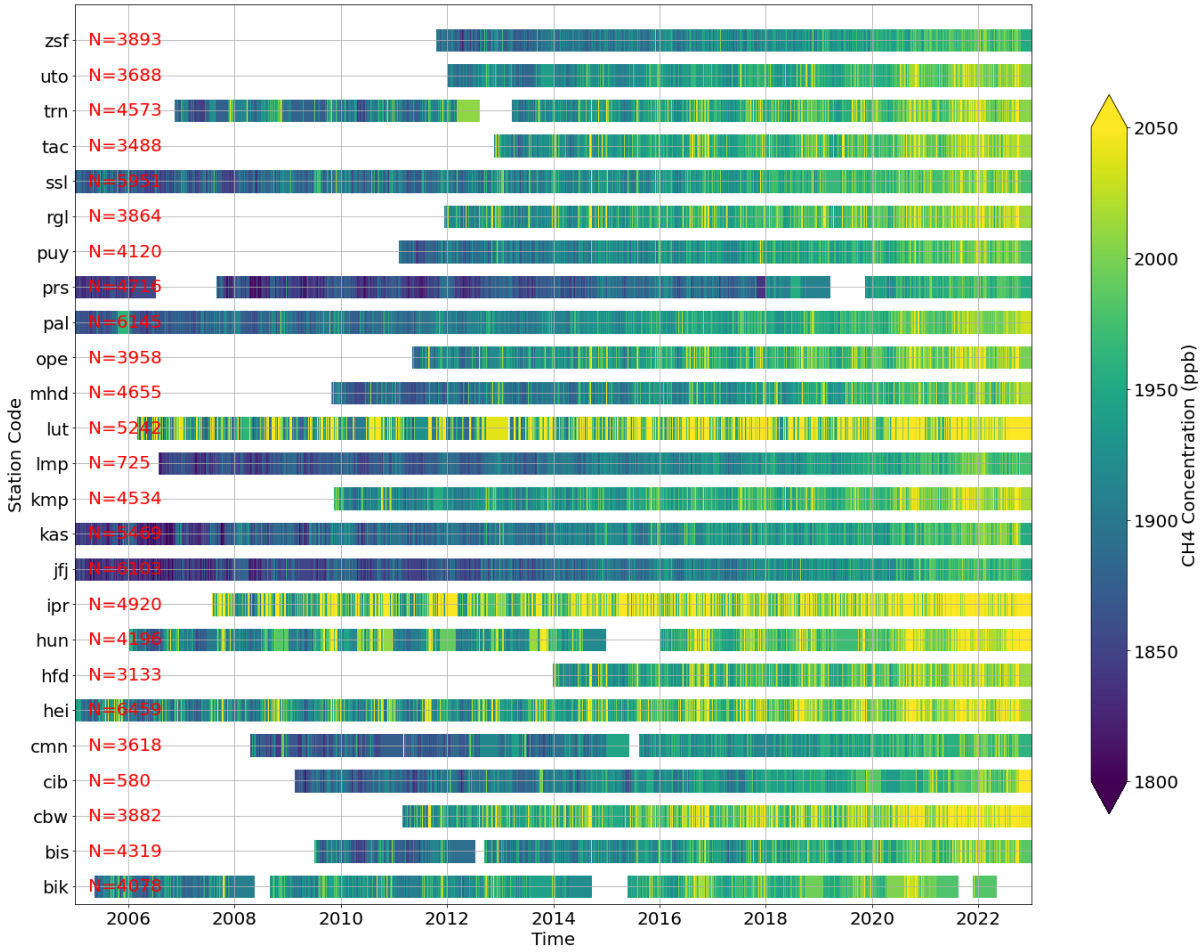

Figure 4.2: Overview of daily mean observed mole fractions (ppb) from 2005 to 2023. White gaps indicate periods with no data available. Each station is indicated by its 3-letter code on the y-axis. The red text indicates the total number of daily mean observations for each station over the full study period.

4.3. Observations

The Integrated Carbon Observation System (ICOS) offers a European compilation of atmospheric CH_4 mole fraction time series data. For the inversions, we used the data from ICOS ObsPack v10 (ICOS RI et al, 2024) and ICOS ATC OBSPACK-Europe-L2-2022 (Apadula et al., 2022). The sites which have more than 50% of data coverage during the study period are selected. In addition, the sites too close to each other are limited as those would not provide additional information about the fluxes. The sites which did not meet those criteria will be later used for validation. These datasets include both quality-controlled ICOS-labelled and non-labelled datasets. For data density and ICOS labelling see Figure 4.2. In addition to the ICOS data, pre-ICOS continuous hourly observations at Ochsenkopf, Germany (OXK) are taken from the VERIFY project (Thompson et al., 2021). The discrete observations at Centro de Investigacion de la Baja Atmosfera, Spain (CIB) are taken from the NOAA ObsPack GLOBALVIEWplusv7.0 (Schuldt et al., 2024) and continuous hourly observations from Kumpula, Finland (KMP) from the Finnish Meteorological Institute (FMI). The CIB data has approximately weekly resolution. The KMP data taken using similar measurement and calibration methods as other FMI stations, which are part of ICOS. The site geographical distribution across Europe is depicted in Figure 4.3. In cases where multiple intake heights were available, such as at the Cabauw station with intake heights at 27, 67, 127, and 207 meters above ground level, we opted to assimilate data solely from the highest intake height. This approach

This project has received funding from the European Union's Horizon Europe research and innovation programme under grant agreement No 101081395

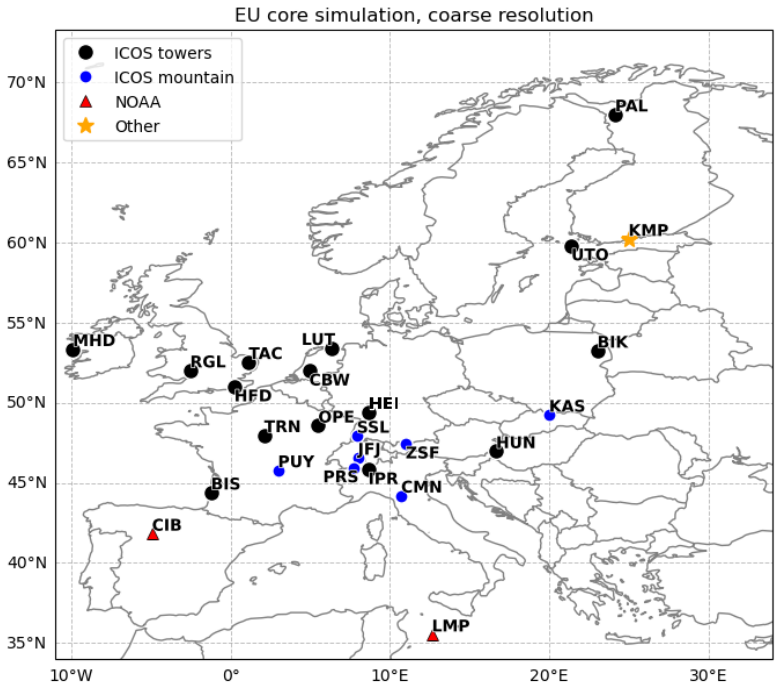

Figure 4.3: Geographic distribution of sites used in data assimilation. Blue dots refer to mountain stations above (1000 masl) while black dots are low altitude stations.

was taken to ensure that the assimilated data represent well-mixed conditions and not just very local influences. We assimilate hourly observations between 14:00 - 16:00 local time. for low altitude stations (<= 1000 m.a.s.l) and between 02:00 - 04:00 local time for high-altitude stations (> 1000 m.a.s.l).

4.4 Results

4.4.1 Comparison of Modelled and observed CH_4 mixing ratio

Figure 4.4 presents representative time series of CH_4 concentrations from six assimilated observation sites: Cabauw (CBW, Netherlands), Centro de Investigación de la Baja Atmósfera (CIB, Spain), Ispra (IPR, Italy), Mace Head (MHD, Ireland), Pallas (PAL, Finland), and Zugspitze (ZSF, Germany). The observed time series from ObsPack are shown together with prior and posterior simulations from the CIF-FLEXPART inversion covering the period 2005–2023. Across all stations, a positive long-term trend in CH_4 is evident, consistent with the global increase in atmospheric methane. Seasonal variability is also observed, with enhanced wintertime concentrations and lower summertime values.

The posterior estimates demonstrate a substantial improvement in reproducing the observed variability compared to the prior. Posterior simulations more closely follow the measured time series, better capturing both background concentrations and episodic enhancements linked to regional-scale emissions. At Cabauw, for instance, RMSE decreased from 60.05 ppb in the prior to 28.15 ppb in the posterior, while bias was reduced from –39.05 ppb to –7.97 ppb. Similar improvements are evident at other stations, particularly at Ispra and Cabauw, where prior simulations exhibited systematic underestimation of observed concentrations. At background and high-altitude sites such as Pallas and Zugspitze, posterior adjustments are smaller, reflecting their role in constraining large-scale background concentrations rather than local emission signals.

This project has received funding from the European Union's Horizon Europe research and innovation programme under grant agreement No 101081395

Figure 4.5 provides a network-wide statistical evaluation of model performance. Three metrics are shown: (a) bias, (b) RMSE, and (c) correlation coefficient. Posterior bias is consistently reduced across nearly all sites, with the largest correction at Ispra, where the strong negative prior bias (> –60 ppb) is substantially corrected. Across the observational network, posterior estimates show substantial improvements relative to the prior. RMSE values decreased systematically, dropping from 36.14 to 23.69 ppb, with reductions exceeding 25% at several stations. Posterior correlations with observations also increased markedly, from 0.835 to 0.916, frequently exceeding 0.85 at individual sites, reflecting a much stronger ability of the posterior modelled mole fractions to capture temporal variability. Bias is substantially reduced, from −10.18 ppb in the prior to −2.48 ppb in the posterior, further demonstrating the improved agreement with observations.

Overall, these results confirm that the CIF-FLEXPART inversion systematically reduces mismatches between model and observations by lowering bias and RMSE while increasing correlation with measured data. This is a necessary condition for the inversion framework to constrain regional methane emissions.

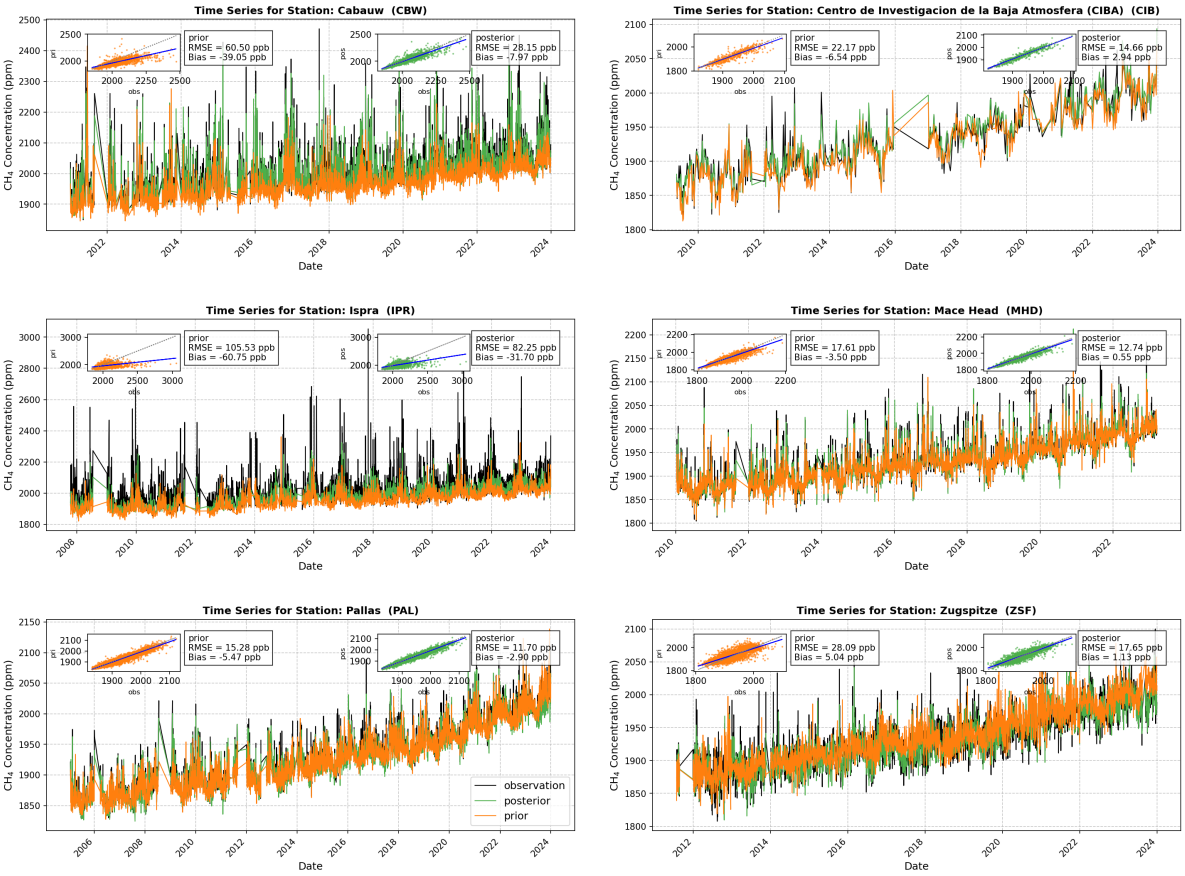

Figure 4.4: Time series of CH_4 mole fractions sampled at six assimilated stations. Observations from ObsPack (black) are compared with CIF-FLEXPART inversion results for posterior mole fractions (green) and prior mole fractions (orange).

This project has received funding from the European Union's Horizon Europe research and innovation programme under grant agreement No 101081395

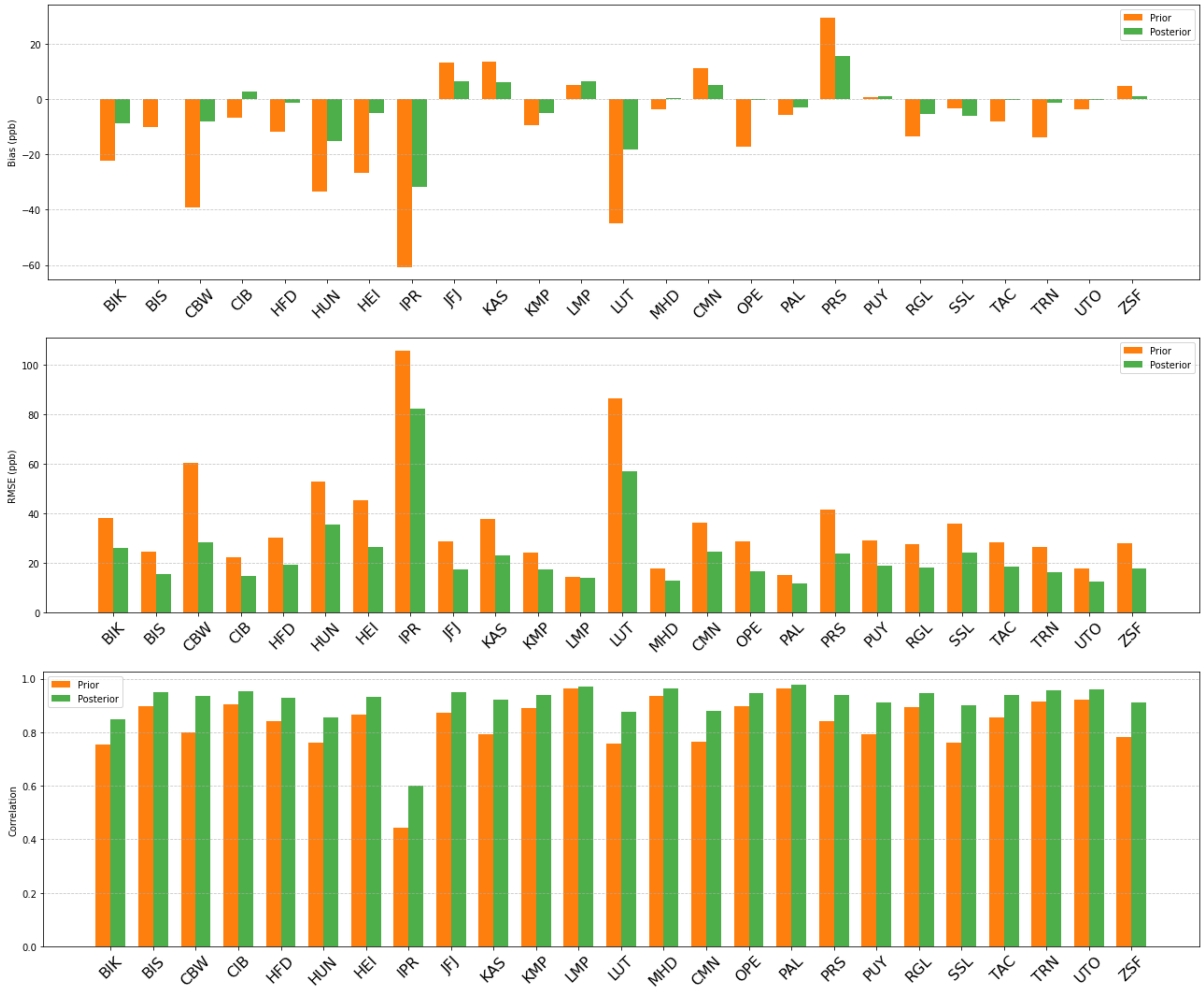

Figure 4.5: Overview of statistical results for assimilated observed mole fractions and CIF-FLEXPART posterior and prior simulated mole fractions from all stations used in the inversion.

4.4.2 Spatial distribution of prior and posterior fluxes

Figure 4.6 presents the spatial distribution of mean methane (CH_4) emissions across Europe over the period 2005 – 2023 derived from the CIF-FLEXPART inversion system at the spatial resolution of 0.5°×0.5°. The figure is divided into three panels: the left panel shows the prior emission estimates, the middle panel displays the posterior estimates, and the right panel illustrates the posterior increment, defined as the difference between posterior and prior emissions. The posterior estimates indicate a modest overall increase relative to the prior, with total emissions ~2.2% larger over the whole domain for 2005–2023 (32.078 to 32.772 Tg yr^{-1}). However, a closer look at the sectoral and spatial breakdowns reveals substantial regional redistributions that underlie this seemingly small net change.

Agriculture & Waste (AGW) shows the largest increase, rising from 20.026 to 21.455 Tg yr^{-1} (~7.1%). This growth is driven by localized increases in western Europe, including Germany, France, and the Benelux region, while decreases occur in the UK, Poland, and Italy. The combination of rises and declines across different regions explains why the overall domain-average change remains modest.

Biomass Burning (BBR) exhibits minimal adjustments, with emissions essentially unchanged at 0.106 Tg yr^{-1} (−0.04%). Small reductions in Eastern Europe and Spain are balanced by minor increases in France and Germany, resulting in negligible impact on the domain mean.

This project has received funding from the European Union's Horizon Europe research and innovation programme under grant agreement No 101081395

Combustion (COM) increases from 1.306 to 1.357 Tg yr^{-1} (~3.9%), with corrections concentrated in central Europe. In particular, there are increases in Germany and Hungary and decreases in northern Italy and southern Poland, reflecting a spatial redistribution across central Europe rather than a net amplification of emissions.

Fossil Fuel Fugitive (FFF) decreases slightly from 3.292 to 3.198 Tg yr^{-1} (−2.9%), with spatially heterogeneous adjustments: reductions dominate in northern and eastern regions, partially offset by localized increases in western Europe and the Balkans.

The **Geological (GEO)** sector undergoes the largest relative correction, declining from 2.933 to 2.354 Tg yr^{-1} (−19.7%). Posterior decreases are observed in Italy and the UK, whereas increases are seen over central Europe resulting in little net change at the domain level.

Wetlands (WET) show a moderate decrease from 4.414 to 4.303 Tg yr^{-1} (−2.5%), primarily driven by systematic reductions across Scandinavia, partially offset by smaller increases in western, southern and eastern Europe.

Overall, while the total domain-average change is modest (~2.2%), due to pronounced regional and sectoral counterbalancing. Agricultural emissions rise in western and central Europe, wetland emissions decrease in northern regions, and fossil and geological fluxes undergo localized redistributions. Collectively, the posterior highlights a spatial reallocation of emissions rather than a uniform increase or decrease across Europe.

This project has received funding from the European Union's Horizon Europe research and innovation programme under grant agreement No 101081395

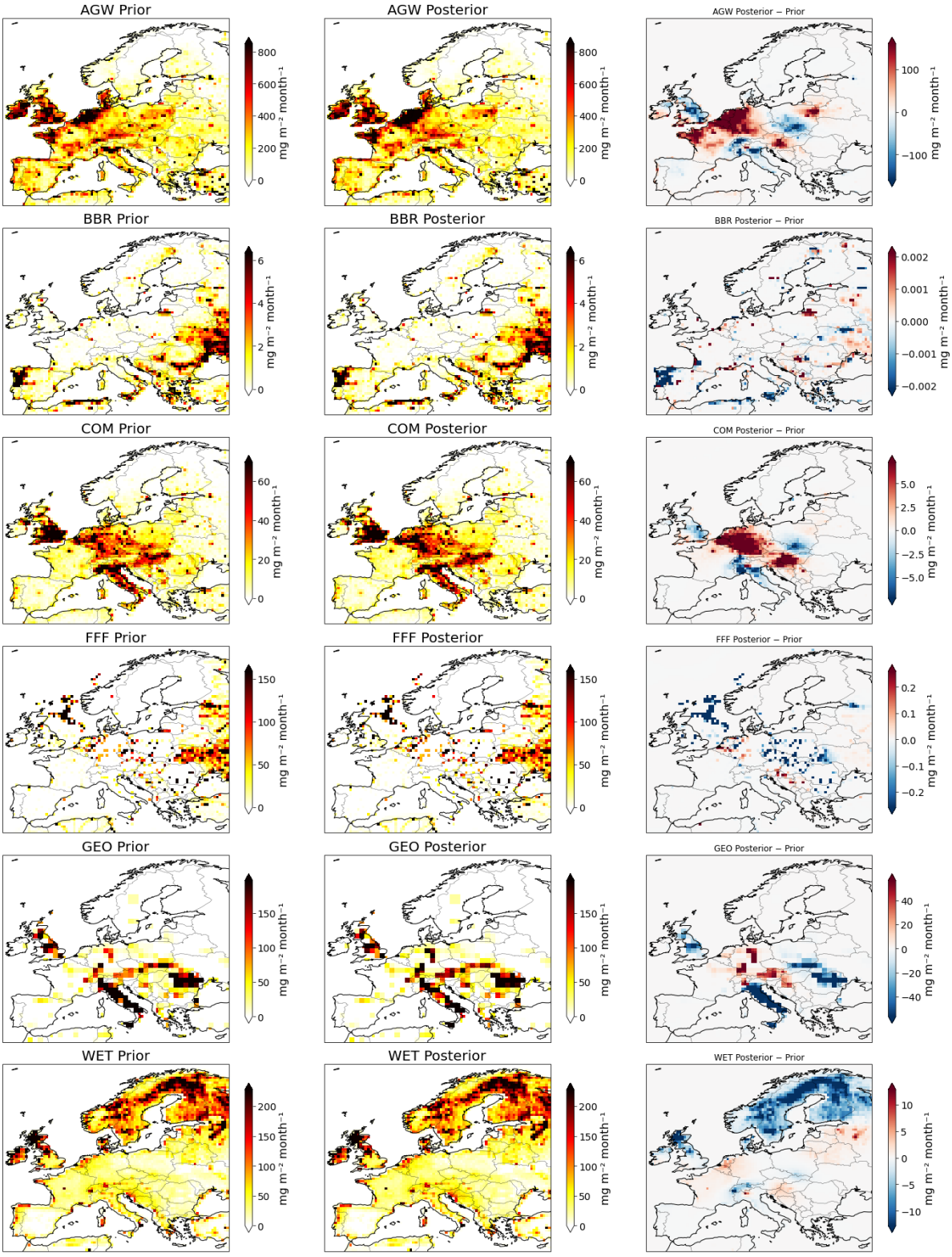

Figure 4.6: Mean spatial distribution of CH_4 fluxes from the CIF-FLEXPART inversion (2005–2023) at 0.5° × 0.5° resolution for six sectors. Shown are prior (left), posterior (middle), and posterior–prior increments (right).

This project has received funding from the European Union's Horizon Europe research and innovation programme under grant agreement No 101081395

4.4.3 Annual and monthly emission estimates

Figure 4.7 presents the time series of total and sectoral methane emissions integrated over EU27+3 covering the years 2005 – 2023. The total CH_4 source exhibits a pronounced seasonal cycle, with summer maxima driven by wetlands and agricultural sources and a small secondary winter maxima driven by combustion sources. The posterior agricultural emissions are generally higher than the prior estimates, while the posterior geological emissions are generally lower than the prior except between 2015 – 2018 and 2022 - 2023. The posterior mean over EU27+UK is 22.8 Tg yr^{-1}, slightly above the prior estimate of 22.3 Tg yr^{-1}, and is close to the range reported by Petrescu et al., 2019, who gives total CH_4 emissions of 23 Tg yr^{-1} (GOSAT) and 24 Tg yr^{-1} (SURF) for the common period 2010–2016 for EU27+UK.

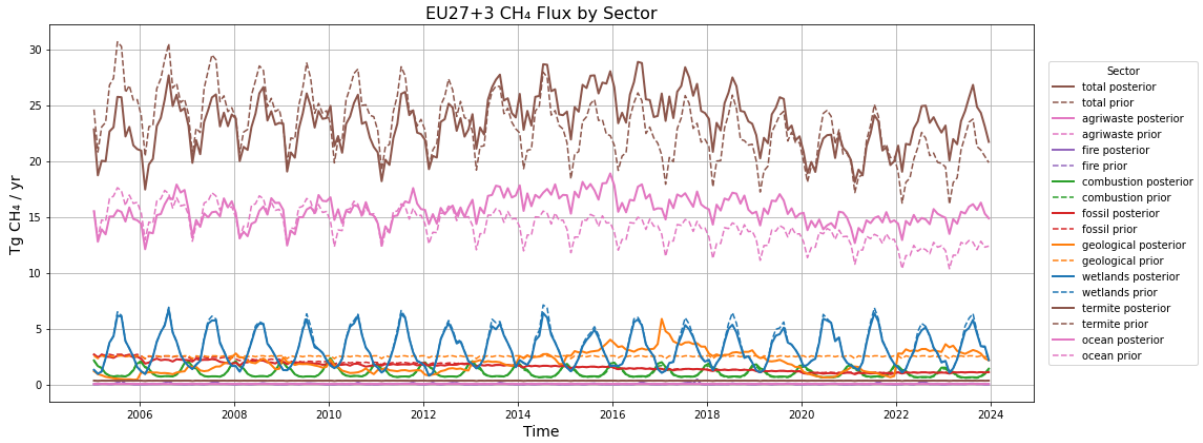

Figure 4.7: Time series of monthly CH_4 emissions for EU27+3 countries showing total and sectoral contributions for the period 2005-2023. Posterior fluxes are shown as solid lines and prior fluxes as dashed lines.

This project has received funding from the European Union's Horizon Europe research and innovation programme under grant agreement No 101081395

5. N_2O inversions

This section describes the CIF-FLEXPART configuration for long-term N_2O inversions over Europe.

5.1 Inversion framework and transport model

To quantify long-term N_2O emissions over Europe, we used the Community Inversion Framework (CIF) in combination with the Lagrangian particle dispersion model FLEXPART v11, collectively referred to as CIF-FLEXPART. The inversion was conducted at a base resolution of 0.5° × 0.5° using atmospheric mole fraction data from ground-based observation networks and covered the period 2005–2023.

Source-Receptor-Relationships (SRRs) were computed at two spatial scales:

- Global domain: 2° × 2° resolution
- European nested domain: 0.5° × 0.5° resolution

All FLEXPART runs were driven by hourly ECMWF ERA5 meteorological data at a resolution of 0.5° × 0.5°. The meteorological variables include wind velocity, temperature, and boundary layer height, which are critical for accurate particle transport simulation.

A 50% relative uncertainty was assigned to the prior N_2O fluxes. A temporal correlation of 90 days is defined. The spatial correlation lengths were defined to according to the heterogeneity of surface fluxes as below:

- Land domains: 200 km
- Ocean domains: 1000 km

Using spatial correlations reduces the degrees of freedom in the inversion and helps further regularize the problem and is particularly important when the observational constraint is weak. This helps to avoid spurious results when two or more grid cells cannot be independently determined based on the available observations.

A variable-resolution inversion grid was implemented to optimize computational efficiency while maintaining fidelity in regions with a strong observational constraint. As illustrated in Figure 5.1, the grid resolution varies depending on the total sensitivity (i.e., the sum of SRRs) of a region:

- High-sensitivity areas: Retain native resolution of 0.5° × 0.5°
- Moderate-sensitivity areas: Aggregated to 1° × 1°
- Low-sensitivity areas: Aggregated to 2° × 2°

This approach effectively reduces the dimension of the inversion problem, thereby lowering memory and computational demands, while avoiding significant aggregation-induced errors in flux estimates.

This project has received funding from the European Union's Horizon Europe research and innovation programme under grant agreement No 101081395

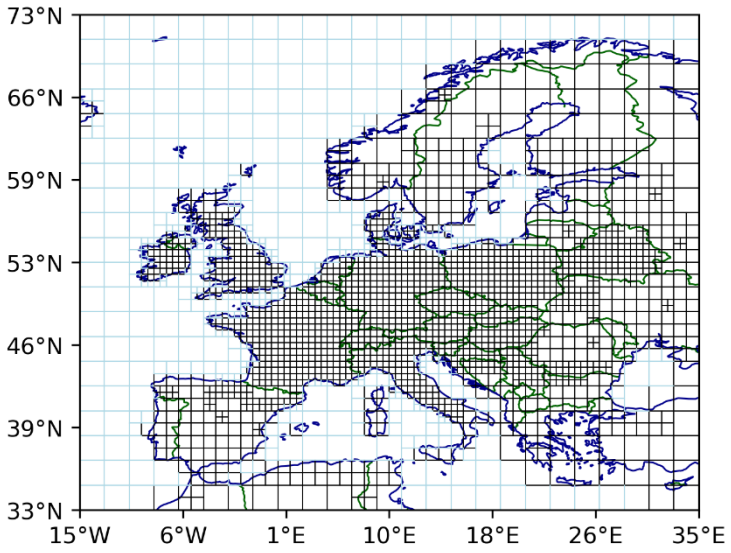

Figure 5.1: Variable-resolution grid used in the inversion

5.1 Prior Fluxes

To generate comprehensive prior estimates of N_2O emissions, we incorporate monthly gridded flux data from the following sources:

- Agricultural emissions: Based on the GAINS model (provided by WP2) for EU27+3 (EU27, United Kingdom, Norway, and Switzerland), including direct emissions from N-fertilizer and manure use and indirect emissions.
- Other anthropogenic emissions: Also from GAINS, covering transport, industrial activities, and waste.
- Biomass burning: Monthly data derived from GFEDv4.1 (Randerson et al., 2017), excluding agricultural waste burning, which is already captured under agriculture.
- Natural soil emissions: From the O-CN land surface model representing unmanaged soils.
- Ocean fluxes: Derived from climatological estimates of the PlankTOM ocean biogeochemistry model.

The spatial distribution of these prior flux components is shown in Figure 5.2. Each panel depicts the magnitude and spatial distribution of N_2O emissions from each source category. It is important to note that while the inversion uses these disaggregated source estimates as prior input, it optimizes only the total emissions in each grid cell.

This project has received funding from the European Union's Horizon Europe research and innovation programme under grant agreement No 101081395

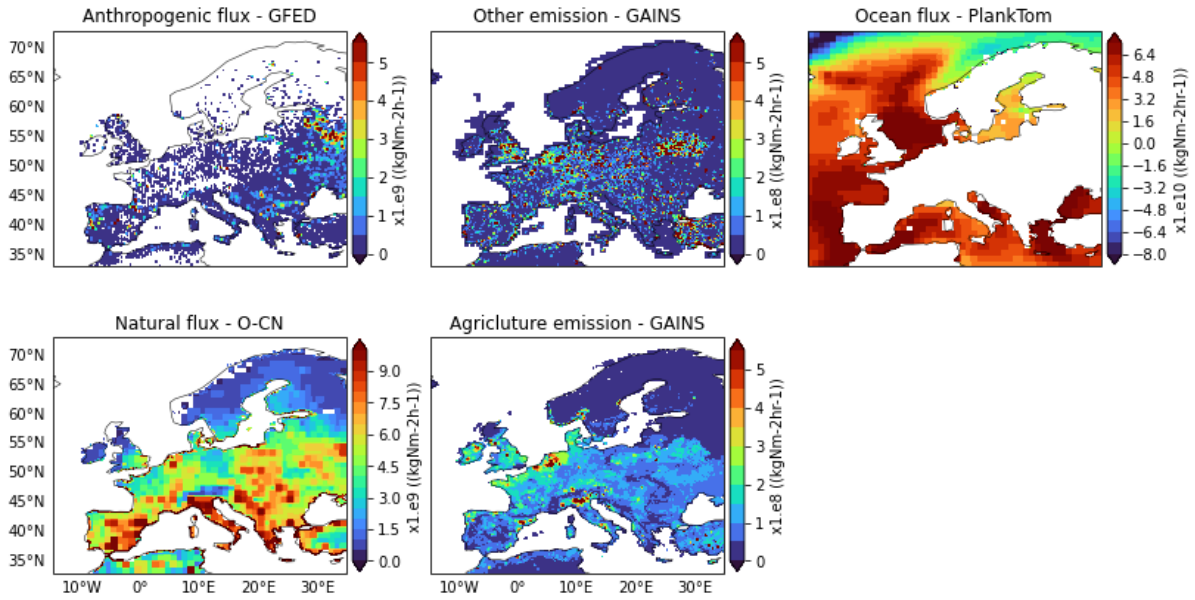

Figure 5.2: Annual mean N_2O emissions. Note that the scales of the maps vary.

5.3 Observations

A harmonized dataset of atmospheric N_2O observations was compiled for Europe as a collaborative effort involving EYE-CLIMA, and Horizon Europe projects AVENGERS and PARIS. We assimilated hourly data from 18 ground-based stations, each with at least 10 years of data between 2005 and 2023. Most stations report data extending to 2023, as shown in Figure 5.3. The data sources are from the previous European project, InGOS (pre-ICOS), the European network, ICOS, other sites obtained from the World Data Centre for Greenhouse Gases (WDCGG), and the NOAA network (Henne et al., 2024, https://meta.icos-cp.eu/collections/FHIS-w3c_eny9-NDoR7ddvTX).

The geographic distribution and altitude of the sites used in the inversion are displayed in Figure 5.4. In cases where stations report multiple intake heights (e.g., Hohenpeissenberg at 131 m and 5 m), only the highest inlet level was selected to ensure the air sampled represented the well-mixed atmosphere. All observations were assimilated as hourly averages. The observation uncertainty was defined as the standard deviation of the observations, with a lower bound set to 0.6 ppb to account also for the model representation and error and to prevent over-fitting the observations.

The altitude of observation sites used in the inversion spans a wide range, from sea level to about 3600 meters above sea level (masl). However, the orography in ERA5 data is resolved only at 0.5° resolution and, therefore, does not accurately represent true altitudes at mountainous locations (defined here as >1000 masl). To address this mismatch, the particle release heights in FLEXPART were adjusted for mountain sites to be the mid-point between the orography height in ERA5 and the actual height above sea level.

This project has received funding from the European Union's Horizon Europe research and innovation programme under grant agreement No 101081395

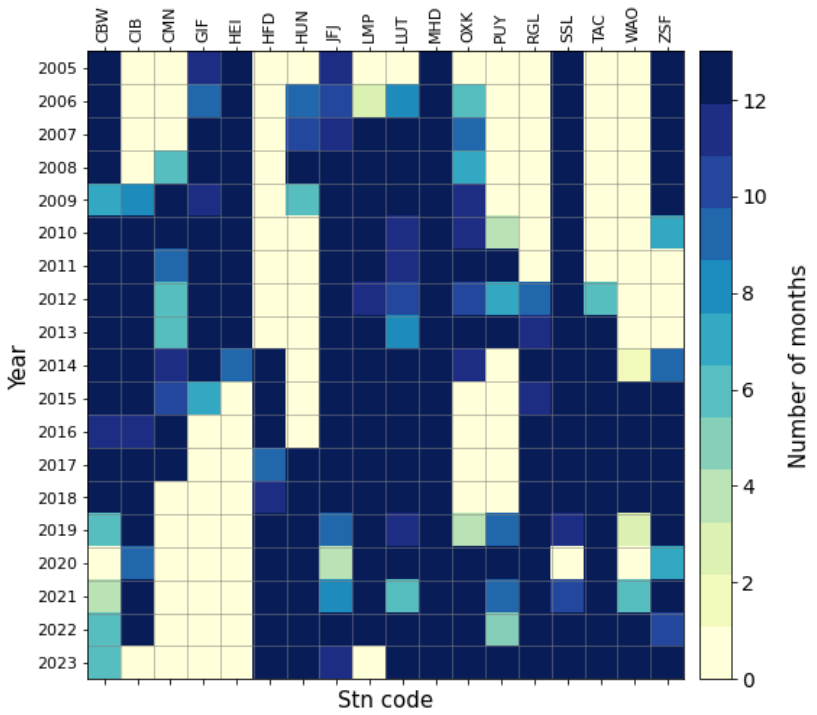

Figure 5.3: Data density in months for each site per year

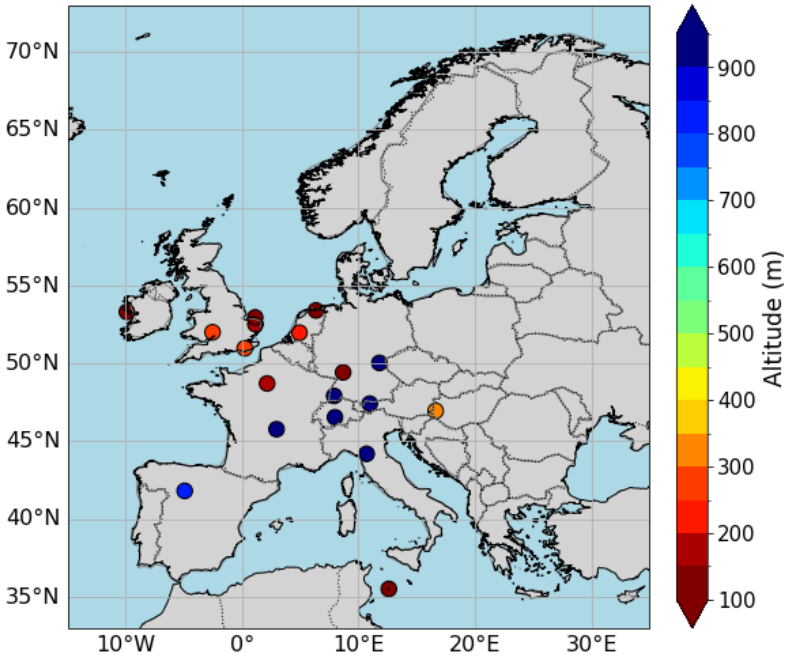

Figure 5.4: Geographical distribution of sites indicating also the particle release height for the representation in FLEXPART

This project has received funding from the European Union's Horizon Europe research and innovation programme under grant agreement No 101081395

5.4 Results

5.4.1 Modelled and observed atmospheric N_2O mole fractions

Figure 5.5 shows daily time series of observed N_2O mole fractions (black dots) and modelled values based on prior (green) and posterior (red) simulations for selected stations: CBW, GIF, LUT, MHD, and RGL. The time series spans from 2005 to 2023 (or up to each station's data availability) and highlights the model's capability to reproduce observed patterns.

Key observations include:

- An increase in the positive long-term trend of the N_2O mixing ratio is evident at most stations, consistent with the global mean trend and a global source that exceeds the global sink.
- All stations exhibit a seasonal cycle, where N_2O mixing ratios peak in spring and are at a minimum in autumn. This seasonality is driven by atmospheric transport and temperature-dependent biogenic emissions.
- After inversion, the posterior simulations more closely follow the observed variability, where the red line aligns more tightly with the black observational data.
- The posterior simulations better capture episodic enhancements (e.g., local emission spikes), indicating improved representation of regional-scale emission hotspots that the prior failed to capture.

This improvement in the agreement between observed and modelled values across diverse European stations is one necessary criterion for a correct inversion.

Figure 5.6 provides a comparative assessment of model performance before and after inversion across multiple monitoring stations, based on three key statistical metrics: Root Mean Square Error (RMSE), bias, and the coefficient of determination (R^2).

Top panel shows the Root Mean Square Error (RMSE) and bias:

- RMSE (red bars) quantifies the average model error magnitude. At most stations, posterior RMSE (dark red) is lower than prior RMSE (light red), indicating improved accuracy post-inversion.
- Bias (green bars) reflects systematic deviations. The posterior bias (dark green) is consistently reduced compared to the prior (light green), often approaching zero. This suggests that systematic over- or underestimation in the prior simulations has been largely corrected.
- The greatest improvements in both RMSE and bias are observed at stations like MHD, LUT, and HEI, indicating stronger constraint by observations and inversion performance at these sites.

This project has received funding from the European Union's Horizon Europe research and innovation programme under grant agreement No 101081395

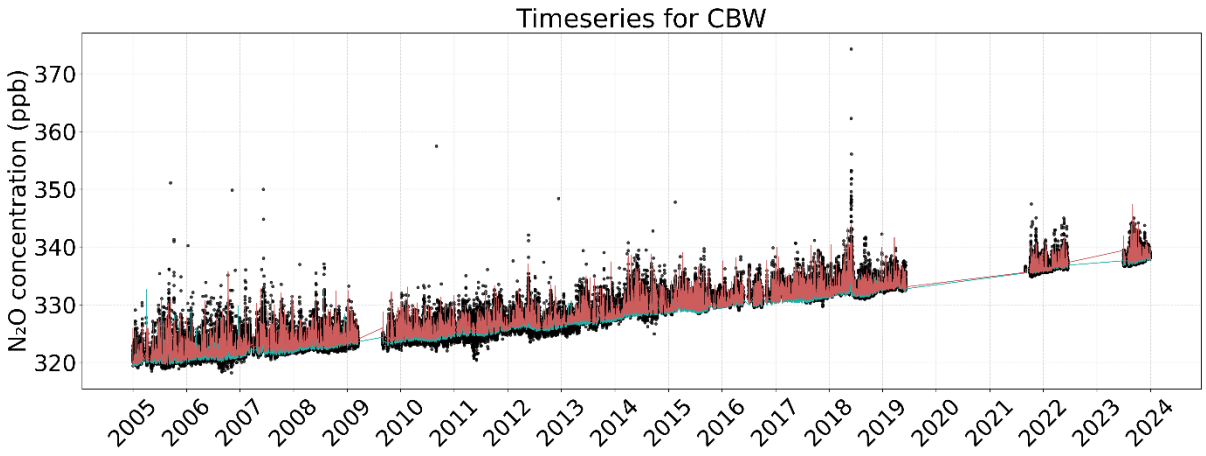

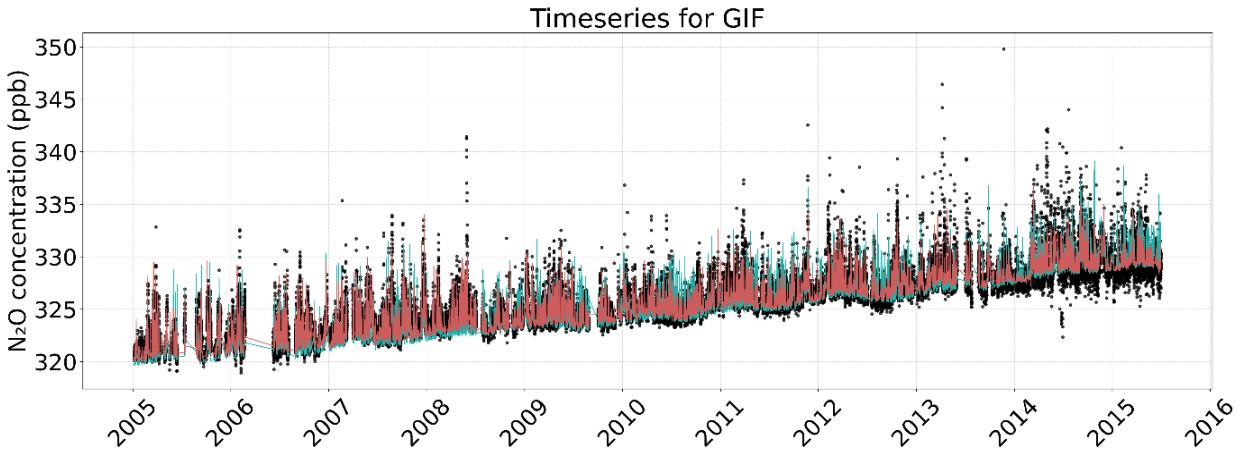

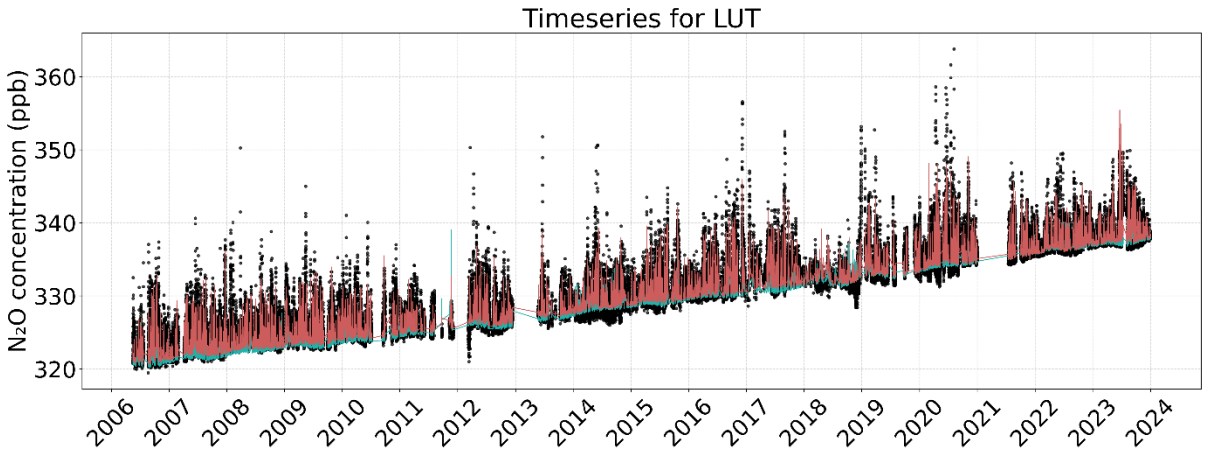

This project has received funding from the European Union's Horizon Europe research and innovation programme under grant agreement No 101081395

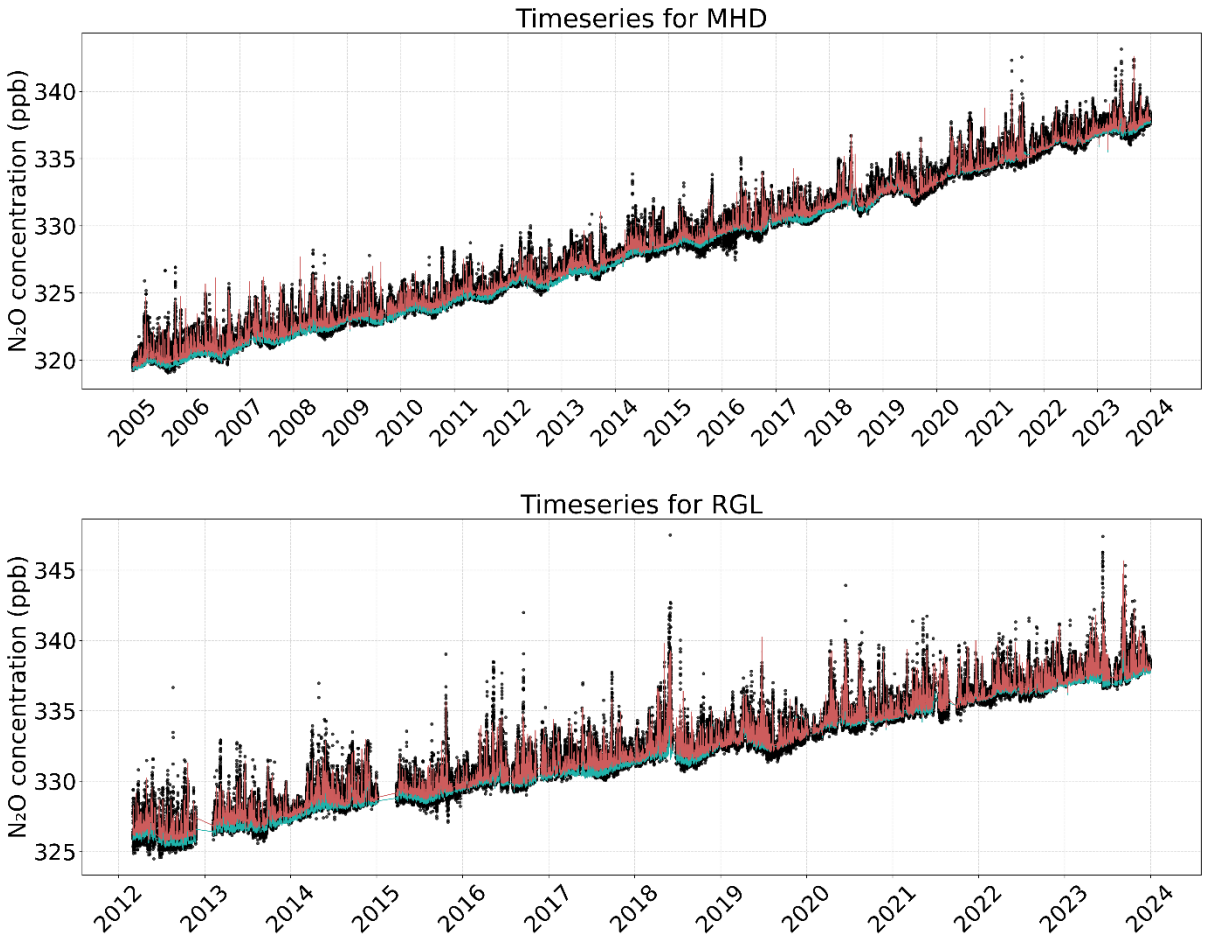

Figure 5.5: Time series of assimilated N_2O mole fractions sampled at different stations used in the inversion. Observed concentrations (black), CIF-FLEXPART inversion results a posteriori (red), and a priori (green).

Bottom panel shows coefficient of determination (R^2):

R^2 values (light blue for prior, blue for posterior) are uniformly high across stations (mostly >0.9), demonstrating strong temporal correspondence between observations and simulations.

- Though some stations (e.g., HEI) initially had slightly lower R^2, inversion has enhanced the correlation with observational data.
- Limited R^2 improvements at some stations (e.g., OXK, ZSF) imply that the model already had good temporal fidelity, and inversion mainly refined magnitude, not pattern.

CBW, LUT, HEI, and MHD stand out as stations where the inversion most significantly improved model performance.

Together, these statistical metrics indicate that the inversion systematically improves the representation of atmospheric N_2O mole fractions at diverse measurement locations, and is a necessary condition for the inversion to have improved the prior fluxes.

This project has received funding from the European Union's Horizon Europe research and innovation programme under grant agreement No 101081395

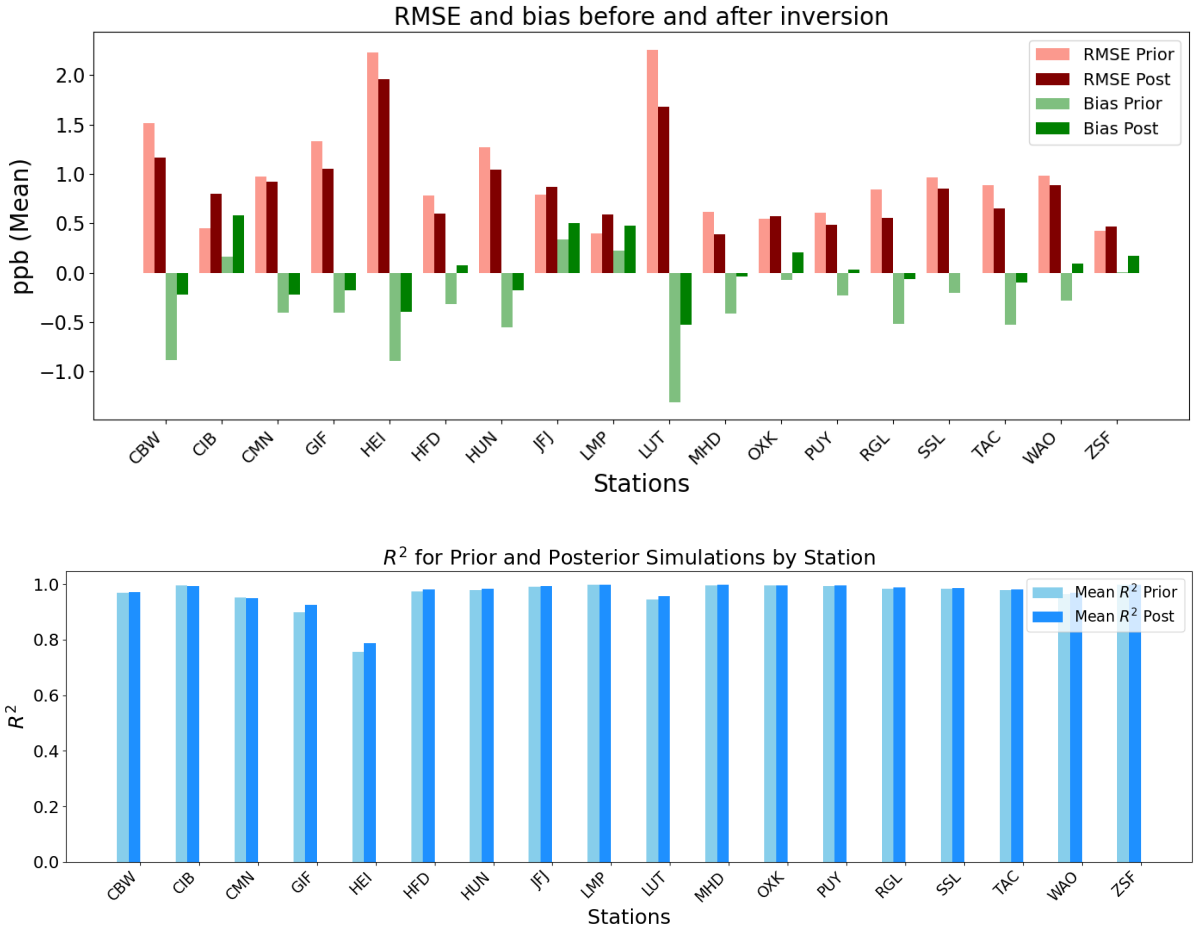

Figure 5.6: Statistical analysis of prior and posterior mole fractions with observations

5.4.2 Spatial and temporal distribution of prior and posterior emissions

Figure 5.7 compares prior and posterior estimates of mean N_2O emissions across Europe over the period 2005 – 2023. The left panel displays the prior emission estimates, while the right panel shows the posterior estimates after atmospheric inversion. The lower panel visualizes the difference between posterior and prior estimates, highlighting areas where corrections were made.

Significant changes in both intensity and spatial distribution are evident post-inversion. Notably:

- Total mean prior emissions over the whole inversion period from 2005-2023 is 1.038 Tg(N_2O) yr^{-1} and increased to 1.519 Tg yr^{-1} after inversion.
- High-emission regions, such as the Netherlands, western Germany, northwest France, and the UK, are prominent in both prior and posterior maps. This consistency suggests that the high prior emissions in these regions is reasonable and likely linked to intensive agricultural activities.
- Northern Italy shows a marked reduction in N_2O emissions in the posterior estimate, indicating that prior emissions were likely overestimated for this region.
- The posterior-prior difference map reveals increased emissions in the UK, Netherlands, parts of France, Spain and Germany, and decreased emissions in Italy. This spatial redistribution may be attributed to improved constraints from observational data and inversion corrections targeting agricultural hotspots.

This project has received funding from the European Union's Horizon Europe research and innovation programme under grant agreement No 101081395

Figure 5.8 illustrates the seasonal and interannual variability in total N_2O emissions for Europe (EU27+3 countries) between 2005 and 2022. Both the prior (brown line) and posterior (green line) emissions exhibit a clear seasonal cycle, characterized by:

- Peaks during late spring to early summer (May–June), coinciding with warmer temperatures and increased agricultural activity such as fertilizer application.
- Troughs in winter months, likely due to reduced microbial activity in soils and lower fertilizer usage.

Key observations include:

- The posterior emissions consistently exceed prior estimates for most years, indicating a systematic underestimation in the initial emission inventories.
- There is visible interannual variability in the amplitude of the seasonal cycle. For instance, 2013 and 2021 stand out with the highest posterior peaks.
- The seasonal pattern is broadly consistent with prior estimates and what is understood to be driving the emissions, notably soil temperature and moisture as well as management practices, such as the timing of fertilizer use. The year-to-year variability reflects the influence of weather variability and possibly inter-annual differences in cropping and fertilizer use.

This temporal analysis emphasizes the importance of accounting for seasonal and climatic drivers in emission estimation frameworks and the value of inversions in correcting for biases in emission inventories.

This project has received funding from the European Union's Horizon Europe research and innovation programme under grant agreement No 101081395

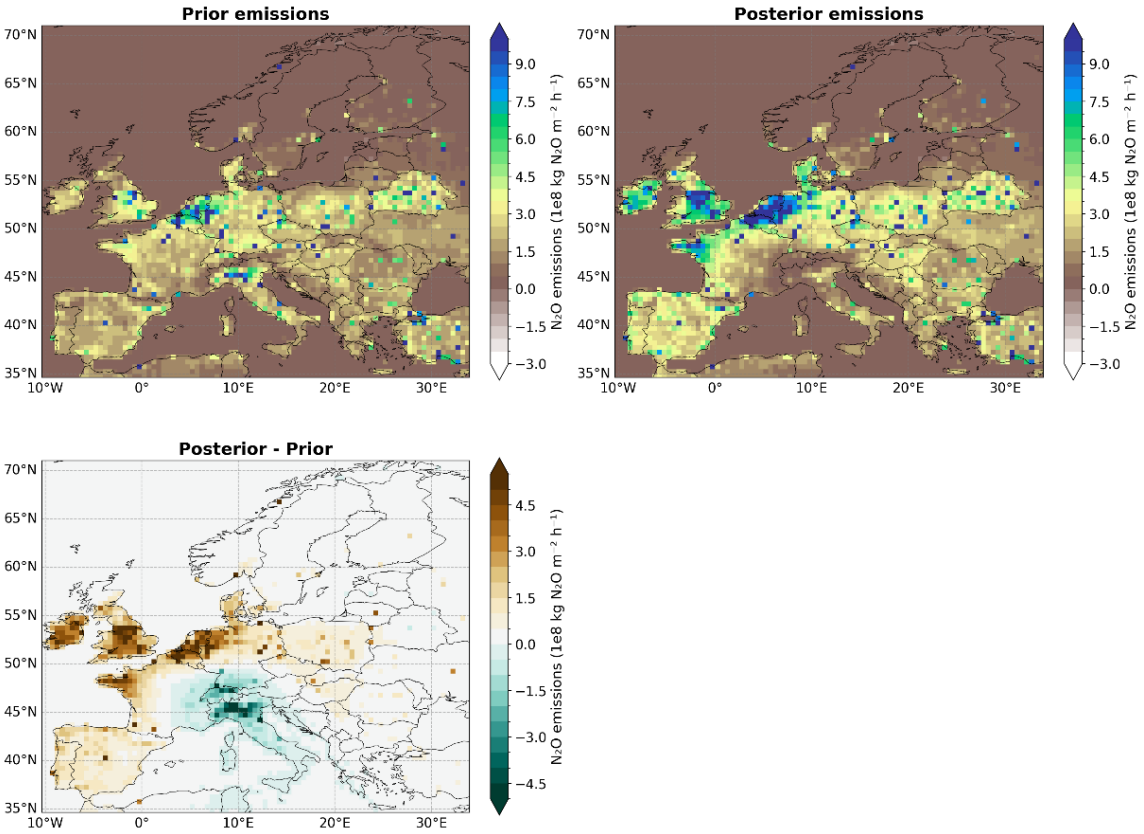

Figure 5.7: Mean N_2O estimates from CIF-FLEXPART inversion at the resolution of 0.5°×0.5° from 2005 to 2023: prior (left upper panel), posterior (right upper panel) and posterior increments computed as (posterior – prior) (bottom panel) shown as area fluxes.

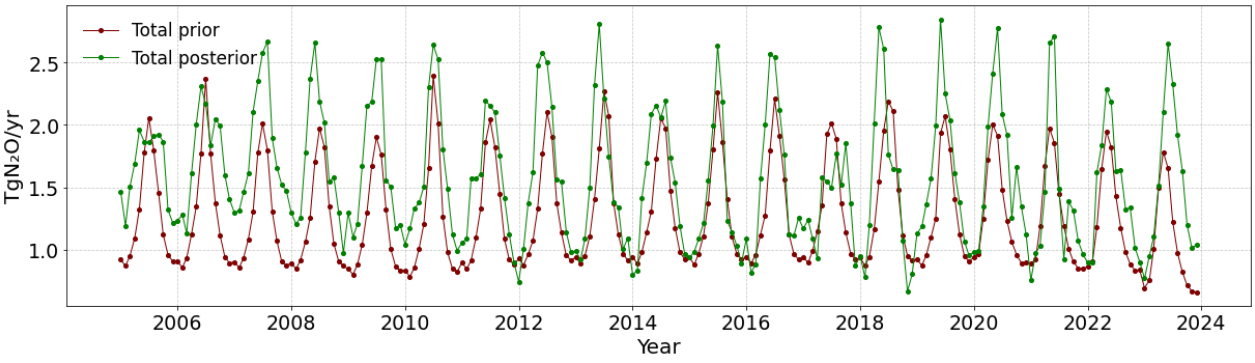

Figure 5.8: Times series of monthly N_2O in $Tg(N_2O)$ yr^{-1} for the inversion period from 2005 to 2023, for the EU27+UK+Norway+Switerland area.

This project has received funding from the European Union's Horizon Europe research and innovation programme under grant agreement No 101081395

6. Conclusions

Carbon dioxide, methane and nitrous oxide European budgets have been produced using different inversion frameworks.

CO_2 inversions using the CIF-CHIMERE model to correct prior estimates of the Net Ecosystem Exchange (NEE) and of the ocean fluxes and of the boundary conditions by assimilating surface and OCO-2 satellite observations show that the model significantly improves the fit between simulated and observed CO_2 concentrations, reducing root-mean-square (RMS) errors and biases. Surface-based inversions generally result in positive corrections (decreasing the CO_2 sink) in regions like Switzerland and Germany, while satellite-based inversions apply more negative corrections (increasing the CO_2 sink), particularly in Central and Eastern Europe. European ecosystems act as CO_2 sinks, with a posterior estimate of the NEE+F_{LUC} average annual budget for EU27+3 over 2005-2023 of about -0.35 PgC.yr^{-1} from the surface-based inversions compared to the prior estimates of about -0.52 PgC.yr^{-1}. The CO_2 uptake estimated from satellite-based inversions is higher than the surface-based ones at the annual scale. The posterior estimates of the NEE+F_{LUC} average annual budget for EU27+3 over 2015-2021 is of about -0.34 PgC.yr^{-1} from the surface-based inversions and of about –0.84 PgC.yr^{-1} from the satellite-based inversions compared to the prior estimates of about -0.55 PgC.yr^{-1}, with weakest sinks seen in 2018, when Europe experienced an extensive heatwave and drought.

For CH_4, the inversion posterior demonstrates substantial improvements in reproducing observed mole fractions compared to the prior. Across the observational network, RMSE values decrease from 36.14 to 23.69 ppb, with reductions exceeding 25%, while correlations increase from 0.835 to 0.916, frequently exceeding 0.85 at individual sites. Bias is also substantially reduced, from −10.18 ppb to −2.48 ppb, reflecting the posterior's enhanced ability to capture temporal variability and overall agreement with observations. At the EU27+3 scale, averaged over 2005–2023, total CH_4 emissions rise modestly from a prior estimate of 23.11 ± 1.79 Tg yr^{-1} to a posterior estimate of 23.47 ± 1.52 Tg yr^{-1} (~2% increase), but this conceals significant regional and sectoral redistributions. Agricultural emissions increase by around 10% across the EU27+3, with particularly large increases in Germany, France, and the Benelux, while decreases occur in the UK, Poland, Switzerland, and Italy. Wetland emissions decline across northern Europe, and fossil and geological fluxes show localized adjustments. Spatially, wetland emissions remain concentrated in northern Europe, whereas anthropogenic emissions dominate western, central, and southern regions, particularly Germany, the Netherlands, UK, and France. Monthly emissions exhibit a pronounced seasonal cycle, largely driven by wetland fluxes.

For N_2O, comparisons of the modelled and observed mole fractions show that the posterior N_2O fluxes significantly improve the agreement compared to the prior fluxes. Posterior simulations reduced both RMSE and bias relative to prior modelled mixing ratios, indicating a better agreement with observations. In addition, the R^2 analysis shows that correlations remain high across stations, with modest improvements after inversion. The spatial maps indicate that posterior emissions are more localized compared to the prior, with strong enhancements in northwestern Europe, particularly over the Netherlands, Germany, and the UK, while reductions are evident in regions such as France, Switzerland, and southern Europe. The time series of total emissions reveals a pronounced seasonal cycle throughout the study period, with posterior emissions generally higher than prior estimates. Total mean prior emissions over the whole inversion period from 2005-2023 is 1.038 Tg(N_2O) yr^{-1} and increased to 1.519 Tg yr^{-1} after inversion.

This project has received funding from the European Union's Horizon Europe research and innovation programme under grant agreement No 101081395

7. References

Berchet, A., Sollum, E., Thompson, R. L., Pison, I., Thanwerdas, J., Broquet, G., Chevallier, F., Aalto, T., Berchet, A., Bergamaschi, P., Brunner, D., Engelen, R., Fortems-Cheiney, A., Gerbig, C., Groot Zwaaftink, C. D., Haussaire, J.-M., Henne, S., Houweling, S., Karstens, U., Kutsch, W. L., Luijkx, I. T., Monteil, G., Palmer, P. I., van Peet, J. C. A., Peters, W., Peylin, P., Potier, E., Rödenbeck, C., Saunois, M., Scholze, M., Tsuruta, A., and Zhao, Y.: The Community Inversion Framework v1.0: a unified system for atmospheric inversion studies, Geoscientific Model Development, 14, 5331–5354, https://doi.org/10.5194/gmd-14-5331-2021, 2021.

Broquet, G., Chevallier, F., Rayner, P., Aulagnier, C., Pison, I., Ramonet, M., Schmidt, M., Vermeulen, A., and Ciais, P.: A European summertime CO 2 biogenic flux inversion at mesoscale from continuous in situ mixing ratio measurements, Journal of Geophysical Research: Atmospheres, 116, D23 303 1–22, https://doi.org/10.1029/2011JD016202, 2011.

Broquet, G., Chevallier, F., Bréon, F.-M., Kadygrov, N., Alemanno, M., Apadula, F., Hammer, S., Haszpra, L., Meinhardt, F., Morguí, J. A., Necki, J., Piacentino, S., Ramonet, M., Schmidt, M., Thompson, R. L., Vermeulen, A. T., Yver, C., and Ciais, P.: Regional inversion of CO2 ecosystem fluxes from atmospheric measurements: reliability of the uncertainty estimates, Atmospheric Chemistry and Physics, 13,175 9039–9056, https://doi.org/10.5194/acp-13-9039-2013, 2013.

Bruhwiler, L., Dlugokencky, E., Masarie, K., Ishizawa, M., Andrews, A., Miller, J., Sweeney, C., Tans, P., and Worthy, D.: CarbonTracker-CH4: An assimilation system for estimating emissions of atmospheric methane, Atmospheric Chemistry and Physics, 14, 8269–8293, https://doi.org/10.5194/acp-14-8269-2014, 2014.

Chevallier, F.: Fluxes of Carbon Dioxide from Managed Ecosystems Estimated by National Inventories Compared to Atmospheric Inverse Modeling, Geophysical Research Letters, 48, e2021GL093 565, https://doi.org/https://doi.org/10.1029/2021GL093565, e2021GL093565 2021GL093565, 2021.

Chevallier, F., Fisher, M., Peylin, P., Serrar, S., Bousquet, P., Bréon, F.-M., Chédin, A., and Ciais, P.: Inferring CO2 sources and sinks from satellite observations: Method and application to TOVS data, Journal of Geophysical Research: Atmospheres, 110, https://doi.org/https://doi.org/10.1029/2005JD006390, 2005.

Chevallier, F., et al., CO_2 surface fluxes at grid point scale estimated from a global 21 year reanalysis of atmospheric measurements, *J. Geophys. Res.*, 115, D21307, doi:10.1029/2010JD013887, 2010.

Chevallier, F., Remaud, M., O'Dell, C. W., Baker, D., Peylin, P., and Cozic, A.: Objective evaluation of surface- and satellite-driven carbon dioxide atmospheric inversions, Atmospheric Chemistry and Physics, 19, 14 233–14 251, https://doi.org/10.5194/acp-19-14233-2019, 2019.

Denier van der Gon, H., Hendriks, C., Kuenen, J., Segers, A., and Visschedijk, A.: TNO Report Description of current temporal emission patterns and sensitivity of predicted AQ for temporal emission patterns EU FP7 MACC deliverable report DD – EM IS1.3, Tech. rep., 2019.

Fortems-Cheiney, A., Pison, I., Broquet, G., Dufour, G., Berchet, A., Potier, E., Coman, A., Siour, G., and Costantino, L.: Variational regional inverse modeling of reactive species emissions with PYVAR-CHIMERE-v2019, Geoscientific Model Development, 14, 2939–2957, https://doi.org/10.5194/gmd-14-2939-2021, 2021.

Friedlingstein, P., O'Sullivan, M., Jones, M. W., Andrew, R. M., Gregor, L., Hauck, J., Le Quéré, C., Luijkx, I. T., Olsen, A., Peters, G. P., Peters, W., Pongratz, J., Schwingshackl, C., Sitch, S., Canadell, J. G., Ciais,

This project has received funding from the European Union's Horizon Europe research and innovation programme under grant agreement No 101081395

P., Jackson, R. B., Alin, S. R., Alkama, R., Arneth, A., Arora, V. K., Bates, N. R., Becker, M., Bellouin, N., Bittig, H. C., Bopp, L., Chevallier, F., Chini, L. P., Cronin, M., Evans, W., Falk, S., Feely, R. A., Gasser, T., Gehlen, M., Gkritzalis, T., Gloege, L., Grassi, G., Gruber, N., Gürses, O.,Harris, I., Hefner, M., Houghton, R. A., Hurtt, G. C., Iida, Y., Ilyina, T., Jain, A. K., Jersild, A., Kadono, K., Kato, E., Kennedy, D., Klein Goldewijk, K., Knauer, J., Korsbakken, J. I., Landschützer, P., Lefèvre, N., Lindsay, K., Liu, J., Liu, Z., Marland, G., Mayot, N., McGrath, M. J., Metzl, N., Monacci, N. M., Munro, D. R., Nakaoka, S.-I., Niwa, Y., O'Brien, K., Ono, T., Palmer, P. I., Pan, N., Pierrot, D., Pocock, K., Poulter, B., Resplandy, L., Robertson, E., Rödenbeck, C., Rodriguez, C., Rosan, T. M., Schwinger, J., Séférian, R., Shutler, J. D., Skjelvan, I., Steinhoff, T., Sun, Q., Sutton, A. J., Sweeney, C., Takao, S., Tanhua, T., Tans, P. P., Tian, X., Tian, H., Tilbrook, B., Tsujino, H., Tubiello, F., van der Werf, G. R., Walker, A. P., Wanninkhof, R., Whitehead, C., Willstrand Wranne, A., Wright, R., Yuan, W., Yue, C., Yue, X., Zaehle, S., Zeng, J., and Zheng, B.: Global Carbon Budget 2022, Earth System Science Data, 14, 4811–4900, https://doi.org/10.5194/essd-14-4811-2022, 2022.

Koch, F.-T., Gerbig, C., 2023. European anthropogenic CO2 emissions based on EDGARv4.3 and BP statistics 2023 for 2005-2022. https://doi.org/10.18160/RFJD-QV8J

Gilbert, J. and Lemaréchal, C.: Some numerical experiments with variable storage quasi-Newton algorithms, Math. Program., 45, 407–435, https://doi.org/10.1007/BF01589113, 1989.

Hersbach, H., Bell, B., Berrisford, P., Hirahara, S., Hor´anyi, A., Mu˜noz-Sabater, J., Nicolas, J., Peubey, C., Radu, R., Schepers, D., Simmons, A., Soci, C., Abdalla, S., Abellan, X., Balsamo, G., Bechtold, P., Biavati, G., Bidlot, J., Bonavita, M., De Chiara, G., Dahlgren, P., Dee, D., Diamantakis, M., Dragani, R., Flemming, J., Forbes, R., Fuentes, M., Geer, A., Haimberger, L., Healy, S., Hogan, R. J., H´olm, E., Janisková, M., Keeley, S., Laloyaux, P., Lopez, P., Lupu, C., Radnoti, G., de Rosnay, P., Rozum, I., Vamborg, F., Villaume, S., and Th´epaut, J. N.: The ERA5 global reanalysis, Quarterly Journal of the Royal Meteorological Society, 146, 1999–2049, https://doi.org/10.1002/qj.3803, 2020.

ICOS RI, Bergamaschi, P., Colomb, A., De Mazière, M., Emmenegger, L., Kubistin, D., Lehner, I., Lehtinen, K., Lund Myhre, C., Marek, M., Platt, S. M., Plaß-Dülmer, C., Schmidt, M., Apadula, F., Arnold, S., Blanc, P.-E., Brunner, D., Chen, H., Chmura, L., Conil, S., Couret, C., Cristofanelli, P., Delmotte, M., Forster, G., Frumau, A., Gheusi, F., Hammer, S., Haszpra, L., Heliasz, M., Henne, S., Hoheisel, A., Kneuer, T., Laurila, T., Leskinen, A., Leuenberger, M., Levin, I., Lindauer, M., Lopez, M., Lunder, C., Mammarella, I., Manca, G., Manning, A., Marklund, P., Martin, D., Meinhardt, F., Müller-Williams, J., Necki, J., O'Doherty, S., Ottosson-Löfvenius, M., Philippon, C., Piacentino, S., Pitt, J., Ramonet, M., Rivas-Soriano, P., Scheeren, B., Schumacher, M., Sha, M. K., Spain, G., Steinbacher, M., Sørensen, L. L., Vermeulen, A., Vítková, G., Xueref-Remy, I., di Sarra, A., Conen, F., Kazan, V., Roulet, Y.-A., Biermann, T., Heltai, D., Hensen, A., Hermansen, O., Komínková, K., Laurent, O., Levula, J., Pichon, J.-M., Smith, P., Stanley, K., Trisolino, P., ICOS Carbon Portal, ICOS Atmosphere Thematic Centre, ICOS Flask And Calibration Laboratory, and ICOS Central Radiocarbon Laboratory: European Obspack compilation of atmospheric carbon dioxide data from ICOS and non-ICOS European stations for the period 1972-2023; obspackco2466GLOBALVIEW plus v8.02023-04-6, https: //doi.org/10.18160/CEC4 – CAGK, 2023.

Janssens-Maenhout, G., Crippa, M., Guizzardi, D., Muntean, M., Schaaf, E., Dentener, F., Bergamaschi, P., Pagliari, V., Olivier, J. G. J., Peters, J. A. H. W., van Aardenne, J. A., Monni, S., Doering, U., Petrescu, A. M. R., Solazzo, E., and Oreggioni, G. D.: EDGAR v4.3.2 Global Atlas of the three major greenhouse gas emissions for the period 1970–2012, Earth System Science Data, 11, 959–1002, https://doi.org/10.5194/essd-11-959-2019, 2019.

Jung, M., Schwalm, C., Migliavacca, M., Walther, S., Camps-Valls, G., Koirala, S., Anthoni, P., Besnard, S., Bodesheim, P., Carvalhais, N., Chevallier, F., Gans, F., Goll, D. S., Haverd, V., Köhler, P., Ichii, K.,

This project has received funding from the European Union's Horizon Europe research and innovation programme under grant agreement No 101081395

Jain, A. K., Liu, J., Lombardozzi, D., Nabel, J. E. M. S., Nelson, J. A., O'Sullivan, M., Pallandt, M., Papale, D., Peters, W., Pongratz, J., Rödenbeck, C., Sitch, S., Tramontana, G., Walker, A., Weber, U., and Reichstein, M.: Scaling carbon fluxes from eddy covariance sites to globe: synthesis and evaluation of the FLUXCOM approach, Biogeosciences, 17, 1343–1365, https://doi.org/10.5194/bg-17-1343-2020, 2020.

Jöckei, P., Tost, H., Pozzer, A., Brühl, C., Buchholz, J., Ganzeveld, L., Hoor, P., Kerkweg, A., Lawrence, M. G., Sander, R., Steil, B., Stiller, G., Tanarhte, M., Taraborrelli, D., Van Aardenne, J., and Lelieveld, J.: The atmospheric chemistry general circulation model ECHAM5/MESSy1: Consistent simulation of ozone from the surface to the mesosphere, Atmospheric Chemistry and Physics, 6, 5067–5104, https://doi.org/10.5194/acp-6-5067-2006, 2006.

Kangasaho, V., Tsuruta, A., Backman, L., M¨akinen, P., Houweling, S., Segers, A., Krol, M., Dlugokencky, E. J., Michel, S., White, J. W. C., and Aalto, T.: The Role of Emission Sources and Atmospheric Sink in the Seasonal Cycle of CH4 and δ13-CH4: Analysis Based on the Atmospheric Chemistry Transport Model TM5, Atmosphere, 13, 888, https://doi.org/10.3390/atmos13060888, 2022.

Kountouris, P., Gerbig, C., Totsche, K.-U., Dolman, A. J., Meesters, A. G. C. A., Broquet, G., Maignan, F., Gioli, B., Montagnani, L., and Helfter, C.: An objective prior error quantification for regional atmospheric inverse applications, Biogeosciences, 12, 7403–7421, https://doi.org/10.5194/bg-12-7403-2015, 2015.

Krinner, G., Viovy, N., de Noblet-Ducoudré, N., Ogée, J., Polcher, J., Friedlingstein, P., Ciais, P., Sitch, S., and Prentice, I. C.: A dynamic global vegetation model for studies of the coupled atmosphere-biosphere system, Global Biogeochemical Cycles, 19, https://doi.org/https://doi.org/10.1029/2003GB002199, 2005.

Krol, M., Houweling, S., Bregman, B., van den Broek, M., Segers, A., van Velthoven, P., Peters, W., Dentener, F., Bergamaschi, P., Broek, M. V. D., Segers, A., Velthoven, P. V., Peters, W., Dentener, F., van den Broek, M., Segers, A., van Velthoven, P., Peters, W., Dentener, F., Bergamaschi, P., Broek, M. V. D., Segers, A., Velthoven, P. V., Peters, W., and Dentener, F.: The two-way nested global chemistry-transport zoom model TM5: algorithm and applications, Atmospheric Chemistry and Physics, 5, 417–432, https://doi.org/10.5194/acp-5-417-2005, 2005.

Lienert, S. and Joos, F.: A Bayesian ensemble data assimilation to constrain model parameters and land-use carbon emissions, Biogeosciences, 15, 2909–2930, https://doi.org/10.5194/bg-15-2909-2018, 2018.

Mahadevan, P., Wofsy, S. C., Matross, D. M., Xiao, X., Dunn, A. L., Lin, J. C., Gerbig, C., Munger, J. W., Chow, V. Y., and Gottlieb, E. W.: A satellite-based biosphere parameterization for net ecosystem CO2 exchange: Vegetation Photosynthesis and Respiration Model (VPRM), Global Biogeochemical Cycles, 22, https://doi.org/https://doi.org/10.1029/2006GB002735, 2008.

Mailler, S., Menut, L., Khvorostyanov, D., Valari, M., Couvidat, F., Siour, G., Turquety, S., Briant, R., Tuccella, P., Bessagnet, B., Colette, A., Létinois, L., Markakis, K., and Meleux, F.: CHIMERE-2017: from urban to hemispheric chemistry-transport modeling, Geoscientific Model Development, 10, 2397–2423, https://doi.org/10.5194/gmd-10-2397-2017, 2017.

McGrath, M. J., Petrescu, A. M. R., Peylin, P., Andrew, R. M., Matthews, B., Dentener, F., Balkovi˘c, J., Bastrikov, V., Becker, M., Broquet, G., Ciais, P., Fortems, A., Ganzenmüller, R., Grassi, G., Harris, I., Jones, M., Knauer, J., Kuhnert, M., Monteil, G., Munassar, S., Palmer, P. I., Peters, G. P., Qiu, C., Schelhaas, M.-J., Tarasova, O., Vizzarri, M., Winkler, K., Balsamo, G., Berchet, A., Briggs, P., Brockmann,

This project has received funding from the European Union's Horizon Europe research and innovation programme under grant agreement No 101081395

P., Chevallier, F., Conchedda, G., Crippa, M., Dellaert, S., Denier van der Gon, H. A. C., Filipek, S., Friedlingstein, P., Fuchs, R., Gauss, M., Gerbig, C., Guizzardi, D., Günther, D., Houghton, R. A., Janssens-Maenhout, G., Lauerwald, R., Lerink, B., Luijkx, I. T., Moulas, G., Muntean, M., Nabuurs, G.-J., Paquirissamy, A., Perugini, L., Peters, W., Pilli, R., Pongratz, J., Regnier, P., Scholze, M., Serengil, Y., Smith, P., Solazzo, E., Thompson, R. L., Tubiello, F. N., Vesala, T., and Walther, S.: The consolidated European synthesis of CO2 emissions and removals for EU27 and UK: 1990–2020, Earth System Science Data Discussions, 2023, 1–123, https://doi.org/10.5194/essd-2022-412, 2023.

Menut, L., Bessagnet, B., Khvorostyanov, D., Beekmann, M., Blond, N., Colette, A., Coll, I., Curci, G., Foret, G., Hodzic, A., Mailler, S., Meleux, F., Monge, J.-L., Pison, I., Siour, G., Turquety, S., Valari, M., Vautard, R., and Vivanco, M. G. : CHIMERE 2013: a model for regional atmospheric composition modelling, Geoscientific Model Development, 6, 981–1028, https://doi.org/10.5194/gmd-6-981-2013, 2013.

Monteil, G., Broquet, G., Scholze, M., Lang, M., Karstens, U., Gerbig, C., Koch, F.-T., Smith, N. E., Thompson, R. L., Luijkx, I. T., White, E., Meesters, A., Ciais, P., Ganesan, A. L., Manning, A., Mischurow, M., Peters, W., Peylin, P., Tarniewicz, J., Rigby, M., Rödenbeck, C., Vermeulen, A., and Walton, E. M.: The regional European atmospheric transport inversion comparison, EUROCOM: first results on European-wide terrestrial carbon fluxes for the period 2006–2015, Atmospheric Chemistry and Physics, 20, 12 063–12 091, https://doi.org/10.5194/acp-20-12063-2020, 2020.

Munassar, S., Rödenbeck, C., Koch, F.-T., Totsche, K. U., Gałkowski, M., Walther, S., and Gerbig, C.: Net ecosystem exchange (NEE) estimates 2006–2019 over Europe from a pre-operational ensemble-inversion system, Atmospheric Chemistry and Physics, 22, 7875–7892, https://doi.org/10.5194/acp-22-7875-2022, 2022.

O'Dell, C. W., Eldering, A., Wennberg, P. O., Crisp, D., Gunson, M. R., Fisher, B., Frankenberg, C., Kiel, M., Lindqvist, H., Mandrake, L., Merrelli, A., Natraj, V., Nelson, R. R., Osterman, G. B., Payne, V. H., Taylor, T. E., Wunch, D., Drouin, B. J., Oyafuso, F., Chang, A., McDuffie, J., Smyth, M., Baker, D. F., Basu, S., Chevallier, F., Crowell, S. M. R., Feng, L., Palmer, P. I., Dubey, M., García, O. E., Griffith, D. W. T., Hase, F., Iraci, L. T., Kivi, R., Morino, I., Notholt, J., Ohyama, H., Petri, C., Roehl, C. M., Sha, M. K., Strong, K., Sussmann, R., Te, Y., Uchino, O., and Velazco, V. A.: Improved retrievals of carbon dioxide from Orbiting Carbon Observatory-2 with the version 8 ACOS algorithm, Atmospheric Measurement Techniques, 11, 6539–6576, https://doi.org/10.5194/amt-11-6539-2018, 2018.

Petrescu, A. M. R., McGrath, M. J., Andrew, R. M., Peylin, P., Peters, G. P., Ciais, P., Broquet, G., Tubiello, F. N., Gerbig, C., Pongratz, J., Janssens-Maenhout, G., Grassi, G., Nabuurs, G.-J., Regnier, P., Lauerwald, R., Kuhnert, M., Balkovič, J., Schelhaas, M.-J., Denier van der Gon, H. A. C., Solazzo, E., Qiu, C., Pilli, R., Konovalov, I. B., Houghton, R. A., Günther, D., Perugini, L., Crippa, M., Ganzenmüller, R., Luijkx, I. T., Smith, P., Munassar, S., Thompson, R. L., Conchedda, G., Monteil, G., Scholze, M., Karstens, U., Brockmann, P., and Dolman, A. J.: The consolidated European synthesis of CO_2 emissions and removals for the European Union and United Kingdom: 1990–2018, Earth Syst. Sci. Data, 13, 2363–2406, https://doi.org/10.5194/essd-13-2363-2021, 2021.

Rödenbeck, C., Bakker, D. C. E., Metzl, N., Olsen, A., Sabine, C., Cassar, N., Reum, F., Keeling, R. F., and Heimann, M.: Interannual sea–air CO2 flux variability from an observation-driven ocean mixed-layer scheme, Biogeosciences, 11, 4599– 4613, https://doi.org/10.5194/bg-11-4599-2014, 2014.

Sasakawa, M., Shimoyama, K., Machida, T., Tsuda, N., Suto, H., Arshinov, M., Davydov, D., Fofonov, A., Krasnov, O., Saeki, T., Koyama, Y., and Maksyutov, S.: Continuous measurements of methane from a

This project has received funding from the European Union's Horizon Europe research and innovation programme under grant agreement No 101081395

tower network over Siberia, Tellus, Series B: Chemical and Physical Meteorology, 62, 403–416, https://doi.org/10.1111/j.1600-0889.2010.00494.x, 2010.

Saunois, M., Stavert, A. R., Poulter, B., Bousquet, P., Canadell, J. G., Jackson, R. B., Raymond, P. A., Dlugokencky, E. J., Houweling, S., Patra, P. K., Ciais, P., Arora, V. K., Bastviken, D., Bergamaschi, P., Blake, D. R., Brailsford, G., Bruhwiler, L., Carlson, K. M., Carrol, M., Castaldi, S., Chandra, N., Crevoisier, C., Crill, P. M., Covey, K., Curry, C. L., Etiope, G., Frankenberg, C., Gedney, N., Hegglin, M. I., Höglund-Isaksson, L., Hugelius, G., Ishizawa, M., Ito, A., Janssens-Maenhout, G., Jensen, K. M., Joos, F., Kleinen, T., Krummel, P. B., Langenfelds, R. L., Laruelle, G. G., Liu, L., Machida, T., Maksyutov, S., McDonald, K. C., McNorton, J., Miller, P. A., Melton, J. R., Morino, I., Müller, J., Murguia-Flores, F., Naik, V., Niwa, Y., Noce, S., O'Doherty, S., Parker, R. J., Peng, C., Peng, S., Peters, G. P., Prigent, C., Prinn, R., Ramonet, M., Regnier, P., Riley, W. J., Rosentreter, J. A., Segers, A., Simpson, I. J., Shi, H., Smith, S. J., Steele, L. P., Thornton, B. F., Tian, H., Tohjima, Y., Tubiello, F. N., Tsuruta, A., Viovy, N., Voulgarakis, A., Weber, T. S., van Weele, M., van der Werf, G. R., Weiss, R. F., Worthy, D., Wunch, D., Yin, Y., Yoshida, Y., Zhang, W., Zhang, Z., Zhao, Y., Zheng, B., Zhu, Q., Zhu, Q., and Zhuang, Q.: The Global Methane Budget 2000–2017, Earth System Science Data, 12, 1561–1623, https://doi.org/10.5194/essd-12-1561-2020, 2020.

Saunois, M., Martinez, A., Poulter, B., Zhang, Z., Raymond, P. A., Pierre Regnier, Canadell, J. G., Jackson, R. B., Patra, P. K., Bousquet, P., Philippe Ciais, Dlugokencky, E. J., Lan, X., Allen, G. H., Bastviken, D., Beerling, J., D., Belikov, D. A., Blake, D. R., Castaldi, S., Crippa, M., Deemer, B. R., Dennison, F., Etiope, G., Gedney, N., Höglund-Isaksson, L., Holgerson, M. A., Hopcroft, P. O., Hugelius, G., Ito, A., Jain, A. K., Janardanan, R., Johnson, M. S., Kleinen, T., Krummel, P. B., Lauerwald, R., Li, T., Liu, X., McDonald, K. C., Melton, J. R., Mühle, J., Müller, J., Murguia-Flores, F., Niwa, Y., Noce, S., Pan, S., Parker, R. J., Peng, C., Ramonet, M., Riley, W. J., Rocher-Ros, G., Rosentreter, J. A., Sasakawa, M., Segers, A., Smith, S. J., Stanley, E. H., Thanwerdas, J., Tian, H., Tsuruta, A., Tubiello, F. N., Weber, T. S., Werf, G. R. v. d., Worthy, D. E. J., Xi, Y., Yoshida, Y., Zhang, W., Bo Zheng, Zhu, Q., Zhu, Q., and Zhuang, Q.: Global Methane Budget 2000-2020, Earth System Science Data Discussions, pp. 1–147, https://doi.org/10.5194/essd-2024-115, 2024.

Schuldt, K. N., Aalto, T., Andrews, A., Aoki, S., Arduini, J., Baier, B., Bergamaschi, P., Biermann, T., Biraud, S. C., Boenisch, H., Brailsford, G., Chen, H., Colomb, A., Conil, S., Cristofanelli, P., Cuevas, E., Daube, B., Davis, K., Mazière, M. D., Delmotte, M., Desai, A., DiGangi, J. P., Dlugokencky, E., Elkins, J. W., Emmenegger, L., Fischer, M. L., Gatti, L. V., Gehrlein, T., Gerbig, C., Gloor, E., Goto, D., Haszpra, L., Hatakka, J., Heimann, M., Heliasz, M., Hermanssen, O., Hintsa, E., Holst, J., Ivakhov, V., Jaffe, D., Joubert, W., Kang, H.-Y., Karion, A., Kazan, V., Keronen, P., Ko, M.-Y., Kominkova, K., Kort, E., Kozlova, E., Krummel, P., Kubistin, D., Labuschagne, C., Langenfelds, R., Laurent, O., Laurila, T., Lauvaux, T., Lee, J., Lee, H., Lee, C.-H., Lehner, I., Leppert, R., Leuenberger, M., Lindauer, M., Loh, Z., Lopez, M., Machida, T., Mammarella, I., Manca, G., Marek, M. V., Martin, M. Y., Matsueda, H., McKain, K., Miles, N., Miller, C. E., Miller, J. B., Moore, F., Morimoto, S., Munro, D., Myhre, C. L., Mölder, M., Müller-Williams, J., Nichol, S., Niwa, Y., O'Doherty, S., Obersteiner, F., Piacentino, S., Pichon, J. M., Pittman, J., Plass-Duelmer, C., Ramonet, M., Richardson, S., Rivas, P. P., Saito, K., Santoni, G., Sasakawa, M., Scheeren, B., Schuck, T., Schumacher, M., Seifert, T., Sha, M. K., Shepson, P., Sloop, C. D., Smith, P., Steinbacher, M., Stephens, B., Sweeney, C., Timas, H., Torn, M., Trisolino, P., Turnbull, J., Tørseth, K., Viner, B., Vitkova, G., Watson, A., Wofsy, S., Worsey, J., Worthy, D., Zahn, A., and Sarra, A. G. d.: Multi-laboratory compilation of atmospheric carbon dioxide data for the period 1983-2020; obspack ch4 1 GLOBALVIEWplus v4.0 2021-10-14, https://doi.org/10.25925/20211001, 2021.

Sitch, S., Friedlingstein, P., Gruber, N., Jones, S. D., Murray-Tortarolo, G., Ahlström, A., Doney, S. C., Graven, H., Heinze, C., Huntingford, C., Levis, S., Levy, P. E., Lomas, M., Poulter, B., Viovy, N., Zaehle,

This project has received funding from the European Union's Horizon Europe research and innovation programme under grant agreement No 101081395

S., Zeng, N., Arneth, A., Bonan, G., Bopp, L., Canadell, J. G., Chevallier, F., Ciais, P., Ellis, R., Gloor, M., Peylin, P., Piao, S. L., Le Quéré, C., Smith, B., Zhu, Z., and Myneni, R.: Recent trends and drivers of regional sources and sinks of carbon dioxide, Biogeosciences, 12, 653–679, https://doi.org/10.5194/bg-12-653-2015, 2015.

Steinbach, J., Gerbig, C., Rödenbeck, C., Karstens, U., Minejima, C., and Mukai, H.: The CO2 release and Oxygen uptake from Fossil Fuel Emission Estimate (COFFEE) dataset: effects from varying oxidative ratios, Atmospheric Chemistry and Physics, 11, 6855–6870, https://doi.org/10.5194/acp-11-6855-2011, 2011

Thompson, R. L., Broquet, G., Gerbig, C., Koch, T., Lang, M., Monteil, G., Munassar, S., Nickless, A., Scholze, M., Ramonet, M., Karstens, U., van Schaik, E., Wu, Z., and Rödenbeck, C.: Changes in net ecosystem exchange over Europe during the 2018 drought based on atmospheric observations, Philos. T. R. Soc. B, 375, 20190512, 2020.

Tsuruta, A., Aalto, T., Backman, L., Hakkarainen, J., van der Laan-Luijkx, I. T., Krol, M. C., Spahni, R., Houweling, S., Laine, M., Dlugokencky, E., Gomez-Pelaez, A. J., van der Schoot, M., Langenfelds, R., Ellul, R., Arduini, J., Apadula, F., Gerbig, C., Feist, D. G., Kivi, R., Yoshida, Y., and Peters, W.: Global methane emission estimates for 2000–2012 from CarbonTracker Europe-CH4 v1.0, Geoscientific Model Development, 10, 1261–1289, https://doi.org/10.5194/gmd-10-1261-2017, 2017.

Tsuruta, A., Aalto, T., Backman, L., Krol, M. C., Peters, W., Lienert, S., Joos, F., Miller, P. A., Zhang, W., Laurila, T., Hatakka, J., Leskinen, A., Lehtinen, K. E. J., Peltola, O., Vesala, T., Levula, J., Dlugokencky, E., Heimann, M., Kozlova, E., Aurela, M., Lohila, A., Kauhaniemi, M., and Gomez-Pelaez, A. J.: Methane budget estimates in Finland from the CarbonTracker Europe-CH4 data assimilation system, Tellus B: Chemical and Physical Meteorology, 71, 1–20, https://doi.org/10.1080/16000889.2018.1565030, 2019.

van der Laan-Luijkx, I. T., van der Velde, I. R., van der Veen, E., Tsuruta, A., Stanislawska, K., Babenhauserheide, A., Zhang, H. F., Liu, Y., He, W., Chen, H., Masarie, K. A., Krol, M. C., and Peters, W.: The CarbonTracker Data Assimilation Shell (CTDAS) v1.0: implementation and global carbon balance 2001–2015, Geoscientific Model Development, 10, 2785–2800, https://doi.org/10.5194/gmd-10-2785-2017, 2017.

van der Werf, G. R., Randerson, J. T., Giglio, L., van Leeuwen, T. T., Chen, Y., Rogers, B. M., Mu, M., van Marle, M. J. E., Morton, D. C., Collatz, G. J., Yokelson, R. J., and Kasibhatla, P. S.: Global fire emissions estimates during 1997–2016, Earth System Science Data, 9, 697–720, https://doi.org/10.5194/essd-9-697-2017, 2017.

Weber, T., Wiseman, N. A., and Kock, A.: Global ocean methane emissions dominated by shallow coastal waters, Nature Communications, 10, 4584, https://doi.org/10.1038/s41467-019-12541-7, 2019.

This project has received funding from the European Union's Horizon Europe research and innovation programme under grant agreement No 101081395

Appendix A: Inversion Protocol for CO_2

Authors: Audrey Fortems-Cheiney and Gregoire Broquet (LSCE)
Date: January 2026
Version: 1.1

1. Objectives

This **protocol** describes the standard configuration of the European scale CO_2 inversions assimilating surface and/or satellite observations in EYE-CLIMA, in terms of

- **period, domain and spatial and temporal resolution of the inversion**, i.e., of the control variables underlying the targeted flux estimates, assuming capabilities for solving high dimensional inversion problems (i.e. controlling fluxes over each cell of a relatively fine resolution grid covering the domain of analysis)
- **variables underlying the targeted flux estimates to be controlled by the inversion** at this spatial and temporal resolution, and **ancillary control variables**
- **prior or fixed estimates of the different components of the ocean and land surface to atmosphere fluxes**
- **prior of fixed estimates of the domain initial, lateral and top boundary conditions**
- **CO_2 observations to be assimilated**
- **constraints on the statistics of the prior and observation uncertainties (on their covariance matrices)**
- **constraints regarding the output file content and format**

The reference inversions in the project should be based on this standard configuration. Tests of sensitivities to the parameters of this configuration will be conducted in parallel to these reference inversions.

2. Domain, period and control resolution for the flux estimates and of the transport model

The European scale CO_2 inversions should cover at least the domain from 15°W to 35°E and 34°N to 73°N. The minimum temporal coverage of the inversion will depend on the control resolution of the control vector for the flux estimate (see below) and on the types of observations that are assimilated as detailed in Table 1.

Table 1. Minimum inversion period as a function of the control resolution and of the type of observations that are assimilated.

	0.5° control resolution	**0.2° control resolution**
Assimilation of surface observations	2005-2023	2018-2023
Assimilation of satellite (OCO-2) observations	2015-2023	(no constraint: no required inversion)

In order to cover such periods of analysis, the inversion interval can be broken down, and sequences of independent inversions over shorter and overlapping windows can be used. In that case, sufficient overlapping between the independent inversion windows should be used to account for the influence of observations on flux backward in time and to exploit the temporal correlation in the flux

This project has received funding from the European Union's Horizon Europe research and innovation programme under grant agreement No 101081395

uncertainties (propagating information from the observation both backward and forward in time). For example (accounting for the typical lag-time between observations in Europe and the typical period of representativity of their emission footprint in Europe, and accounting for the typical temporal correlation used for the characterization of the prior uncertainties in the controlled variables) the results for 2005-2023 can be generated via 13-month inversions centred on each calendar year: for a given year y (over Jan 1 to Dec 31), the results are extracted from the inversion over mid Dec of year y-1 and mid-Jan of year y+1. In this example, each 13-month inversion is independent (and does not use outputs from other inversions to derive its initial or boundary conditions, or to adjust its prior estimate of the surface fluxes).

Two ensemble of reference inversions should be conducted with two configurations for the spatial resolution of the control vector for the flux estimates: 0.5° and 0.2° (over the minimum inversion periods provided in Table 1). The spatial resolution of the transport model is not constrained, but if the model configuration is flexible, it should preferably be identical to that of the control vector for the flux estimates.

The temporal resolution of the control vector for the flux estimate can be set-up in various ways but should bear some flexibility to adjust the diurnal cycle of the fluxes with a separate control of the different 6-hour windows of the day in Europe, defined here as 0:00-6:00, 6:00-12:00, 12:00-18:00 and 18:00-0:00 UTC time. In practice, this temporal resolution can be 6 hours or it can be defined by the control of n-day averages for each of the four 6-hour windows of the days (with 7 to 14 as typical values for n).

3. Control variables

The main control variables, underlying the targeted component of the land biosphere fluxes in Europe, should consist in the sum of the Net Ecosystem Exchange (NEE, sum of the Net Primary Productivity NPP and of the Heterotrophic Respiration R_h) and of the fluxes F_{LUC} of CO_2 due to the Land Use Change (LUC) (these fluxes being limited here to emissions from deforestation), i.e.

$NEE + F_{LUC} = NPP + R_h + F_{LUC}$.

The inversions should control the net sea/ocean fluxes **F_{OCEAN}.** The spatial and temporal resolution for this control can be kept the same as for NEE + F_{LUC}, but it can also be highly coarsened.

The inversions should also control initial and lateral conditions. Ideally, for Eulerian transport models, it should control these conditions at the transport model 3D spatial resolution and 1-day temporal resolution.

4. Prior / fixed flux estimates

All products should be interpolated at the transport model resolution using a mass conservation interpolation following the preprocessing CIF configuration yml file joined to this document.

a) Land biosphere fluxes

Two products should be used to derive prior or fixed estimates of the land-biosphere fluxes of CO_2:

- ORCHIDEE simulation CRUERA-v5 at 0.125° resolution over Europe (35°-73°N and 25°W-45°E) and at hourly temporal resolution, providing
- **NPP** and **Rh** at 3-hour resolution
- **F_{LUC}** (land use change fluxes restricted, here in practice, to emissions of carbon due to deforestation)

This project has received funding from the European Union's Horizon Europe research and innovation programme under grant agreement No 101081395

- local emissions of the total amount of carbon removed (without spatial displacement in ORCHIDEE) from the local carbon stocks by wood and crop harvest: $\mathbf{F_{WOODHARVEST}}$ and $\mathbf{F_{CROPHARVEST}}$ at annual resolution but spread at 1-hour resolution as a constant flux over the year
- GFAS (v1.2) [1] estimate of net biomass burning emissions at 0.1° resolution, until year 2025:
- $\mathbf{F_{BB}}$ at 1-day resolution

The F_{BB} fluxes from GFAS should be used as a fixed flux component in the inversions.

b) Land fluxes from the "lateral" export of carbon from the ecosystems (including biofuel emissions)

The estimate of land fluxes due to "lateral" export of carbon from the ecosystems (when addressing the export of crops and wood: the associated sources only, assuming that the associated sinks are accounted for in the land biosphere flux estimates) will be derived using the last version of the database of Ciais et al. (2021)[2]: v6[3]. These estimates are provided globally at 0.083°x0.083° and 1-year resolution over 1961-2022. The estimates for 2022 have been used to impose the values for 2023. The following selection of fluxes from this database should be used:

- ALLWOODSOURCE (emissions from wood biofuel combustion and other wood products)
- ALLCROPSOURCE (emissions from crop biofuel combustion and other crop products such as human/animal respiration)
- ALLCROPSINK (estimate of the carbon sink corresponding to the crop harvest)
- ALLWOODSINK (estimate of the carbon sink corresponding to the wood harvest)
- RIVERSINK (transfer from soils to rivers)
- LAKERIVEREMIS (inland water outgassing)

c) Prior and fixed estimates of the land fluxes

For the sake of consistency between the sinks and sources associated to these lateral transfers in the prior estimate of the fluxes, the prior estimate of the NEE from ORCHIDEE should be adjusted by adding a linear scaling of the ORCHIDEE $F_{CROPHARVEST}$ and $F_{WOODHARVEST}$ fields α x ($F_{CROPHARVEST}$ or $F_{WOODHARVEST}$) with α_{crop} and α_{wood} respectively defined so that the integral of this correction over Europe and the year equals the differences between the EU-27+3 and 1-year scale budget of $F_{CROPHARVEST}$ and $F_{WOODHARVEST}$ versus the ALLCROPSINK and ALLWOODSINK estimates from Ciais et al.

[1] Available at: https://ads.atmosphere.copernicus.eu/datasets/cams-global-fire-emissions-gfas?tab=overview

[2] Philippe Ciais, Yitong Yao, Thomas Gasser, Alessandro Baccini, Yilong Wang, Ronny Lauerwald, Shushi Peng, Ana Bastos, Wei Li, Peter A Raymond, Josep G Canadell, Glen P Peters, Rob J Andres, Jinfeng Chang, Chao Yue, A Johannes Dolman, Vanessa Haverd, Jens Hartmann, Goulven Laruelle, Alexandra G Konings, Anthony W King, Yi Liu, Sebastiaan Luyssaert, Fabienne Maignan, Prabir K Patra, Anna Peregon, Pierre Regnier, Julia Pongratz, Benjamin Poulter, Anatoly Shvidenko, Riccardo Valentini, Rong Wang, Grégoire Broquet, Yi Yin, Jakob Zscheischler, Bertrand Guenet, Daniel S Goll, Ashley-P Ballantyne, Hui Yang, Chunjing Qiu, Dan Zhu, Empirical estimates of regional carbon budgets imply reduced global soil heterotrophic respiration, *National Science Review*, Volume 8, Issue 2, February 2021, nwaa145, https://doi.org/10.1093/nsr/nwaa145

[3] Available at: https://thredds-su.ipsl.fr/thredds/fileServer/tgcc_thredds/work/p24cheva/LateralFluxes/lateralfluxes_v6.tar see the updated metadata

This project has received funding from the European Union's Horizon Europe research and innovation programme under grant agreement No 101081395

(2021), implicitly assuming that the budget from the latter is more accurate. Of note is that there is no sub-annual temporal resolution for the $F_{CROPHARVEST}$ and $F_{WOODHARVEST}$ fields out of the ORCHIDEE simulations. Therefore, these fluxes should be prescribed as constant fluxes within a year, which thus applies to the adjustment of ORCHIDEE.

The estimates of $F_{WOODSOURCE}$ (=ALLWOODSOURCE), $F_{CROPSOURCE}$ (=ALLCROPSOURCE), and $F_{LAKERIVER}$ (=LAKERIVEREMIS+RIVERSINK) should be used as a fixed flux components in the inversions. The ORCHIDEE $F_{CROPHARVEST}$ and $F_{WOODHARVEST}$ from ORCHIDEE themselves, which are redundant with the ALLWOODSOURCE and ALLCROPSOURCE but which are assumed to rely on a less accurate estimate of the harvests, and which ignore the import/export of harvest across the boundaries of Europe, should be discarded.

d) Fossil emissions

Anthropogenic emissions from EDGARv8 should be used as recommended by WP2 (Milestone 2). These are provided at monthly resolution[4] for the following sectors (the sector codes are given in parentheses): i) Energy for buildings (BUILDINGS), ii) Fuel exploitation (FUEL_EXPLOITATION), iii) Industrial combustion (IND_COMBUSTION), iv) Industrial processes (IND_PROCESSES), v) Power industry (POWER_INDUSTRY), vi) Transport (TRANSPORT) and vii) Waste (WASTE).

EDGARv8 provides separate estimates for CO_2 emissions from fossil sources (Ffco2) versus bio-fuel sources for the above sectors. The biofuel files include "CO2bio" in the file name and should be excluded.

EDGARv8 provides weekly and hourly profiles per country and source sector, which should be used to calculate hourly varying emissions[5]. The sectors, however, correspond to the sector grouping used for the annual emissions, and not the monthly ones. Table 2 describes the "mapping" of monthly to annual sectors which can be used to determine which temporal profile to use.

The Ffco2 flux from EDGARv8 should be used as a fixed flux component in the inversions.

Table 2. List of aggregated sectors for which monthly emissions are provided and the corresponding sector(s) for which the temporal profiles are provided.

Aggregated sector	Sectors	Recommended for temporal profile	Description
ENERGY	RCO	RCO	Energy for buildings
FUEL_EXPLOITATION	REF_TRF	REF	Oil refineries and transformation industry
IND_COMBUSTION	IND	IND	Combustion for manufacturing
IND_PROCESSES	NMM, CHE, IRO, NFE, NEU	NMM	Non-metallic minerals production
POWER_INDUSTRY	ENE	ENE	Power industry
TRANSPORT	TNR, TRO	TRO	Road transport
WASTE	SWD_INC	SWD	Solid waste

[4] file available from https://edgar.jrc.ec.europa.eu/dataset_ghg80
[5] these are provided in the "Auxilliary Tables" available from https://edgar.jrc.ec.europa.eu/dataset_temp_profile

This project has received funding from the European Union's Horizon Europe research and innovation programme under grant agreement No 101081395

e) Open and coastal ocean fluxes

The estimate of sea/ocean fluxes within the inversion domain should be based on a hybrid product combining the coastal ocean flux estimates from the University of Bergen and a global ocean estimate from MPI-BGC-Jena (Rödenbeck et al., 2014[6]; McGrath et al., 2023[7]). The data is provided from 2005 to 2020 at a 0.125°×0.125° horizontal resolution and at daily temporal resolution. The estimates for 2020 should be used to impose the values for more recent years.

This product should be used as a prior estimate of the F_{OCEAN} fluxes in the inversions.

f) Components ignored in the set of prior/fixed flux estimates

Some secondary flux components which should not have a critical impact for the CO_2 inversions, and for which there is a lack of suitable estimate over the whole period of analysis, are ignored in the set of prior/fixed flux estimates, CO_2 emissions from liming (missed by ORCHIDEE), decomposition of peat etc.

g) Providing the LULUCF fluxes

The provision of "LULUCF estimates" from the inversions for comparisons with inventories should be based on a correction of the NEE+F_{LUC} prior and posterior estimates, to include some fixed land fluxes such as F_{BB}, and to correct for the fluxes which do not lead to change in the local stock of carbon, e.g. cancelling from the NEE the amount of carbon removed by harvesting (via the $F_{WOODSINK}$ and $F_{CROPSINK}$ estimates).

5. Prior / Fixed estimate of the boundary conditions and completion of the stratosphere

For the estimate of the initial, lateral and top boundary conditions, inversions should use the CAMS global greenhouse gas inversion product, v22r1 available up to 2022-12.

This global inversion product should also be used to complement the vertical columns of CO_2 above the top boundary of regional CTM (if its top boundary is lower than the height of the columns) when comparing the model to XCO_2 satellite observations.

6. Other input to inversions

a) Meteorological forcing

The CTM should be driven by the European Centre for Medium-Range Weather Forecasts (ECMWF) meteorological forecast or by the ERA5 reanalysis.

[6] Rödenbeck, C., Bakker, D. C. E., Metzl, N., Olsen, A., Sabine, C., Cassar, N., Reum, F., Keeling, R. F., and Heimann, M.: Interannual sea–air CO2 flux variability from an observation-driven ocean mixed-layer scheme, Biogeosciences, 11, 4599–4613, https://doi.org/10.5194/bg-11-4599-2014, 2014.

[7] McGrath, M. J., Petrescu, A. M. R., Peylin, P., Andrew, R. M., Matthews, B., Dentener, F., Balkovič, J., Bastrikov, V., Becker, M., Broquet, G., Ciais, P., Fortems-Cheiney, A., Ganzenmüller, R., Grassi, G., Harris, I., Jones, M., Knauer, J., Kuhnert, M., Monteil, G., Munassar, S., Palmer, P. I., Peters, G. P., Qiu, C., Schelhaas, M.-J., Tarasova, O., Vizzarri, M., Winkler, K., Balsamo, G., Berchet, A., Briggs, P., Brockmann, P., Chevallier, F., Conchedda, G., Crippa, M., Dellaert, S. N. C., Denier van der Gon, H. A. C., Filipek, S., Friedlingstein, P., Fuchs, R., Gauss, M., Gerbig, C., Guizzardi, D., Günther, D., Houghton, R. A., Janssens-Maenhout, G., Lauerwald, R., Lerink, B., Luijkx, I. T., Moulas, G., Muntean, M., Nabuurs, G.-J., Paquirissamy, A., Perugini, L., Peters, W., Pilli, R., Pongratz, J., Regnier, P., Scholze, M., Serengil, Y., Smith, P., Solazzo, E., Thompson, R. L., Tubiello, F. N., Vesala, T., and Walther, S.: The consolidated European synthesis of CO2 emissions and removals for the European Union and United Kingdom: 1990–2020, Earth Syst. Sci. Data, 15, 4295–4370, https://doi.org/10.5194/essd-15-4295-2023, 2023.

This project has received funding from the European Union's Horizon Europe research and innovation programme under grant agreement No 101081395

b) Atmospheric observations

For ground-based observations, the European Obspack dataset should be used (https://meta.icos-cp.eu/objects/xfK_Mjw7m3jN1LIzq-wtsCYq). This dataset encompasses ICOS as well as non-ICOS sites and covers the period 1972-01 to 2024-07. The inversion assimilates 1-hour averages of the corresponding measurements.

For satellite observations, retrievals from the OCO-2 v11 satellite should be used.

Selection of the observations

Following the observation selection defined in Broquet et al. (2013)[8], hourly observations at low altitude stations (with inlets below 1000masl) are assimilated during the afternoon (here 12:00-17:00 LTC) only, and hourly observations at high altitude stations (with inlets above 1000masl) are assimilated during the night time (here 0:00-6:00 LTC) only. When several levels of measurements are available at a given station, the inversions assimilate the data from the highest level only. Please note that we exclude the urban stations HEI (Heidelberg in Germany) and GIF (Gif sur Yvette in France) and some stations which are challenging to represent with mesoscale atmospheric transport models and/or which provide data over a relatively short time over the entire period 2005-2023 (LMU, VAC, GIC, SGC and EEC in Spain) from the dataset.

For the satellite XCO_2 observations from the OCO-2 NASA-JPL mission, we only consider "good" retrievals as identified by the XCO_2 quality flag of the product, with nadir and glint modes over land (ignoring observations over the ocean). Since Chevallier et al. (2019)[9] claimed that the assimilation of OCO-2 ocean observations still produced unrealistic results in their global atmospheric inversions, they are therefore not considered in this study. After this selection, all individual observations are assimilated and compared to their corresponding CTM horizontal grid-cells (i.e. to the CTM CO_2 vertical column in this horizontal grid cell), defined for a given observation as that containing the centre of the ground projection of the OCO-2 pixel at the observation time: there is no aggregation of the observations at the model resolution.
To make suitable comparisons between simulations and satellite observations, the vertical profiles of CO_2 mole fraction in the corresponding atmospheric columns of the model simulations are first interpolated on the satellite CO_2 retrieval levels (with a vertical mass-conserving interpolation on pressure levels). Then, the appropriate simulated XCO_2 values are computed using both the OCO-2 averaging kernels and prior estimates provided in the OCO-2 retrieval product.

Observations errors

For both the *in situ* and satellite data assimilation, the inversion system accounts for both transport model and observation errors. The observation error covariance matrix of the system is set up as a diagonal matrix (without spatial or temporal correlation across the observations) with the observation error values provided in the observation products (for each hourly in situ observation, and each satellite retrieval), and with values for the transport model error for the in situ and satellite CO_2 observations (the total observation error being the root sum square of the observation and transport model error).

[8] Broquet, G., Chevallier, F., Bréon, F.-M., Kadygrov, N., Alemanno, M., Apadula, F., Hammer, S., Haszpra, L., Meinhardt, F., Morguí, J. A., Necki, J., Piacentino, S., Ramonet, M., Schmidt, M., Thompson, R. L., Vermeulen, A. T., Yver, C., and Ciais, P.: Regional inversion of CO2 ecosystem fluxes from atmospheric measurements: reliability of the uncertainty estimates, Atmos. Chem. Phys., 13, 9039–9056, https://doi.org/10.5194/acp-13-9039-2013, 2013.

[9] Chevallier, F., Remaud, M., O'Dell, C. W., Baker, D., Peylin, P., and Cozic, A.: Objective evaluation of surface- and satellite-driven carbon dioxide atmospheric inversions, Atmos. Chem. Phys., 19, 14233–14251, https://doi.org/10.5194/acp-19-14233-2019, 2019.

This project has received funding from the European Union's Horizon Europe research and innovation programme under grant agreement No 101081395

The following values can be used (but this is not a requirement):

- for satellite observations, a 1 ppm 1-sigma transport model error for each satellite retrieval
- for surface measurements, observation errors set up as a function of stations, of the height of the station level above the ground and of the season, following the estimates by Broquet et al. (2011[10], 2013; based on comparison of simulations and measurements of radon: the corresponding standard deviations for the hourly observations ranges from 3.5 to 17 ppm and are given in Table 3).

Table 3. Seasonal estimates of the model errors for hourly averages of the measurements from surface stations following Broquet et al. (2011, 2013).

Altitude of the station	Selected hours	Season	Model error at the 1-hour scale (in ppm)
>= 1000m	Night, from 0:00 to 6:00 UTC	-	3.5
<1000m	Day, from 12:00 to 17:00 UTC	Winter (JFM)	17
		Spring (AMJ)	4
		Summer (JAS)	8
		Fall (OND)	11

c) Prior uncertainty

The uncertainty covariance matrix associated to the prior estimate of NEE + F_{LUC} is specified using Rh from ORCHIDEE, similarly to what is traditionally done in CO_2 inversions over Europe (Broquet et al., 2011; Monteil et al., 2020[11]). In principle, it should depend on the control resolution which is partially left free. The following details provide an indicative guidance. For a given 0.5° (or 0.2°) grid cell and 6-hour window (corresponding to one of the diagonal terms of this covariance matrix), the standard deviation of this uncertainty is fixed as α_{year}^{config} Rh, α_{year}^{config} being fixed for each control resolution and each year so that the average uncertainty (the RMS of the uncertainties) over land and over the year at the 0.5° (or 0.2°) and 1-day scale is 2.27 µmol CO_2 m^{-2} s^{-1} (Table 4). The spatial and temporal correlations of the uncertainty in the NEE + F_{LUC} fluxes at the 0.5° (or 0.2°) and 6-hour resolution are modelled with no correlation between the four 6-hour windows of the same day but day-to-day correlations for a given 6-hour window of the day, using exponentially decaying function with

[10] Broquet, G., Chevallier, F., Rayner, P., Aulagnier, C., Pison, I., Ramonet, M., Schmidt, M., Vermeulen, A. T., and Ciais, P.: A European summertime CO2 biogenic flux inversion at mesoscale from continuous in situ mixing ratio measurements, J. Geophys. Res., 116, D23303, https://doi.org/10.1029/2011JD016202, 2011.

[11] Monteil, G., Broquet, G., Scholze, M., Lang, M., Karstens, U., Gerbig, C., Koch, F.-T., Smith, N. E., Thompson, R. L., Luijkx, I. T., White, E., Meesters, A., Ciais, P., Ganesan, A. L., Manning, A., Mischurow, M., Peters, W., Peylin, P., Tarniewicz, J., Rigby, M., Rödenbeck, C., Vermeulen, A., and Walton, E. M.: The regional European atmospheric transport inversion comparison, EUROCOM: first results on European-wide terrestrial carbon fluxes for the period 2006–2015, Atmos. Chem. Phys., 20, 12063–12091, https://doi.org/10.5194/acp-20-12063-2020, 2020.

This project has received funding from the European Union's Horizon Europe research and innovation programme under grant agreement No 101081395

homogeneous temporal and spatial scales. Following the diagnostics of Kountouris et al. (2015)[12], these temporal and spatial correlation scales are set to 30 days and 200 km.

The uncertainty covariance matrix associated to the prior estimate of F_{OCEAN} is specified using a $0.2 gCm^{-2}day^{-1}$ uncertainty at 6-hour (or other temporal) and 0.5° (or 0.2°) resolution. Spatial and temporal correlations of the uncertainty at the 0.5° and 6-hour (or other temporal) resolution are modelled with correlations between all the temporal windows, using exponentially decaying function with homogeneous temporal and spatial scales, which are set to 30 days and 1000 km.

The configuration of the uncertainty covariance matrix associated to the prior estimate of the initial and boundary conditions is highly impacted by the type of transport model used for the inversion and there is thus no strong constraint on this. The following is an indicative example for such a configuration for CHIMERE: the uncertainty covariance matrix associated to the prior estimate of the initial and boundary conditions can be set using a 2% relative uncertainty for individual model grid cells at 1-day resolution, horizontal, vertical and temporal correlations modeled with exponentially decaying function with homogeneous temporal and spatial scales, 1000 km length scale for the horizontal correlations, 5 km length scale for the vertical correlations and 5 days temporal scale for the temporal correlations.

Table 4. List of the prior estimates for the control vector and indicative examples of control resolutions and of configuration of the associated error covariance matrix.

Product	**Abbreviation**	**Control resolutions**		**Prior uncertainties (optional)**			
		Spatial	**Temporal**	**Standard deviation**	**Correlations**		
					Spatial	**Temporal**	**Vertical**
ORCHIDEE simulation CRUERA-v5	**NEE + F_{LUC}** = NPP + Rh + F_{LUC}.	0.5° res or 0.2° res (requirement)	6H (optional)	2.27µmol CO_2 m^{-2} s^{-1} at 6-hour and 0.5° resolution on average	200km	30 days (with no correlation from one 6-hour window to the other within a day)	-
Open and coastal fluxes from MPI-BGC-Jena and the University of Bergen	**F_{OCEAN}**	0.5° res or 0.2° res (requirement)	6H (optional)	0.2 $gCm^{-2}day^{-1}$ at 6-hour and 0.5° resolution	1000km	30 days	-
CAMS v22r1	Initial conditions	At the transport model 3D spatial resolution (optional)	-	2% at the model and 1 day resolution	1000km	-	5km

[12] Kountouris, P., Gerbig, C., Totsche, K.-U., Dolman, A. J., Meesters, A. G. C. A., Broquet, G., Maignan, F., Gioli, B., Montagnani, L., and Helfter, C.: An objective prior error quantification for regional atmospheric inverse applications, Biogeosciences, 12, 7403–7421, https://doi.org/10.5194/bg-12-7403-2015, 2015.

This project has received funding from the European Union's Horizon Europe research and innovation programme under grant agreement No 101081395

CAMS v22r1	Lateral conditions	At the transport model 3D spatial resolution at the lateral boundaries (optional)	1D (optional)	2% at the model and 1 day resolution	1000km	5days	5km

7. Output

The following out should respect the AVEYPA format to enable comparison with PARIS and AVENGERS. The file naming convention should follow that outlined in the EYE-CLIMA Data Management Plan (D6.3).

Gridded flux files:

- Prior land-biosphere fluxes
- Prior land-biosphere flux uncertainty
- Posterior land-biosphere fluxes
- Posterior land-biosphere flux uncertainty
- Prior bio-fuel emissions
- Prior fossil emissions
- Prior ocean fluxes
- Prior ocean flux uncertainty (if ocean fluxes are optimized)
- Posterior ocean fluxes (if ocean fluxes are optimized)
- Posterior ocean flux uncertainty (if ocean fluxes are optimized)

The posterior land-biosphere fluxes plus the bio-fuel emissions (with subsequent corrections for lateral fluxes) should be comparable to LULUCF as is reported to the UNFCCC.

Mixing ratio files:

- Prior modelled CO_2 at sites where observations were assimilated
- Posterior modelled CO_2 at sites where observations were assimilated
- Prior background CO_2 at sites where observations were assimilated
- Posterior background CO_2 at sites where observations were assimilated (if background is optimized)
- Prior uncertainty in CO_2

This project has received funding from the European Union's Horizon Europe research and innovation programme under grant agreement No 101081395

Appendix B: Inversion Protocol for CH_4

Author: Aki Tsuruta (FMI)
Date: January 2026
Version: 1.1

1. Objectives

This protocol describes the set-up for CH_4 flux estimates from inversion frameworks for three case studies.

1) **European coarse resolution study:** The inversion domain should cover at least the area **11°W to 34°E and 34°N to 72°N** to include all EU countries, and for the period **2005 to 2023**. Here, flux optimization and transport model resolutions should be **0.5° × 0.5°**.
2) **European high resolution study:** Same domain as above, and for the period **2018 to 2023**. Here, flux optimization and transport model resolutions should be at **0.2° × 0.2°**.
3) **Russian case study:** The inversion domain should cover at least the area **19°E to 170°W and 30°N to 85°N**, and the period **2015 to 2023**. Here, flux optimization resolutions should be at **0.5° × 0.5°**, and transport models are also recommended to run at **0.5° × 0.5°** resolution.

2. Inversion runs

2.1 Core simulation inputs and setups

All three cases should be run with the following inputs and setups for the periods stated in Section 1. Please see Section 3 for more details about the inputs.

Table 1. Datasets to be used in the prior flux estimates

Source sector	**Dataset**
Fugitives from fossil fuels (FFF)	GAINS
Combustion (COM)	GAINS
Agriculture and waste (AGW)	GAINS
Wetlands and soil sinks (WET)	JSBACH-HIMMELI
Freshwater (WET):	
Lakes	Johnson et al. (2022)
Rivers	Rocher-Ros et al. (2023
Biomass burning (BBR)	GFAS
Geological (GEO)	Etiope et al. (2019)
Termites	Castaldi (2013)
Ocean	Weber et al. (2019)
Prior uncertainties	As in Table 2
Boundary conditions	CAMS GHG inversion
Wind fields	ECMWF ERA5
OH	TransCom OH
Observations	ICOS & NOAA ObsPack surface data

This project has received funding from the European Union's Horizon Europe research and innovation programme under grant agreement No 101081395

2.2 Emission Categories

In all the inversions, please optimize the emission categories using prior uncertainties as defined in Table 2. Note that termites and ocean sources will not be optimized, and therefore uncertainties are not defined. Please see also Table 3 for the details about sectors and data sources.

The uncertainties are given as percentages of the prior flux estimate. For anthropogenic sources (using GAINS priors), these are based on the analysis from D2.8.

Table 2. List of emission categories and prior uncertainties

Category abbreviations	**Source Sectors**	**Optimization resolutions**		**Uncertainties**	**Correlations**	
		Spatial	Temporal		Spatial	Temporal
FFF	Fugitives from fossil fuels	Grid-wise	Monthly	15%	100 km	1M
COM	Combustion	Grid-wise	Monthly	51%	100 km	3M
AGW	Agriculture and waste	Grid-wise	Monthly	80%	100 km	3M
WET	Wetlands, soil sinks and freshwater	Grid-wise	Monthly	100%	100 km	1M
BBR	Biomass burning	Grid-wise	Monthly	50%	50 km	1M
GEO	Geological	Grid-wise	Monthly	100%	300 km	6M
TER	Termites	N/A	N/A	N/A	N/A	N/A
OCE	Ocean	N/A	N/A	N/A	N/A	N/A

3. Input Data

Input data described below will be made available at the NILU's sftp server

SFTP: eyeclimasftp@sftp.nilu.no
Password: ec_dataexchange2189
Directory: eyeclimasftp/WP3/inversion_input/ch4/

3.1 Prior fluxes of CH_4

Prior CH_4 fluxes will be provided in daily or monthly resolutions for the period 2005 to 2023 at 0.2°×0.2°, 0.5°×0.5° and 1°×1° spatial resolutions. The data sources are summarized in Table 3.

The data can be found in the NILU's sftp server:

eyeclimasftp/WP3/inversion_input/ch4/priors/

This project has received funding from the European Union's Horizon Europe research and innovation programme under grant agreement No 101081395

Table 3. Data sources of prior CH_4 fluxes

Category Abb.	Source Sector	Data source	Sectors as in original data	Original Resolutions		Time period
FFF	Fugitives from fossil fuels	GAINS v2	D_Fugitives	0.1°×0.1°	monthly	2005-2023
COM	Combustion	GAINS v2	A_PublicPower, B_Industry, C_OtherStationaryComb, F_RoadTransport	0.1°×0.1°	monthly	2005-2023
AGW	Agriculture and waste	GAINS v2	J_Waste, K_AgriLivestock, L_AgriOther	0.1°×0.1°	monthly	2005-2023
WET	Wetlands and soil sinks	JSBACH-HIMMELI EU	Peatlands, mineral soils, soil sinks	0.125°×0.125°	daily	2005-2023
		JSBACH-HIMMELI NHL	Peatlands, mineral soils, soil sinks	0.5°×0.5°	daily	2005-2023
WET	Freshwater	Johnson et al., 2022†	Lakes	0.25°×0.25°	daily	Climatology
WET	Freshwater	Rocher-Ros et al., 2023‡	Rivers	0.25°×0.25°	monthly	Climatology
BBR	Biomass burning	GFAS	Biomass burning	0.1°×0.1°	daily	2005-2023
GEO	Geological	Etiope et al., 2019*	Onshore emissions from geological sources	1°×1°	monthly	Climatology
TER	Termites	Castaldi, 2013	Termites	1°×1°	monthly	Climatology
OCE	Ocean	Weber et al., 2019	Diffusive and ebullitive fluxes from ocean	1°×1°	monthly	Climatology

†Small lakes (<0.1 km^2) are unscaled, large lakes (>5000 km^2) are scaled down to 10% of the fluxes in Johnson dataset. All remaining lakes are scaled such that the global yearly total from lakes is 13 Tg, the lower limit in Saunois et al., Global Methane Budget 2000–2020, Earth Syst. Sci. Data Discuss. [preprint] (2024).

‡Global total scaled down to 12 Tg, the lower limit in Saunois et al., Global Methane Budget 2000–2020, Earth Syst. Sci. Data Discuss. [preprint] (2024).

*Global total scaled down to 15 Tg, and excluding ocean fluxes. (Petrenko, V. V. et al. Minimal geological methane emissions during the Younger Dryas–Preboreal abrupt warming event. Nature 548, 443–446 (2017).)

3.2. Atmospheric observations

NetCDF data for each station can be found in the NILU's sftp server:

eyeclimasftp/WP3/inversion_input/ch4/obs/sitefiles/EU_core_coarse/

eyeclimasftp/WP3/inversion_input/ch4/obs/sitefiles/EU_core_high/

The merged monitor file can be found in the NILU's sftp server:

eyeclimasftp/WP3/inversion_input/ch4/obs/monitor_eyeclima_EU_core_coarse.nc

eyeclimasftp/WP3/inversion_input/ch4/obs/monitor_eyeclima_EU_core_high.nc

This project has received funding from the European Union's Horizon Europe research and innovation programme under grant agreement No 101081395

Table 4: List of ground-based stations to be used in the EU core simulations.

Site ID	Site name	Country/Territory	Laboratory	Latitude (deg. N)	Longitude (deg. E)	Elevation (masl)	Sampling height (magl)	Period (MM/YYYY-MM/YYYY)	Data type (C=continuous, D=discrete)	Data source	Simulation (EU core, Coarse)	(EU core, High)
BIK	Bialystok	Poland	ICOS, MPI	53.23	23.01	183	300	07/2005-12/2023	C	ICOS ObsPack v10 & VERIFY	x	
BIR	Birkenes	Norway	ICOS, NILU	58.39	8.25	219	75	09/2020-07/2024	C	ICOS ObsPack v10		x
BIS	Biscarrosse	France	ICOS, LSCE	44.38	-1.23	73	47	09/2009-03/2024	C	ICOS ObsPack v10	x	x
BSD	Bilsdale	United Kingdom	ICOS, ACRG	54.36	-1.15	382	248	01/2014-08/2021	C	ICOS ObsPack v10		x
CBW	Cabauw	Netherlands	ICOS, TNO	51.97	4.93	0	207	04/1993-07/2024	C	ICOS ObsPack v10	x	x
CIB	Centro de Investigacion de la Baja Atmosfera (CIBA)	Spain	NOAA	41.81	-4.93	845	5	05/2009-07/2024	D	NOAA ObsPack v7.0 & NOAA ObsPack NRT v7.0	x	x
CMN	Monte Cimone	Italy	ICOS, CNR-ISAC	44.19	10.7	2165	8	07/2008-07/2024	C	ICOS ObsPack v10	x	x
CRP	Carnsore Point	Ireland	ICOS, NUI	52.18	-6.37	9	14	08/2010-08/2021	C	ICOS ObsPack v10		x
ERS	Ersa	France	ICOS, LSCE	42.97	9.38	533	40	04/2013-03/2024	C	ICOS ObsPack v10		x
FKL	Finokalia	Greece	ICOS, CEA-CNRS-UVSQ	35.34	25.67	250	15	06/2014-03/2024	C	ICOS ObsPack v10		x
GAT	Gartow	Germany	ICOS, DWD	53.07	11.44	70	341	05/2016-07/2024	C	ICOS ObsPack v10		x
HEI	Heidelberg	Germany	ICOS, IUP	49.42	8.68	113	30	01/1996-03/2024	C	ICOS ObsPack v10	x	x
HEL	Helgoland	Germany	ICOS, DWD	54.18	7.88	43	110	08/2020-07/2024	C	ICOS ObsPack v10		x
HFD	Heathfield	United Kingdom	ICOS, NPL	50.98	0.23	160	100	03/2014-03/2024	C	ICOS ObsPack v10	x	x
HPB	Hohenpeissenberg	Germany	ICOS, DWD	47.8	11.02	934	131	09/2015-07/2024	C	ICOS ObsPack v10		x
HTM	Hyltemossa	Sweden	ICOS, CEC	56.1	13.42	115	150	12/2016-07/2024	C	ICOS ObsPack v10		x
HUN	Hegyhátsál háttérszennyettség-mérő állomás	Hungary	ICOS, HUN-REN	46.96	16.65	248	115	02/2006-05/2024	C	ICOS ObsPack v10 & ICOS_ATC_OBSPACK-Europe-L2-2022	x	x
IPR	Ispra	Italy	ICOS, JRC	45.81	8.64	210	100	10/2007-07/2024	C	ICOS ObsPack v10 & VERIFY	x	x
JFJ	Jungfraujoch	Switzerland	ICOS, CEP	46.55	7.99	3571.8	13.9	02/2005-07/2024	C	ICOS ObsPack v10	x	x
KAS	Kasprowy Wierch	Poland	ICOS, AGH	49.23	19.98	1987	7	07/1996-03/2024	C	ICOS ObsPack v10	x	x
KMP	Kumpula	Finland	FMI	60.2	24.96	53	30	01/2010-12/2024	C	FMI	x	x
KRE	Křešín u Pacova	Czech Republic	ICOS, KAS	49.57	15.08	534	250	04/2017-07/2024	C	ICOS ObsPack v10		x
LIN	Lindenberg	Germany	ICOS, DWD	52.17	14.12	73	98	10/2015-07/2024	C	ICOS ObsPack v10		x
LMP	Lampedusa	Italy	ICOS, ENEA	35.52	12.63	45	8	01/2008-07/2024	C	ICOS ObsPack v10		x
LMP	Lampedusa	Italy	NOAA	35.52	12.63	45	5	10/2006-08/2024	D	NOAA ObsPack v7.0 & NOAA ObsPack NRT v7.0	x	
LUT	Lutjewad	Netherlands	ICOS, RUG	53.4	6.35	1	60	05/2006-07/2024	C	ICOS ObsPack v10	x	x
MHD	Mace Head	Ireland	ICOS, LSCE	53.33	-9.9	5	24	01/2005-03/2023	C	ICOS ObsPack v10 & VERIFY	x	x
MLH	Malin Head	Ireland	ICOS, LATMOS	55.36	-7.33	22	47	09/2010-07/2021	C	ICOS ObsPack v10		x
NOR	Norunda	Sweden	ICOS, CEC	60.09	17.48	46	100	01/2017-07/2024	C	ICOS ObsPack v10		x
OPE	Observatoire pérenne de l'environnement	France	ICOS, ANDRA	48.56	5.5	390	120	04/2011-07/2024	C	ICOS ObsPack v10	x	x
OXK	Ochsenkopf	Germany	ICOS, MPI	50.03	11.81	1022	163	09/2019-07/2024	C	ICOS ObsPack v10		x
PAL	Pallas	Finland	ICOS, FMI	67.97	24.12	565	12	02/2004-07/2024	C	ICOS ObsPack v10	x	x
PDM	Pic du Midi	France	ICOS, LSCE	42.94	0.14	2877	28	05/2014-03/2024	C	ICOS ObsPack v10		x
PRS	Plateau Rosa	Italy	ICOS, RSE	45.93	7.7	3480	10	01/2005-07/2024	C	ICOS ObsPack v10	x	x
PUI	Puijo	Finland	ICOS, FMI	62.91	27.65	232	84	02/2016-07/2024	C	ICOS ObsPack v10		x
PUY	Puy de Dôme	France	ICOS, LSCE	45.77	2.97	1465	10	04/2011-07/2024	C	ICOS ObsPack v10	x	x
RGL	Ridge Hill	United Kingdom	ICOS, ACRG	52	-2.54	207	90	02/2012-07/2024	C	ICOS ObsPack v10	x	x
SMR	Hyytiälä	Finland	ICOS, UHEL	61.85	24.29	181	125	05/2015-07/2024	C	ICOS ObsPack v10		x
SSL	Schauinsland	Germany	ICOS, IUP	47.92	7.92	1205	35	07/1991-07/2024	C	ICOS ObsPack v10 & ICOS_ATC_OBSPACK-Europe-L2-2022	x	x
STE	Steinkimmen	Germany	ICOS, DWD	53.04	8.46	29	252	07/2019-07/2024	C	ICOS ObsPack v10		x
SVB	Svartberget	Sweden	ICOS, SLÜ	64.26	19.78	269	150	05/2017-07/2024	C	ICOS ObsPack v10		x
TAC	Tacolneston	United Kingdom	ICOS, ACRG	52.52	1.14	64	185	01/2013-03/2024	C	ICOS ObsPack v10	x	x
TOH	Torfhaus	Germany	ICOS, DWD	51.81	10.54	801	110	12/2017-07/2024	C	ICOS ObsPack v10		x
TRN	Trainou	France	ICOS, LSCE	47.96	2.11	131	180	01/2007-07/2024	C	ICOS ObsPack v10	x	x
UTO	Utö - Baltic sea	Finland	ICOS, FMI	59.78	21.37	8	57	03/2012-07/2024	C	ICOS ObsPack v10	x	x
ZSF	Zugspitze	Germany	ICOS, UBA	47.42	10.98	2666	3	01/2002-07/2024	C	ICOS ObsPack v10 & ICOS_ATC_OBSPACK-Europe-L2-2022	x	x

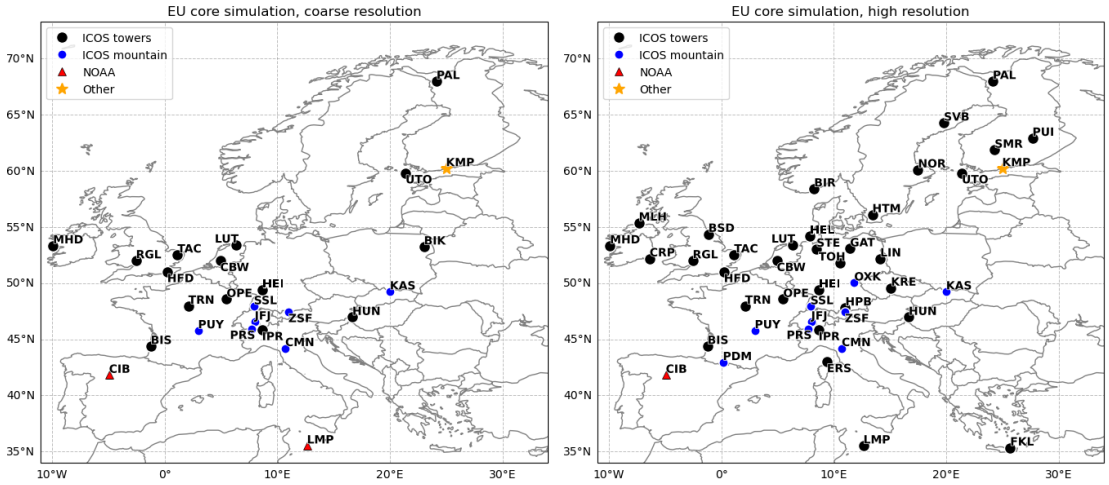

Figure 1: Locations of ground-based stations to be used in the EU core coarse (left) and high (right) resolution simulations.

This project has received funding from the European Union's Horizon Europe research and innovation programme under grant agreement No 101081395

Observed mixing ratios of CH_4 consist of data provided from the ICOS ObsPack v10 and NOAA ObsPack v7.0. The data in the server contain observations since 2004 only. List of sites are summarized in Table 3, and locations are illustrated in Figure 1.

The number of sites is limited based on data coverage (number of days (continuous) or weeks (discrete)) such that the list includes only the ites with more than 50% of coverage within the simulation periods for each case study.

Models can adjust the followings for their own specifications:

- Observation uncertainties (both transport model and measurement errors)
- Sampling height from which modelled mole fractions will be estimated from
- For continuous data, hours of the days to use, and whether to take daily averages from some hours. Recommendations are: 12-16 LT (towers) and 0-4 LT (mountain sites).
- Data outside of the study domain.

3.3. Boundary conditions

CAMS GHG inversion: please use the CAMS data v22r2 until 2022, and v23r1 for 2023, assimilating surface observations only. Data can be downloaded from:

https://ads.atmosphere.copernicus.eu/datasets/cams-global-greenhouse-gas-inversion?tab=download

3.4. OH sink

TransCom OH concentration fields can be found in the NILU's sftp server:

eyeclimasftp/WP3/inversion_input/ch4/lossfields/

4. Validation data

NetCDF data for each validation site can be found in the NILU's sftp server:

eyeclimasftp/WP3/inversion_input/ch4/obs/validation

List of validation data includes:

- ICOS and NOAA sites that did not meet data coverage criteria, but has more than 70% of data coverage in 2021
- NOAA sites with measurement period largely overlapping with ICOS data
- TCCON sites that have GGG2020 data
- Aircraft data from LSCE
- AirCore data from Aire-sur-l'Adour, Cyprus, Kiruna, Reims, Sodankylä and Trainou

Please provide prior and posterior mole fractions corresponding to these observations.

This project has received funding from the European Union's Horizon Europe research and innovation programme under grant agreement No 101081395

5. Output Data

Please upload the results to the NILU's sftp server:

eyeclimasftp/WP3/inversion_output/ch4/

5.1. File formats

To facilitate the inter-comparison of the inversions, please follow common guidelines for the output file formats: AVEYPA_data_format.docx

Files should be named as:

Species_Variable_Sector_Region_Method_Timestep_FromTime_ToTime_Model_Institute_Version.nc

Example file name:

CH4_FLUX_ALL_EUR_INV_MONTH_20050101_20221231_CIF-CHIMERE_CNRS_V01.nc

Please see Table 10 of D6.3 report for details:

https://folk.nilu.no/~rthompson/eyeclima_reports/EYECLIMA_D6.3_v1.pdf

5.2. Fluxes and uncertainties

Please provide the total and sectoral fluxes (as in Table 1) at monthly and spatial resolution of each study as described in Section 1. Please use category abbreviations (FFF, COM, AGW, WET, BBR, GEO, TER, OCE) as "sector_name".

Please also report national and regional total and sectoral emissions using Eye-Clima masks. The mask files can be downloaded from the NILU's sftp server:

eyeclimasftp/WP3/Mask_files_EU27+3

5.3. Mixing ratios and uncertainties

Please provide prior and posterior mixing ratios, as well as uncertainties and background mixing ratios for 2005-2023 for core simulations and 2021 for sensitivity runs and validation sites.

For "conc" outputs, "number_of_identifier" should be as follows:

- 1 = ICOS ObsPack data
- 2 = NOAA ObsPack data
- 3 = other data sources
- 4 = aircraft data
- 5 = AirCore data
- 6 = TCCON data

This project has received funding from the European Union's Horizon Europe research and innovation programme under grant agreement No 101081395

Appendix C: Inversion Protocol for N_2O

Author: Nalini Krishnankutty
Date: January 2026
Version: 1.1

1. Objectives

This protocol describes the set-up and input data for inversions of N2O in the EYE-CLIMA project. Inversions will be run at 0.5°×0.5° resolution from 2005 to at least 2023 and at 0.2°×0.2° from 2018 to at least 2023. The inversion domain should cover the area from 15°W to 35°E and 33°N to 73°N to include all EU-27 countries plus United Kingdom, Norway, and Switzerland (together EU27+3).

2. Input Data

2.1. Prior fluxes of N_2O

Total N2O fluxes are provided for the period 2005 to 2023 at 0.5°×0.5° and 2018 to 2023 at 0.2°×0.2° spatial resolutions. Natural soil and ocean fluxes at 1o×1o spatial resolution were linearly interpolated to 0.5°×0.5° and 0.2°×0.2°. In addition, to accurately attribute land/ocean the fluxes to land/ocean, a redistribution of fluxes has been done using the land-sea mask at 0.5°×0.5° and 0.2°×0.2°. For ocean fluxes, the climatology from 2010 to 2014 has been used.

Table 1. Prior N2O fluxes

Category	Data source	Original resolution		Original Time period
Natural soils	OCN_GCP2019	1°×1°	monthly	1980-2019
Ocean	PlankTOMv10.2	1°×1°	monthly	2010-2014
Agriculture[1]	GAINS	0.1°×0.1°	monthly	1990-2023
Waste[1]	GAINS	0.1°×0.1°	monthly	1990-2023
Transport[1]	GAINS	0.1°×0.1°	monthly	1990-2023
Industry[1]	GAINS	0.1°×0.1°	monthly	1990-2023
Biomass burning	GFED-4.1s	0.25°×0.25°	monthly	1995-2022
	GFED-5	0.25°×0.25°	monthly	2023

[1]Covers Europe from 34.95°W to 44.95°E and 23.95°N to 83.85°N. Data were missing for non-EU27+3 countries, i.e. countries in the Balkans, North Africa, and Ukraine where estimates from EDGARv8 were used. Emissions from Agriculture included the following sectors from EDGARv8: direct and indirect emissions from agricultural soils, manure management).

2.1.1. Prior data description

Agriculture sector:
GAINS: includes direct and indirect soil emissions associated with mineral fertilizer, manure and grazing (sectors K_AgriLivestock and L_AgriOther)

Industry:
GAINS: Chemical processing, Combustion for industrial manufacturing (sector B_Industry)

This project has received funding from the European Union's Horizon Europe research and innovation programme under grant agreement No 101081395

2.2. Atmospheric observations

The N2O harmonized observation dataset at hourly intervals available from the ICOS CP, which was prepared as part of AVENGERS, EYE-CLIMA and PARIS projects. This includes data from NOAA flask sampling sites and other European sites (WDCGG, DECC, AGAGE and ICOS). The grey-highlighted sites are used only in 0.2°×0.2° inversion.

Table 2. List of sites used in inversions

Site ID	Site name	Country	Laboratory	Latitude (deg. N)	Longitude (deg. E)	Altitude (m. asl)	Sampling height (m. agl)	Years
BRM	Beromünster	Switzerland	EMPA	47.18	8.17	797	212	2017-2023
BSD	Bilsdale	UK	UNIVBRIS	54.35	-1.15	382	248	2017-2021
CBW	Cabauw	Netherlands	TNO	51.97	4.92	0	207	2005-2024
CIB	Centro de Investigacion de la Baja Atmosfera	Spain	NOAA	41.81	-4.93	845	5	2009-2022
CMN	Monte Cimone	Italy	UNIURB	44.19	10.70	2165	7	2008-2017
GAT	Gartow	Germany	MOHp	53.06	11.44	69	341	2019-2024
GIF	Gif sur Yvette	France	LSCE	48.71	2.14	160	7	2005-2015
HEI	Heidelberg	Germany	Institut für Umwelt-physik	49.41	8.67	113	30	2005-2014
HEL	Helgoland	Germany	MOHp	54.18	7.88	43	110	2020-2024
HFD	Heathfield	UK	UNIVBRIS	51.99	-2.53	207	100	2014-2024
HPB	Hohenpeissenberg	Germany	NOAA	47.80	11.02	985	131	2006-2023
HUN	Hegyhátsál	Hungary	ELTE	46.95	16.65	248	82	2006-2024
JFJ	Jungfraujoch	Switzerland	EMPA	46.54	7.98	3580	13.9	2005-2024
JUE	Jülich	Germany	MOHp	50.91	6.4	98	120	2019-2024
KIT	Karlsruhe	Germany	MOHp	49.09	8.42	110	200	2019-2024
KRE	Křešín u Pacova	Czech Republic	CAS	49.57	15.08	534	250	2018-2024
LIN	Lindenberg	Germany	MOHp	52.16	14.12	73	98	2018-2024
LMP	Lampedusa	Italy	NOAA	52.16	14.12	45	5	2006-2023
LUT	Lutjewad	Netherlands	RUG-CIO	53.40	6.35	1	60	2006-2024
MHD	Mace Head	Ireland	UNIVBRIS	53.32	-9.90	8.4	10	2005-2024
OPE	Observatoire pérenne de l'environne-ment	France	Andra	48.56	5.50	390	120	2019-2024

This project has received funding from the European Union's Horizon Europe research and innovation programme under grant agreement No 101081395

Site ID	Site name	Country	Laboratory	Latitude (deg. N)	Longitude (deg. E)	Altitude (m. asl)	Sampling height (m. agl)	Years
OXK	Ochsenkopf	Germany	MOHp	50.03	11.80	1022	163	2006-2024
PAL	Pallas	Finland	FMI	67.97	24.11	560	12	2022-2023
PUY	Puy de Dôme	France	LSCE	45.77	2.96	1465	10	2010-2024
SAC	Saclay	France	CEA	48.72	2.14	160	100	2019-2024
RGL	Ridge Hill	UK	UNIVBRIS	51.99	-2.53	207	90	2012-2024
SSL	Schauinsland	Germany	UBAG	47.91	7.91	1205	12	2005-2024
STE	Steinkimmen	Germany	MOHp	53.04	8.45	252	252	2019-2024
TAC	Tacolneston	UK	UNIVBRIS	52.51	1.13	64	100	2012-2024
TOH	Torfhaus	Germany	MOHp	51.80	10.53	801	147	2019-2024
TRN	Trainou	France	LSCE	47.96	2.11	131	180	2010-2024
WAO	Weybourne	UK	UEA	52.95	1.21	31	10	2014-2024
ZSF	Zugspitze	Germany	UBAG	47.41	10.97	2656	3	2005-2024

2.3. Boundary conditions

For the reference inversion, CAMS v22r1 boundary conditions are used.

Table 3. N_2O Initial mixing ratios

Data source	Resolution	Time period
CAMSv22r1	3.75°×1.875° 3-hourly 39 pressure levels	2005-2022

This project has received funding from the European Union's Horizon Europe research and innovation programme under grant agreement No 101081395

3. Reference inversion set-up

Resolution	**0.5°x0.5°**	**0.2°x0.2°**
Time period	2005-2023	2018-2023
Model	CIF-FLEXPART	CIF-FLEXPART
Prior fluxes	Global (CAMS, 2°×2°, monthly) Nested (GAINS, 0.5°x0.5°, monthly)	Global (CAMS, 2°×2°, monthly) Nested (GAINS, 0.2°x0.2°, monthly)
Prior uncertainty	50% of prior fluxes	50% of prior fluxes
Initial mixing ratios	CAMS v22r1 (3.75°×1.875° 3-hourly 39 pressure levels)	CAMS v22r1 (3.75°×1.875° 3-hourly 39 pressure levels)
Observations	Hourly averages (for mountain regions (altitude > 790m), the release height correction is done based on ECMWF orography fields)	Hourly averages (for mountain regions (altitude > 790m), the release height correction is done based on ECMWF orography fields)
Observation uncertainty	Standard deviation, where available; otherwise, 0.5 ppb	Standard deviation, where available; otherwise, 0.5 ppb

4. Data availability

Prior fluxes and CIF Yaml files are available from NILU's sftp server:

eyeclimasftp@sftp.nilu.no
Password: ec_dataexchange2189
Directory: /eyeclimasftp/WP3/inversion_input/n2o/

For the reference inversion the prior flux files for 0.5°x0.5° and 0.2°x0.2° are:
N2O_EYECLIMA_YYYY_05x05.nc and N2O_EYECLIMA_YYYY_02x02.nc respectively

Observations are available at the ICOS portal (https://fileshare.icos-cp.eu/s/erQYE4CaQoT8c3t).

Initial mixing ratios from CAMS are available via the Copernicus Atmospheric Data Store: https://ads.atmosphere.copernicus.eu/datasets/cams-global-greenhouse-gas-inversion?tab=overview

This project has received funding from the European Union's Horizon Europe research and innovation programme under grant agreement No 101081395

5. Output Data

Inversion results are to be uploaded to NILU's sftp server:
/eyeclimasftp/WP3/inversion_output/n2o/

5.1. Fluxes and uncertainties

Estimated fluxes and their respective uncertainties (in the same file) should be provided in gridded format at 0.5°x0.5° and 0.2°x0.2° spatial resolutions separately.

File name:
SPECIES_FLUX_SECTOR_REGION_METHOD_Timestep_FromTime_ToTime_MODEL_INSTITUTE_Version.nc

The file format is the common format for fluxes for the AVENGERS, EYE-CLIMA and PARIS (AVEYPA) projects and is described in: AVEYPA_data_format.docx

5.2. Mixing ratios

Observed and modelled mixing ratios used in the inversion should be provided in the NetCDF format with one file for each inversion experiment in the following format:

File name:

Species_CONC_Sector_Region_Method_Timestep_FromTime_ToTime_Model_Institute_Version

The file format is the common format for mixing ratios for the AVENGERS, EYE-CLIMA and PARIS (AVEYPA) projects and is described in: AVEYPA_data_format.docx

This project has received funding from the European Union's Horizon Europe research and innovation programme under grant agreement No 101081395

https://eyeclima.eu

BRUSSELS, 26 01 2026

Funded by the European Union. Views and opinions expressed are however those of the author(s) only and do not necessarily reflect those of the European Union. Neither the European Union nor the granting authority can be held responsible for them.

This project has received funding from the European Union's Horizon Europe research and innovation programme under grant agreement No 101081395